Fabrication of Quantum Dots and its application in DFWM and its corresponding application for optoelectronic devices

Shyamalima Chowdhury
Registration Number 121 of 2004

A thesis submitted in partial fulfillment of the requirements for the degree of Doctor of Philosophy

November, 2005

School of Science & Technology
Department of Physics
Tezpur University
Napaam, Tezpur - 784 028
(India)

Dedicated to my parents

Late (Dr.) Debendra Kr. Chowdhury

&

Mrs. Khirama Chowdhury

Abstract

Quantum dots are three dimensionally confined systems where motion of the charge carrier is restricted in all three dimensions. For semiconductor, such confinement is possible when the radius of the semiconductor crystallite approaches the Bohr radius of the exciton. Practically semiconductor crystallites having size 1-100 nm are termed as quantum dots. They exhibit physical and chemical properties different from either the individual molecule or the extended solid, and their size, shape, and composition can all be tailored to create a variety of desired properties. Apart from quantum size effect or quantum confinement effect, the other main features of quantum dots are high surface to volume ratio and high oscillator strength, For the last few years, a great deal of interest has been shown by many research workers to prepare semiconductor nanoparticles and to study their optoelectronic and optical properties. Producing monocrystalline, monodispersed and uniformly distributed quantum particles involve many physical parameters and machine complexities all of which cannot be controlled ideally and simultaneously in a specific route. And so, each synthetic route has its own advantage and limitations. The various physical and chemical synthetic processes for nanoparticle formation include: molecular beam epitaxy, electrochemical deposition, RF sputtering, dc magnetron sputtering, sol-gel, photochemical, low pressure chemical vapour deposition (LPCVD), chemical precipitation in colloids, mechanical grinding/alloying, magnetron co-sputtering, vapour deposition on cold substrates and on heated substrates, Selective area metal organic chemical vapour deposition (SA-MOCVD) etc. These fabricated structures are being studied for practical applications in electronic as well as linear and nonlinear optical devices. Much larger nonlinear effects have been observed in quantum dots than in bulk crystals of the same material. As a

result, quantum dots have been considered for many optical and electronic devices including light emitters, all-optical analog-to-digital converters, nanoelectronic devices, high-density information storage devices, and catalyses etc.

Recently, ion beam has become an important aspect for synthesis, modification characterizations of nanoparticles. The synthetic procedures include ion-implantation, ion beam mixing, ion beam assisted self organized nanostructure formation and template synthesis.

In this work we have fabricated lead sulphide (PbS), cadmium sulphide (CdS) and zinc sulphide (ZnS) quantum dots with narrow size distribution using poly vinyl alcohol (PVA) as matrix following chemical route. The quantum dots samples were characterized with the help of various characterization techniques, viz, XRD, UV-Vis absorption, TEM and Photoluminescence (PL). The sizes of the quantum dots were found to be 5-10 nm.

Next, in order to control nanocrystalline growth and increase stability, the surface of these low dimensional systems are coated. For coating the prepared nanoparticles, viz, PbS, CdS and ZnS we used PVA/silica hybrid. To the best of our knowledge this is the first approach of this kind. For the synthesis of PVA/silica hybrid we have followed a cheap, non-toxic and environment friendly route where sodium silicate was used as the inorganic source. The coated quantum dots were found to be within the size limit 4.8-9 nm.

In case of bare samples the PL peaks were observed in low energy regime which was attributed mainly to surface state emission surface state as well as band edge emission for PbS and due to surface defects like dangling bonds and vacancies in case of ZnS quantum dots. In case of CdS quantum dots the low energy peak is attributed due to formation of Cd-O complex. After applying silica coating the PL spectra of CdS and ZnS quantum dots show high energy emission. We believe that the origin of high energy emission is electron hole recombination at the surface of the nanoparticle. The occurrence of such

peak in case of coated sample indicates that coating may enhance the possibility of electron hole recombination.

We have also investigated the effect of ageing in quantum dots. The PL spectra of quantum dots were taken after 30 and 60 days. The PL intensity significantly increases with time in case of bare samples. However no significant increase in intensity has been observed in case of coated samples.

Swift heavy ion (SHI) beam impact on quantum dot is relatively new area in nanoparticle research. The effect of SHI irradiation on particle size and luminescence properties has been studied extensively in this work. The irradiation experiment was carried out on each of the bare and coated quantum dots samples. The samples were mounted on a vacuum shielded vertical sliding ladder having six rectangular faces. They were irradiated in the GPSC chamber under high vacuum (5×10^{-6} Torr) by using the 160 MeV Ni^{12+} beam with approximate beam current of 1.0 pnA (particle nanoampere), available from the 15UD tandem Pelletron Accelerator at NSC, New Delhi. The samples were irradiated with fluences 10^{12}, $5x10^{12}$ and 10^{13} ions/cm^2 respectively. Using Monte Carlo simulation program SRIM the projectile range for PbS, CdS and ZnS sample were calculated as 42.38, 36.48 and 34.44 μm. Following the SRIM calculation for SHI irradiation the sample thickness was kept ~20 μm so that the possibility for ion implantation can be ruled out.

After SHI irradiation we have observed particle growth in case of bare samples whereas the coated samples were found stable. Some high peaks were also appeared in PL spectra of the samples after irradiation.

In recent years, there are extensive studies on optical responses of semiconductor nanocrystals. Such studies enhances the possibilities of there application in nonlinear optical and optoelectronic devices. We have carried out DFWM experiment to explore nonlinear optical phenomena shown by embedded PbS quantum dots and presence of large high third order nonlinearity has been observed in such systems. For application of quantum

dots in optoelectronic devices we have studied the optoelectronic switching characteristics of the prepared quantum dots.

The frequency dependent electrical behaviour of PbS quantum dots have also been studied in terms of their capacitance -voltage (C-V) and current voltage (I-V) responses. The C-V characteristics show that in low frequency range (300-900 Hz) they can be used as passive elements like capacitors. Also at mid frequency range (20-40 kHz) single electron effects has been indicated for such systems.

DECLARATION

I hereby declare that the thesis entitled '**Fabrication of Quantum Dots and its application in DFWM and its corresponding application for optoelectronic devices**' being submitted to Tezpur University, Tezpur, Assam in partial fulfillment of the requirements for the award of the Degree of Doctor of Philosophy is a record of research work done by me during the Ph.D. course. This work has not been submitted in part or full for the award of any degree, diploma, associateship, fellowship or any other similar title or recognition from any other institute or organization.

Shyamalima Chowdhury

(Shyamalima Chowdhury)
Department of Physics
Tezpur University
Tezpur-784028(Assam)

Date: 28.11.05

Department of Physics :: Tezpur University

Napaam, Tezpur, Assam-784 028

Dr. Amarjyoti Choudhury
Prof. & Head

Phone: 03712-267007-9 Extn-5551, 5552
Fax: (+91) 3712-267005,6
E-mail- ajc@tezu.ernet.in

CERTIFICATE

This is to certify that the thesis entitled " **Fabrication of Quantum Dots and its application in DFWM and its corresponding application for optoelectronic devices**" submitted to the Tezpur University in the Department of Physics, under the School of Science and Technology, in partial fulfillment for the award of the degree of Doctor of Philosophy (Ph.D.) in Physics is a record of research work carried out by **Ms. Shyamalima Chowdhury** under my personal supervision and guidance.

All helps received by her from various sources have been duly acknowledged.

No part of this thesis has been reproduced elsewhere for award of any other degree.

(A. Choudhury)
Professor
School of Science and Technology
Department of Physics

Date: 21.11.05

Place: Napaam, Tezpur

CONTENTS

LIST OF TABLES

LIST OF FIGURES

ACKNOWLEDGMENTS

I would like to express my deep sense of gratitude to Prof. A. Choudhury for introducing me to the fascinating world of nano science and for his constant guidance and valuable suggestions throughout my research work. I feel myself fortunate enough to work under his able supervision.

I am indebted to Prof. S. K. Dolui for his suggestions regarding fabrication and characterization of the samples. His constructive comments and encouragements will remain noteworthy.

I extend my sincere thanks to Dr. A. Kumar, Dr. N. S. Bhattacharyya, Dr. D Mohanta, Dr. J. K. Sarma, Dr. N. Das and Dr. K. Baruah for their encouragement, criticism and discussions to carry out this research work. I am grateful to Dr. G. A. Ahmed for his help to carry out the DFWM experiment.

Help extended by IUAC-New Delhi, USIC & Dept. of Chemistry-G.U., RSIC-NEHU, Consortium for Scientific Research-DAE Facility Indore, Department of Chemical Sciences, T.U., in SHI irradiation and analytical support are acknowledged. Help extended by library staff of Tezpur University central library and IUAC library staff is also acknowledged.

I would like to appreciate Mr. A. Bordoloi, Mrs. A.Goswami, Siddhartha Juti, Diganta, Nandini, Robin and Swapnali for their help and company during my days in Tezpur University. I feel in short of words to express my gratitude to Abu, for his help in most of my works during the last one and half years.

I would like to thank Principal, Vice Principal and HoD-Physics, Chaiduar College, for their help and goodwill. I also appreciate my colleagues for their support and encouragement. Special thanks are due to Mr. P. Dutta (Dutta Sir) and Dr. R. M. Borah (Rita Ba) for their suggestions and help during these years.

Throughout this work, directly or indirectly, I have received valuable help from a number of individuals. Among them I remember Dr. (Mrs.) J.Baruah and staff of C.I.C., Tezpur, with pleasure.

I am indebted to my mother for her support through out this work. It is only her help, sacrifice and faith on me that makes me daring enough to start research. Thanks Ma, for being always there for me! I heartily acknowledge my brother and sister-in-law and my younger sister for their enduring support. Help extended by my relatives at different stages of my work are also acknowledged.

This work relies on many published facts mostly from the post-1990 era, scientist like Alivisatos, Rosseti, Brus, Wang, Nanda, Fernée, Bhargava and Kayanuma, to name a few, have formed new ideas that paved the path for more practical ideas. So, my gratitude goes out to everyone who writes important thoughts down on paper, so it shall be discovered and rediscovered in the future, opening up new gates and windows for humanity.

Last but not the least, for His blessings, I bow to the Almighty.

Shyamalima Chowdhury

Place: Napaam, Tezpur *(Shyamalima Chowdhury)*

Date: 28.11.05.

CHAPTER I

In recent years there has been much excitement surrounding the possible applications of ultra small systems on the 10-1000 Å length scale in the areas of electronics and optoelectronics. Structures whose dimensions are of this length scale are often called nanostructures. In a wider sense of the term, any material containing grains or clusters below 100 nm, or layers or filaments of that dimension, can be considered as nanostructure.

Though the changes in fundamental optical and electronic properties with decreasing size is observed in any materials but, for a given temperature, this occurs at a very large size in semiconductors, as compared to metals, insulators and van der Walls or molecular crystals [1]. For example, the band gap of CdS, a II-VI semiconductor, can be made to vary more or less continuously between the bulk value of 2.4 eV to 4.0 eV for a 15Å nanocrystal by merely tuning the size of the CdS nanocrystals [2]. Thus the quantum mechanical behaviour can be easily observed in a low dimensional semiconductor structure and therefore while discussing low dimensional structures we have confined our attention to semiconductor nanostructures only.

1.1 Types of nanostructured materials:

In semiconductor, the principle of reducing dimensions is based on confinement of charge carriers in one, two or all of the three dimensions, unlike in the case of bulk structure, where they are free to move in all three dimensions. On reducing the size, the dimension of the structure which becomes comparable to the de-Broglie wavelength at Fermi energy, the motion of the charge carriers along that particular direction, will be confined. These

reduced structures having size in nanometer regime are known as nanostructures.

Depending on how many dimensions are comparable to the de-Broglie wavelength there may be three types of nanostructures (1) quantum well (2) quantum wire and (3) quantum dot as shown in fig 1.1.

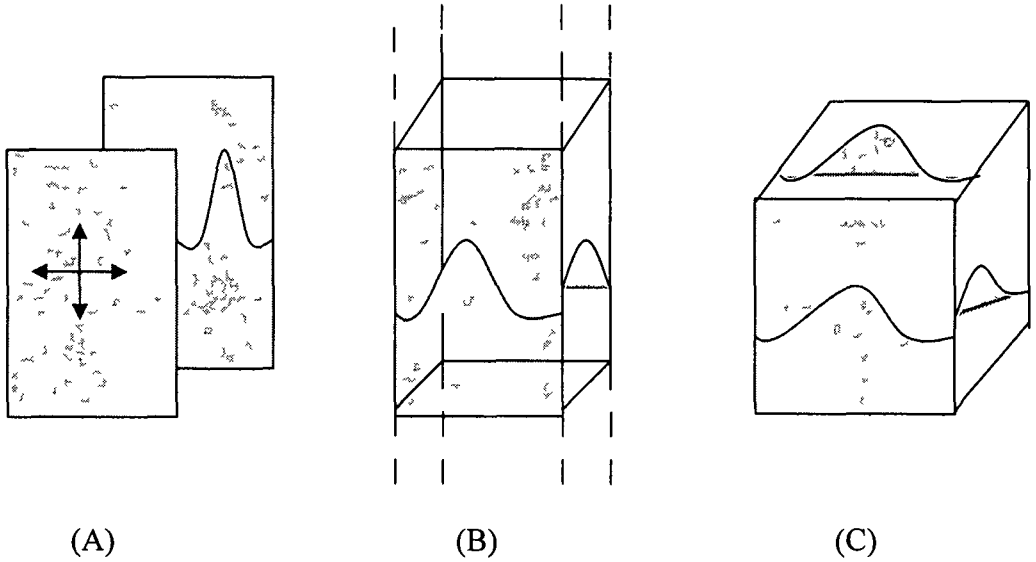

Figure 1 1: Carrier confinement in low dimensional systems (A) quantum well (B) quantum wire and (C) quantum dot

In quantum well, electron motion is restricted only along one dimension (say, thickness). These quasi two dimensional systems show pronounced optical nonlinearities even at room temperature. The research on electronic structure of quantum well begins in 1970 and GaAs is used most commonly for fabricating quantum wells.

In quantum wires, two dimensions, e.g. thickness and width, are made comparable to de-Broglie wavelength, thus confining the electron motion in these two dimensions. At the beginning of 1980s quantum wires are fabricated in the form of miniature strips, etched in sample containing a quantum well.

Quantum dots are three dimensionally confined systems where motion of the charge carriers is restricted in all three dimensions. Thus in quantum dots, all the three dimensions (i.e. thickness, width and length), are made comparable to de-Broglie wavelength. For semiconductor, such confinement is

possible when the radius of the semiconductor crystallite approaches the Bohr radius of the exciton. Practically semiconductor crystallites having size 1-100 nm are termed as quantum dots.

In a semiconductor, when an electron is excited from the valance to conduction band, leaving a hole in the valance band, the electron and the hole can form a loosely bound state, the Mott-Wannier exciton. A quantum dot is formed when the radius of the semiconductor crystallite approaches the exciton Bohr radius (the distance between the electron and the hole).

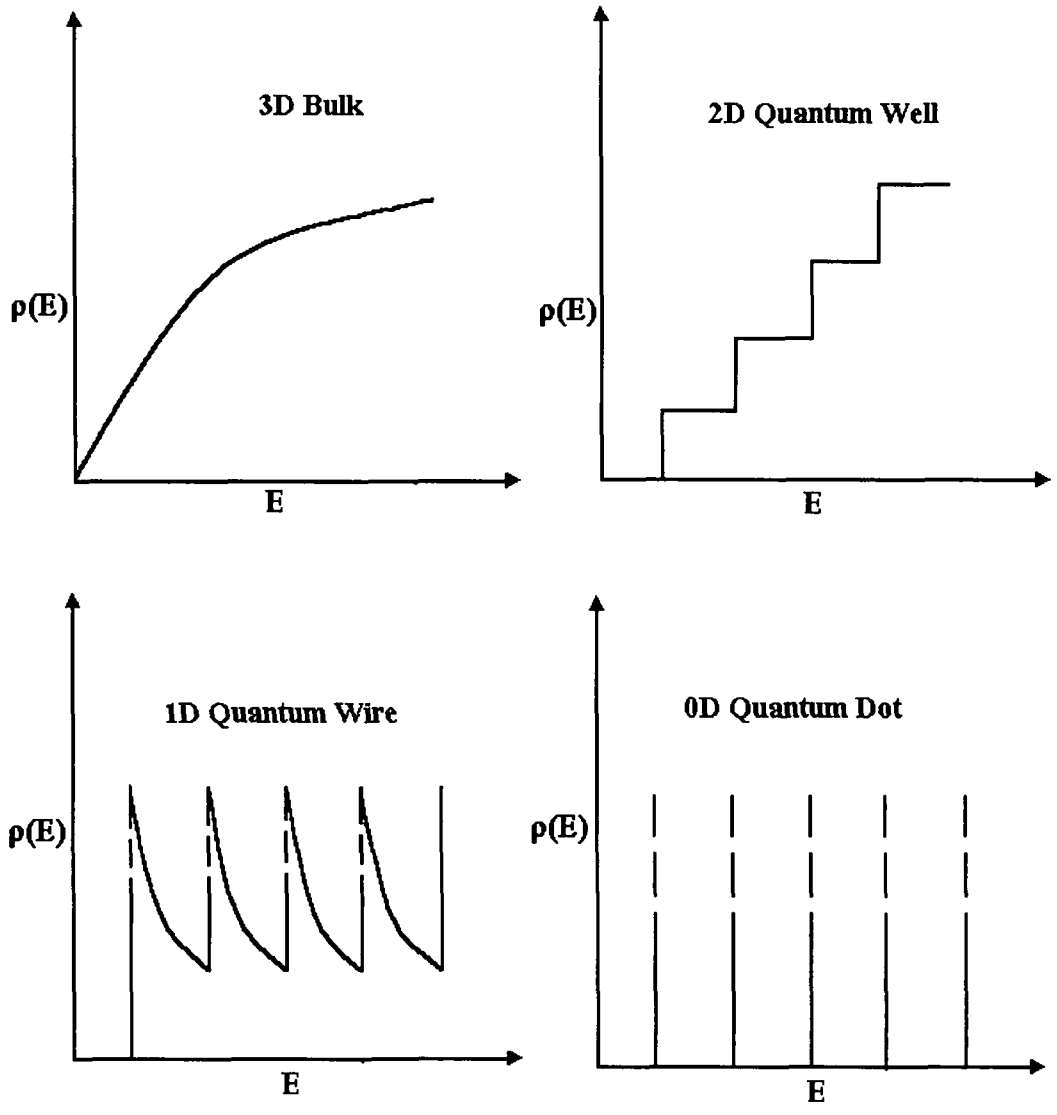

Figure 1.2: Density of states of 3D-bulk and reduced dimensional systems

An important aspect of semiconductor quantum dots is the modification of energy level and density of states (DOS) owing to the confinement of the charge carriers.

The density of states for a bulk semiconductor has the form

$$\frac{dN}{dE} \propto \frac{dE^{\frac{3}{2}}}{dE} = E^{\frac{1}{2}} \qquad (1.1)$$

for a two- dimensional system (quantum well) is a step function,

$$\frac{dN}{dE} \propto \frac{d}{dE} \sum_{\varepsilon_i<E} (E-\varepsilon_i) = \sum_{\varepsilon_i<E} 1 \qquad (1.2)$$

for a one- dimensional system (quantum wire has a peculiarity),

$$\frac{dN}{dE} \propto \frac{d}{dE} \sum_{\varepsilon_i<E} (E-\varepsilon_i)^{1/2} = \sum_{\varepsilon_i<E} (E-\varepsilon_i)^{-1/2} \qquad (1.3)$$

And for a zero-dimensional system (quantum dot) has the shape of δ– peaks

$$\frac{dN}{dE} \propto \frac{d}{dE} \sum_{\varepsilon_i<E} \Theta(E-\varepsilon_i) = \sum_{\varepsilon_i} \delta(E-\varepsilon_i) \qquad (1.4)$$

Where ε_i are discrete energy levels, Θ is the Heaviside step function, and δ is the Dirac function [3]. The variation of density of states (from continuous to discrete) with reducing system dimensionality is shown in fig. 1.2.

The quantum dots systems are also termed as nanocrystal, nanoparticles, artificial atoms etc. They exhibit physical and chemical properties different from either the individual molecule or the extended solid, and their size, shape, and composition can all be tailored to create a variety of desired properties.

Such quasi zero dimensional system was first fabricated by scientists from Texas Instruments Incorporated. Reed *et al.* [4] reported the creation of Quantum Dot with a side length of 250 nm, etched by means of lithography. Soon after Quantum Dots with diameters 30-45 nm were fabricated in Bell Laboratories and Bell Communication Research Incorporated.

The synthesis of colloidal suspensions of nanocrystalline semiconductor particles in the 1980s initiated an enormous amount of research on quantum dots. Semiconductor nanocrystals with the same interior bonding geometry as bulk often exhibit strong variations in their optical and electronic properties with size [5, 6]. The change of the optical properties of semiconductor was reported as early as 1926. Jaeckel [7] related the red shift of the absorption onset observed for glasses containing CdS particle to the growth of the CdS particles. Later in 1967, Berry reported a blue shift of the absorption spectrum for small crystals of AgBr [8] and AgI [9] compared to macroscopic crystal. Interestingly, it was suggested that the blue shift should not be regarded as due to band gap widening. However some 15 years later it was established by the groups of Ekimov [10] and Rosseti [5, 6] that it was indeed the widening of the band gap that caused the observed blue shift in the absorption spectrum and was due to so called quantum size effect.

1.2 Distinguished physical properties of Quantum Dots:

Quantum dots have chemical and physical properties different from those of the bulk and isolated atoms or molecules with the same chemical composition. Here we discuss some of the important properties of these small crystallites:

1.2.1: Quantum Confinement Effect:

The quantum confinement concept is really the reason quantum dots are becoming so important. The exciton Bohr radius (a_B) is given by;

$$a_B = \frac{4\pi \epsilon_0 \epsilon_\alpha \hbar^2}{m_0 e^2}\left(\frac{1}{m_e^*}+\frac{1}{m_h^*}\right) = a_0\, \epsilon_\alpha \left(\frac{1}{m_e^*}+\frac{1}{m_h^*}\right) \qquad (1.5)$$

In equation (1.5) a_0 is the Bohr radius of hydrogen atom (0.529Å), ε_α is the high frequency relative dielectric constant of the medium, m^*_e and m_h^* are the effective masses of the electron and hole respectively both in units of m_0, the rest mass of electron. The resulting Bohr radius for exciton is much larger than

that of hydrogen atom, since the effective masses of the charge carriers are only a small fraction of the electron rest mass and ϵ_α is considerably larger than 1 in semiconductor. As the size of the semiconductor particle approaches Bohr radius of the exciton, the electron hole pair gets spatially confined and assumes a state of higher energy. In this regime of spatial confinement of the charge carriers, the kinetic energy becomes quantized and the energy bands will split into discrete levels. This phenomenon is known as quantum size effect or quantum confinement effect [11]. The increase in band gap is observed as a blue shift in optical absorption spectra. The particles with reduced dimensions exhibit size-dependent optical and electronic behaviour resulting from three-dimensional (3D) carrier confinement [12].

Quantum confinement effect can be qualitatively explained with the help of simple particle in a box model. The solution of the Schrödinger equation gives the eigenfunctions

$$\Psi_n(x) = \sqrt{\frac{1}{2L}}\, sin(kx); \quad k_n = \pi n/L \tag{1.6}$$

And the corresponding energy eigenvalues are given by

$$E_n = \frac{\hbar^2 k_n^2}{2m} = \frac{\hbar^2 \pi^2 n^2}{2mL^2} \tag{1.7}$$

Thus with the reduction of the size of the box, the energy level spacing increases since it is inversely proportional to L^2, the square of the length of the box.

Quantitatively, there are two approaches to explain and understand quantum size effect. The first approach uses the effective mass approximation [13-15] following which the band gap (E) of a semiconductor nanoparticle can be derived as [14]

$$E = E_g + \frac{\pi^2 \hbar^2}{2R^2}\left(\frac{1}{m_e^*} + \frac{1}{m_h^*}\right) - \frac{1.8e^2}{\epsilon R} + \text{smaller terms} \tag{1.8}$$

where R is the radius of the semiconductor nanoparticle, E_g is the band gap of the bulk semiconductor. The second term in equation (1.8) represents the quantum localization energy and has $1/R^2$ dependence. The third term represents the Coulomb energy with $1/R$ dependence. In the limit of large R the value of E, approaches that of E_g. Although the effective mass approximation is not valid for very small particles, equation (1.8) has often been used to describe quantum size effects in semiconductor nanocrystallites.

Equation (1.8) implies that when the radius of a semiconductor particle decreases its band gap increases. As a result of the spatial confinement of the charge carriers, the kinetic energy becomes quantized. The quantization of the kinetic energy manifests itself as a gradual transition of continuous energy bands to discrete energy levels.

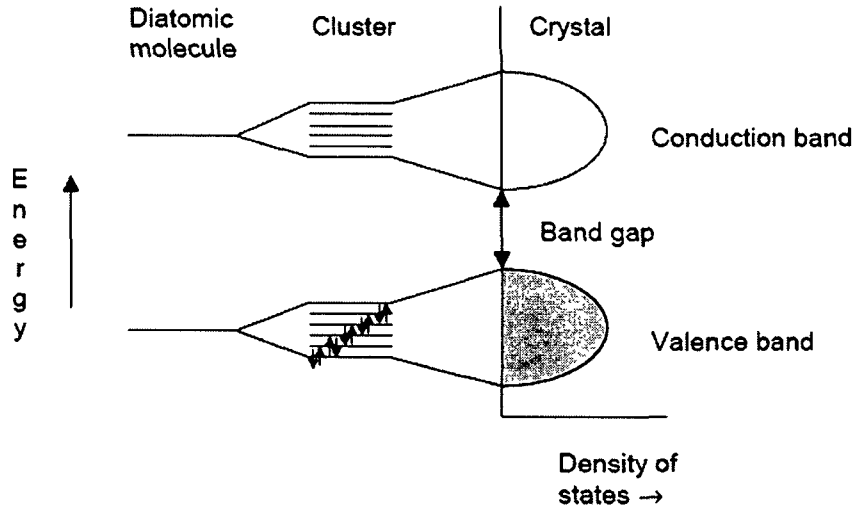

Figure 1.3: From diatomic molecules to crystals: evolution of molecular orbitals into bands

The second approach to explain and understand quantum size effects based on the linear combination of atomic orbital-molecular orbital (LCAO-MO) to calculate the energy levels in a small semiconductor particle. In this approach nanometer size semiconductor particles are described as very large molecules. Fig.1.3 illustrates these approaches qualitatively. In case of large crystals the large numbers of atomic orbitals as well as molecular orbitals form

energy bands. The highest occupied molecular orbital (HOMO) forms the valance band while the lowest unoccupied molecular orbital (LUMO) forms the bottom the conduction band. The energy difference between the HOMO and LUMO is the band gap of the material. As is clear from the fig. 1.3 the band gap increases and the bands split into discrete energy levels with a decreasing number of atoms or reduction in size. Contrary to the effective mass approximation the LCAO-MO theory provides a good way to calculate the energy structure of very small semiconductor clusters.

1.2.2: Large surface to volume ratio:

Besides quantum size effects, statistical effects influence the optical/electronic and optoelectronic properties of quantum dots as well. One of the statistical effects of reducing the size of semiconductor particle is the existence of large surface to volume ratio (S/V), for example, a 50 Å CdS cluster has ~ 15% of the atoms on the surface [11]. The large S/V ratio results in producing electronic states within the band gap of the semiconductor. These are called surface states. These surface states have a large influence on the physical and chemical properties of nanocrystalline semiconductors. For example, in case of photoluminescence, unlike in bulk specimen, in quantum dots excited electrons may be captured by these states, either before or after the direct radiative recombination which ultimately influences the luminescence property. Again, bulk CdS melts at about 1600 ^{0}C, whereas a 25 Å nanocrystal of the same material has a melting temperature of about 400 ^{0}C [16]. Such effects are observed because of the higher surface energy of the nanomaterial.

1.2.3: High oscillator strength:

The intensity of a UV-Visible absorption band is a function of the energy of the transition and to the square of the oscillator strength. In a bulk semiconductor, the electron and hole are bound together by the Coulomb attraction with binding energy of a few to tens of meV. This exciton is easily

ionized at thermal energies, which accounts for the absence of the 'strong exciton bands' in bulk semiconductors at room temperature. In case of quantum dots, due to reduction in size the overlapping of electron and hole wavefunction enhances significantly which results in high oscillator strength. This also explains the presence of excitonic features in absorption spectra of quantum dots.

The oscillator strength of the exciton is given as [10]

$$f = \frac{2m}{\hbar^2}\Delta E|\mu|^2|U(O)|^2 \qquad (6)$$

Where m is the electron mass, ΔE is the transition energy μ is the transition dipole moment and $|U(0)|^2$ represents the probability of finding the electron and hole at the same site (the overlap factor). For clusters with $R>>a_B$, $|U(0)|^2$ is independent of size and it is the macroscopic transition dipole moment that determines the oscillator strength. For cluster with size $R < a_B$, the overlap between electron and hole wavefunction increases and the oscillator strength of the cluster weakly depends on size. However, exciton absorption bands are difficult to observe practically due to inhomogeniety of the sample and also due to surface defects.

1.2.4: Fast transition speed:

In quantum dots the electronic transition between surface states and valance band and surface states and conduction band is faster due to the fast trapping and detrapping of the charge carriers by surface states. This property of quantum dots makes them very efficient for fast optic and photonic switch.

1.3 Coating the surface of Quantum dots:

Quantum dots are characterized by large surface to volume ratio. Thus the surface has a profound effect on the physical and chemical properties of the quantum dots. It is usual practice to modify the surface in someway in order to reduce or prevent the charge carriers interacting with the surface. Surface

passivation with various organic ligands or epitaxial overcoating with a wide band gap semiconductor is already reported [17-18]. Such surface coating enhances optical properties and stability of the nanostructured materials. For example, in colloidal CdS, surface defects have been passivated by $Cd(OH)_2$, with a significant increase in fluorescence [19]. Significant increase in nonlinear absorption coefficient has also been reported in case of 1-thioglycerol capped ZnS nanoparticle [20].Mulvaney *et al.* used silica coating for nanostructuring metal and semiconductor nanoparticles [21]. The unusual property of silica, especially in aqueous media, provides nanoparticles enhanced colloidal stability, so that they remain stable for considerable duration in solution condition. Apart from preventing coagulation during chemical or electronic process, the silica coating leads to a decrease in the polydispersity of the particles and reduces the van der Waals attraction, which enhances the colloid stability and the ability to form colloidal crystals, and such a shell is chemically inert and optically transparent [22].

1.4 Fabrication techniques:

Producing monocrystalline, monodisperse and uniformly distributed quantum particles involve many physical parameters and machine complexities all of which cannot be controlled ideally and simultaneously in a specific route. And so, each synthetic route has its own advantages and limitations.

The various physical and chemical synthetic processes for nanoparticle formation include: molecular beam epitaxy (MBE) [23-25], electrochemical deposition [26,27], RF sputtering [28, 29], dc magnetron sputtering [30, 31], sol-gel [32], photochemical [33, 34], low pressure chemical vapour deposition (LPCVD) [35-37], chemical precipitation in colloids [38], mechanical grinding/alloying [39], magnetron co-sputtering [40, 41], vapour deposition on cold substrates and on heated substrates [42, 43], Selective area metal organic chemical vapour deposition (SA-MOCVD) [44-47] etc.

Recently, ion beam has become an important itinerary for synthesis, modification and characterizations of nanoparticles. The synthetic procedures

include ion-implantation [48-54], ion beam mixing [55-57], ion beam assisted self organized nanostructure formation [58, 59] and template synthesis [60-62].

1.5 Overview of the recent work on quantum dot research:

For the last few years, a great deal of interest has been shown by many research workers to prepare semiconductor nanoparticles and to study their optoelectronic and optical properties. Passler *et al.* [63] prepared the films of ZnS, ZnSe, and ZnTe nanoparticles on GaAs substrate by MBE and studied their temperature dependent optical spectroscopy while Ganeev *et al.* [64] used laser ablation method for the preparation of CdS nanoparticle. Using sol-gel technique Boroditsky *et al.* [65] prepared Mn doped CdS quantum dots and exclusively carried out the photoluminescence studies on III-V semiconductor nanostructures to develop ultra small light emitting diodes. Bera *et al.* prepared Silicon nanocrystals with the help of dc magnetron sputtering technique [66]. Mahamuni *et al.* [67] reported the synthesis of ZnO nanostructure by chemical route and studied its photoluminescence behaviour that revealed its ultra fast switching phenomena. Zhang *et al.* [68] and others [69-71] studied the X-ray absorption of dendrimer stabilized CdS quantum dots. Chen *et al.* [72] has detected the surface states of ZnS nanoparticle by UV/VIS absorption spectroscopy and luminescence study. Also, they have reported the ultra fast trapping and detrapping of electrons by these surface states. Chen *et al.* also investigated different mechanisms of photoluminescence of Si nanocrystals formed by pulsed laser deposition in argon and oxygen gas [73]. Coe *et al.* [74] carried out electroluminescence study of CdSe nanoparticle to develop highly efficient quantum dot LED's. CdS, ZnS and Zn-CdS nanoparticles are synthesized by Kulkarni *et al.* [75] through wet chemical route. Tanaka [76] had studied photoluminescence properties of Mn doped ZnS and CdS nanocrystals dispersed in polyvinyl alcohol while strong photoluminescent emission was observed by Fernée *et al.* [77] in case of surface passivated PbS quantum dots. Desnica *et al.* [78] reported direct ion beam synthesis of II-VI nanocrystals.

1.6 Advantage of chemical route:

The primary advantage of chemical methods over other methods is good chemical homogeneity, as chemical synthesis offers mixing at the molecular level. It also provides basic understanding of the principles of crystal chemistry, thermodynamics, phase equilibrium and reaction kinetics. The prime motivation towards adopting chemical routes is:

* Simplicity of fabrication.
* Requirement of only inexpensive instruments.
* Relatively short synthesis time.
* Possibility of large scale productions.
* Possibility of surface passivation with less difficulty.
* Feasibility of synthesis of metals, alloys, insulators, semiconductors and even compound nanoparticles.
* Possibility of producing single crystalline (monocrystalline) nanoparticles.
* Possibility of doping of large number of materials (Mn, Ni, Fe, Cu etc.) even at room temperature.
* Possibility of coating, capping and coupling of synthesized nanoparticles as per desired stoichiometric proportions.
* Accurate synthesis of nanoparticles in the form of colloids, powders and thin films.

Semiconductor quantum dots have been grown in different host materials like micelles [79, 80], porous host lattice such as zeolites [81], polymers [82] and glasses [83].

1.7 Application of Quantum Dots:

The size-dependent optical and electronic properties of quantum dots make them interesting for potential applications in related areas. Next we highlight on some such promising application of quantum dots.

Quantum dots can be used to produce light emitters of various colors just by tuning the band gap rather than the current complex techniques of synthesizing compound semiconductors [84]. In semiconductors, the direct recombination of photogenerated charge carriers produces a narrow emission band at energy close to the absorption onset. For semiconductor quantum dots this means that the luminescence is size tunable. Thus LEDs with a whole range of output colors can be fabricated using quantum dots. Alivisatos [85] produced light-emitting diodes (LED) with high conversion efficiencies by using quantum dots embedded in polymer matrices. Recently Hwang *et al.* [86] investigated the use of ZnS:Mn quantum dots for polymer light-emitting diodes.

Another potential application of quantum dots is the fabrication of optical memories. A 3-D array of quantum dots which are addressed optically can pack much larger amounts of information than conventional microelectronic memory devices. This can be done, for instance, by spectral hole burning in which those quantum dots in resonance with a specific laser wavelength will be excited and thus 'bleach'. This enables writing a '0' or a '1' memory 'state' with a resolution smaller than the size of the laser spot.

The need for faster switching times in microelectronics, demands reduction in the size of the electronic components. In the conventional technique, one switching cycle in a transistor gives rise to the movement of many thousands of electrons, requiring a considerable amount of switching energy and producing excessive heat which can hardly be dissipated in high-frequency applications. This calls for developing single-electron devices, in which the switching occurs with the motion of only a single electron. Such a device may be realized by a quantum dot in which the charge of an added electron effectively blocks the flow of other electrons by the so-called 'Coulomb blockade'. Both switching, which performs logic operations, and storage of information are possible with these devices.

Enhancement of the nonlinear optical properties of quantum dots by quantum size effects are also of great interest. Due to the nonlinear optical

behaviour quantum dots are suitable for fast optical switches and optical fibers based on the nonlinear optical behaviour. In nonlinear optical materials, the refractive index can be changed either by carrier injection or by applying electrical fields. This change in the refractive index allows electronic modulation of light, enabling, for instance, faster electro-optical switching as compared to electronic switching.

Quantum dots have also been used as gas sensors. The simplest nanomaterial based sensor concept involves measuring the changes in the electrical resistance of a nanocrystalline metal when exposed to hydrogen. Labeau *et al.* [87] investigated the sensitivity of a nanocrystalline SnO_2 gas sensor doped with Pt and Pd nanoparticle. Gautheron *et al.* [88] observed that the CO sensitivity was increased by a factor of 30 by adding Pd nanoparticles to the nanocrystalline SnO_2 gas sensor.

1.8 Motivation of the present work:

Fabrication of quantum dots with uniform size distribution has always been a prime objective in the concerned area of research. In the present work we tried to fabricate IV-VI (PbS) and II-VI (CdS and ZnS) semiconductor quantum dots through chemical route with narrow size distribution.

Due to the high surface to volume ratio of the nanocrystallite its surface is very much sensitive to the surrounding environment. An effective surface coating may enhance chemical stability as well as modify certain physical properties of the quantum dots. Investigation of the effect of coating on luminescence of quantum dots is interesting as it provides knowledge about the charge carriers and energy states involved in the transition.

Swift heavy ion (SHI) irradiation of quantum dot is a relatively new area and detail study about the physical and chemical changes occurring after SHI irradiation needs to be carried out.

In the quantum confined region, nanoparticle exhibit large optical nonlinearity. The four wave mixing experiments with quantum dots will be an

important application in this regard. The quantum dots have large potential for application in optoelectronic device and hence the study of quantum dots for such possible device application is a fruitful area of research. The study of frequency dependent electrical properties of quantum dots will reveal the scope of their use as electrical components.

1.9 Thesis Plan:

The thesis is divided into seven chapters, each of which again split into various sub-sections. Chapter I presents general introduction of different low dimensional systems, modification of energy level and density of states (DOS) owing to the confinement of the charge carriers, characteristic features of quantum dots and fabrication methods etc. along with a brief outlook on foregoing research work in this field. The method of synthesis of semiconductor quantum dots and different characterizing techniques used in this work along with the theoretical models are discussed in chapter II. In chapter III, the experimental results on various unirradiated quantum dots are presented and discussed in details. The experimental results and discussion of SHI irradiated quantum dots are presented in chapter IV. Chapter V presents theory and principle of degenerate four wave mixing (DFWM) along with the result of DFWM experiment to measure the third order nonlinear susceptibility of PbS quantum dots. The optoelectronic and electronic switching behaviour of quantum dots have also been discussed in this chapter. The electrical behaviour of PbS quantum dots in terms of capacitance-voltage and current -voltage responses is presented in chapter VI. The conclusions and future prospects are presented in chapter VII.

References:

1. Alivisatos A.P., *J. Phys. Chem.*, **100** (1996), 13226.
2. Nanda J., Kuruvilla B.A., Shafi K.V.P and Sarma D.D., *Physics of Semiconducting Nanostructures*, Ed. K.P. Jain, Narosa Publication, pp25 (1997).
3. Jacak L., Hawrylak P. and W´ojs A., *Quantum Dots* Springer, Berlin (1998).
4. Reed M.A., Bate R.T., Bradshaw K., Duncan W.M, Frensley W.M, Lee J.W. and Smith H.D., *J. Vacuum Sci. Technol. B*, **4** (1986) 358.
5. Rosseti R., Nakahara S, Brus L.E., *J.Chem. Phys.*, **79** (1983) 1086.
6. Rossetti R., Elision J.L., Gibson J.M. and Brus L.E., *J. Chem. Phys.*, **80** (1984) 4464.
7. Jaeckel G.Z., *Tech. Phys.*, **6** (1926) 301.
8. Berry C.R., *Phys. Rev.*, **153** (1967) 989.
9. Berry C.R., *Phys. Rev.*, **161** (1967) 848.
10. Ekimov A.I., Onushchenko A.A., *Semiconductors*, **16** (1982) 1215.
11. Wang Y. and Herron N., *J. Phys. Chem.*, **95** (1991) 525.
12. Klimov V., Haring Bolivar P. and Kurz H., *Phys Rev. B*, **53** (1996) 1463
13. Brus L.E., *J.Chem.Phys.*, **80** (1984) 4403.
14. Brus L.E., *J. Phys. Chem.*, **90** (1986) 2555.
15. Wang Y., Suna A., Maher W. and Kasowski R., *J. Chem. Phys.*, **87** (1987) 7315.
16. Goldstein A.N., Echer C.M. and Alivisatos A.P., *Science*, **256** (1992)1425.
17. Hines M. A. and Sionnest P.G., *J. Phys. Chem.*, **100** (1996) 468.
18. Patel A.A., Wu F., Zhang J.Z., Torres-Martinez C.L., Mehra R.K., Yang Y. and Risbud S.H., *J. Phys. Chem. B*, **104** (2000) 11598.
19. Malik M.A., O'Brien P. and Revaprasadu N., *Chem. Mater.*, **14** (2002) 2004.
20. Nikesh V.V., Dharmadhikari A., Ono H., Nozaki S., Kumar G.R. and Mahamuni S., *Appl. Phys. Lett.*, (2004) **84** 4602.
21. Arellano M. A., Ung T., Blanco A., Mulvaney P. and Liz-Marzan L. M., *Pure Appl. Chem.*, **72** (2000) 257.

22. Mu J., Gu D., and Xu Z., *Appl. Phys. A: Materials Science & Processing,* (2004). (Online issue).
23. Leobandung E., Guo L., Wang Y., and Chou S.Y., *Appl. Phys. Lett.,* **67** (1995) 938.
24. Muranaka T., Jiang C., Ito A. and Hasegawa H., *Thin Solid Films,* **380** (2000)189.
25. Matsumoto K., Ishii M., Segawa K., Oka Y., Vartanian B. J. and Harris J.S., *Appl. Phys. Lett.,* **68** (1996) 34.
26. Sahu S.N., Patel B., Behera S.N and Nanda K.K., *Indian J. Phys.,* **74 A(2)** (2000) 93.
27. Mahamuni S., Borgohain K., Bendre B.S, Leppert V.J. and Risbud S.H., *J. Appl. Phys.* **85** (1999) 2861.
28. Edelstein A.S., *Nanophase materials,* ed. by G.C. Hadjipanagis and R.W. Siegel, Kluwar Academic Publishers (1994) pp73-80.
29. Ramaswamy S., *Proc. of the Solid-state Phys. Sympo.,* **41** (1998) 30.
30. Mandal S.K, Chaudhury S. and Pal A. K, *Indian J. Phys.,* **74A** (2000) 143.
31. Pal A.K, *Bull. Mat. Sci.,* **22** (1999) 341.
32. Song T.K., Kim J. and Kwyn S.I., *Solid State Commun.,* **97** (1996) 143
33. Kim H.S, Ryu J.H, Jose B., Lee B.G, Ahn B.S and Kang Y.S, *Langmuir,* **17** (2001) 5817.
34. Pokhrel M.R., Janik K. and Bossmann S .H, *Macromolecules,* **33** (2000) 3577.
35. Yoon T. S., Kwon J.Y., lee D.H., Kim K.B., Min S .H., Chae D.H., Kim D.H., Lee J.D., Park B.G. and Lee H. L., *J. Appl. Phys.,* **87** (5) (2000) 2449.
36. Classen W.A.P. and Bloem J, *J. Electrochem. Soc.,* **127** (1980) 194.
37. Kato M., Sato T., Murota J. and Mikoshiba N., *J. Cryst. Growth,* **99** (1990) 240.
38. Herron N., Wang Y. and Eckett H., *J. Am. Chem. Soc.,* **112** (1990) 1322.
39. Mei G., *J. Phys: Condens. Matter,* 4 (1992) 7521.
40. Shi J., Zhu K., Zheng Q., Zhang L., Ye L., Wu J., and Zuo J., *Appl. Phys. Lett.,* **70** (1997) 2586.

41. Maeda Y., Tsumkamato M.A., Yazawa Y., Kanemitsu Y and Matsumoto Y, *Appl. Phys. Lett.*, **59** (1999) 3168

42. Umehera A., Nitta S., Furukawa H. and Nonomura S., *Appl. Surf. Sci.*, **119** (1997) 176.

43. Melendres C.A., Narayanasamy A., Maroni V.A. and Siegel R.W., *J. Mater. Res.*, **4** (1989) 1246.

44. Fukui T., Ando S., Tokura Y. and Toriyama T., *Appl. Phys. Lett.*, **58** (1991) 2018.

45. Kumakura K., Motohisa J. and Fukui T., *J. Cryst. Growth* ,**170** (1997) 700

46. Lebens A., Tsai C.S., Vahala K.J. and Kuech T.F., *Appl. Phys. Lett.*, **56** (1990) 2642.

47. Fukui T., Nakajima F., Kumakura K. and Motohisa J., *Bull. Mater. Sci.*, **22(3)** (1999) 531.

48. Arakawat Y., Nagamunez Y., Nishiokat M and Tsukamotot S., *Semicond. Sci. Technoi.* **8** (1993) 1082.

49. Matsuura D., Kanemitsu Y., Kushida T., White C.W., Budai J.D. and Meldrum A., *Appl Phys. Lett.*, **77** (2000) 2289.

50. Meldrum A., White C.W., Boatner L.A., Anderson L.M., Zuhr R.A., Sonder E., Budai J. D. and Henderson D.O., *Nucl. Instr. and Meth. B*, **148** (1999) 957.

51. Bonafos C., Garrido B., Lopez M., Rodriguez A.R., Varona O.G., Rodriguez A.P. and Morante J.R., *Appl. Phys. Lett.*, **72** (1998) 3488.

52. Meldrum A., Zuhr R.A., Sonder E., Budai J.D., white C.W., Boatner L.A., Ewin R.C. and Henderson D.O., *Appl. Phys. Lett.*, **74** (1999) 69.

53. Takeda Y., Gritsyna V.T., Umeda N., Lee C.G. and Kishimot N., *Nucl.Instr. and Meth. B*, **148** (1999) 1029.

54. Liu Z., Li H., Feng X., Ren S., Wang H., Liu Z. and Lu B., *J. Appl. Phys.*, **84** (1998) 1913.

55. Gangopadhyaya P., Kesavamoorthy R., Nair K.G.M. and Dhandapani R., *J. Appl. Phys.*, **88** (2000) 4975.

56. Bhattacharya R.S. and Rai A.K., *J. Mat. Res.*, **2** (1996) 211.

57. Milosavljevic M., Shao G., Bibic N., McKinty C.N., Jeynes C. and Homewood K. P., *Nucl. Instru. and Meth. B*, **188** (2002) 166.

58. Das A.K., Ghose S.K., Dev B.N., Kuri G. and Yang T.R., *Appl. Surf. Sci.*, **165** (2000) 260.

59. He G. and Atwater H.A., *Nucl. Instru. and Meth. B*, **106** (1995) 126.

60. Chakravarti S.K. and Vetter J., *Nucl. Instru. and Meth. B*, **62** (1991) 109.

61. Martin C.R., *Science*, **266** (1994) 1961.

62. Chakratter J., *J. Microchem. and Microengg.*, **3** (1993) 57.

63. Passler R., Griebl E., Riepl H., Lautner G., Bauer S., Preis H., Gebhardt W., Buda B., As D.J., Schikora D., Lischka K., Papagelis K., and Ves S., *J. Appl. Phys.*, **86** (1999) 4403.

64. Ganeev R.A., Ryasnyansky A.I., Tugushev R.I., Usmanov T., *J. Opt. A: Pure Appl. Opt.*, **5** (2003) 409.

65. Boroditsky M., Gontijo I., Jackson M., Vrijen R., Yablonovitch E., Krauss T., Cheng C.C., Scherer A., Bhat R., Krames M., *J. Appl. Phys.*, **87** (2001) 3497.

66. Bera S.K., Chaudhuri S., Bandyopadhyay A.K., Chakraborty B.R. and Pal A.K., *J. Phys. D: Appl. Phys.*, **34** (2001) 273

67. Mahamuni S., Bendre B.S., Leppert V.J., Smith C.A., Cooke D., Risbud S.H. and Lee H.W.H., *Nano. Struct. Mater.*, 7 (1996) 659.

68. Zhang P., Naftel J., Sham T. K., *J. Appl. Phys.*, **90** (2001) 2755.

69. Tanaka M., Masumoto Y., *Chem. Phys. Lett.*, **324** (2000) 249.

70. Bol A., Meijerink A., *Phys. Chem. Chem. Phys.*, **3** (2001) 2105.

71. Nanda J. and Sarma D.D., *J. Appl Phys.*, **90** (2001) 2504.

72. Chen W., Wang Z., Lin J. and Lin L., *J. Appl. Phys.*, **82** (1997) 3111.

73. Chen X .Y.,Lu Y.F., Wu Y.H., Cho B.J., Liu M.H., Dai D.Y. and Song W.D., *J. Appl. Phys.*, **93** (2003) 6311.

74. Coe S., Woe W.K., Bawendi M. and Bulovic V., *Lett. To Nature*, **420** (2002) 800.

75. Kulkarni S. K., Winkler U., Deshmukh N., Borse P.H., Fink R. and Umbach E., *Appl. Surf. Sci.*, **169-170** (2001) 438.

76. Tanaka M., *J. Luminescence*, **100** (2002) 163,

77. Fernée M.J., Watt A., Warner J., Cooper S., Heckenberg N. and Dunlop H.R., *Nanotechnology*, **14** (2003) 991

78. Desnica U.V., Buljan M., Desnica-Frankovic I.D., Dubcek P., Bernstorff S., Ivanda M. and Zorc H., *Nucl. Instru. and Meth. B*, **216** (2004) 407.

79. Steigerwald M.L. and Brus L.E., *Acc. Chem. Res.*, **23** (1990) 183.

80. Pileni M.P., Motte L. and Petit C., *Chem. Mater.*, **4** (1992) 338.

81. Heo N. H., Park J. S., Kim Y. J., Lim W. T., Jung S. W., and Seff K. *J. Phys. Chem., B* **107** (2003) 1120.

82. Spanhel L., Hasse H., Weller H. and Henglein A., *J. Am. Chem. Soc.*, **109** (1987) 5649.

83. Borrelli N.F., Hall D.W., Holland H.J., Smith D.W., *J. Appl. Phys.*, **61** (1987) 5399.

84. Service R.F., *Science*, **271** (1996) 920.

85. Alivisatos A.P., *Science*, **271** (1996) 933.

86. Hwang J., Oh M.O., Kim I., Lee J.K., Ha C.S., *Curr. Appl. Phys.*, **5** (2005) 31.

87. Labeau M., Gautheron B., Cellier F., Vallet-Regi M., Garcia E. and Gonzale Calbet J.M., *J. Sol. St. Chem.*, **102** (1993) 434.

88. Gautheron B., Labeau M., Delabouglise G. and Schmatz U., *Sensors and Actuators B*, **15-16** (1993) 357.

CHAPTER II

In this chapter the chemical synthesis of quantum dots and various experimental and measurement techniques used to characterize the fabricated quantum dot samples have been discussed. The prepared quantum dot samples were characterized by XRD (X-Ray diffraction), Ultraviolet-visible (UV-Vis) optical absorption, Transmission Electron Microscopy (TEM) and photoluminescence (PL) study.

2.1 Synthesis of quantum dots:

We have fabricated bare and coated quantum dots through chemical method using polyvinyl alcohol as the dielectric matrix for the encapsulation of the quantum particles. We have studied small (PbS) and wide band gap materials (CdS and ZnS) as both of these systems in reduced dimensionality are capable of showing excitonic absorption even at room temperature due to enhancement in excitonic binding energies. Synthesis of bare quantum dots is schematically shown in figure 2.1.

2.1.1 PbS quantum dots:

For preparation of PbS quantum dots in poly vinyl alcohol (PVA), first the matrix was prepared. For this, a 5 wt% PVA solution was prepared in double distilled water, by stirring in a magnetic stirrer with stirring rate at ~200 rpm at a constant temperature of 70 ^{0}C until a transparent solution is formed. To this solution 0.01 M $PbNO_3$ solution was added in the volume ratio 2:1 followed by stirring at the same rate. The temperature is maintained at ~55 ^{0}C. To this solution, 0.01M Na_2S was added drop wise, until the whole solution turns dark brown. The atomic structure of PbS is shown in fig. 2.2 a. After keeping this solution in a dark chamber for 12 hours for stabilization, it was

caste over glass substrate and dried. The film contains PbS quantum dots embedded in PVA matrix.

2.1.2 CdS quantum dots:

For preparation of CdS quantum dots, 5 gm of PVA is dissolved into 100 ml double distilled water and the mixer is stirred in a magnetic stirrer at a stirring rate of ~200 rpm in the constant temperature of 70 ^{0}C for 3 hours until a transparent solution is formed. To this solution 0.01 M $CdCl_2$ solutions is added in the volume ratio 2:1. The mixture i s stirred at the rate of 200 rpm at a constant temperature of 55 ^{0}C while 0.01M Na_2S solution is put into it by dropping funnel slowly unless the whole solution turns into yellow color. The solution is kept in dark chamber at room temperature for 12 hours for its stabilization followed by casting over glass substrate. This film contains CdS quantum dots embedded in PVA matrix. Fig. 2.2 b shows the atomic geometry of CdS.

2.1.3 ZnS quantum dots:

A PVA solution of 5wt% in double distilled water is prepared in the similar way as in case of PbS and CdS quantum dots. Next 0.01M aqueous solution of $ZnCl_2$ and 0.01M solution of Na_2S are prepared so that the molecular weight ratio of $ZnCl_2$ and Na_2S becomes 1:1. The solutions of PVA and $ZnCl_2$ are mixed in the ratio of 1:2 and then stirred at about 200 rpm at 55 ^{0}C while with dropping funnel, Na_2S solution is put into it, until the whole solution appears completely milky. The prepared solution is kept in dark chamber at room temperature for 12 hours for stabilization. Finally, the solution is cast over glass substrate and then dried. The film over substrate contains the quantum dots of ZnS embedded in PVA matrix. The atomic structure of ZnS is shown in fig. 2.2c.

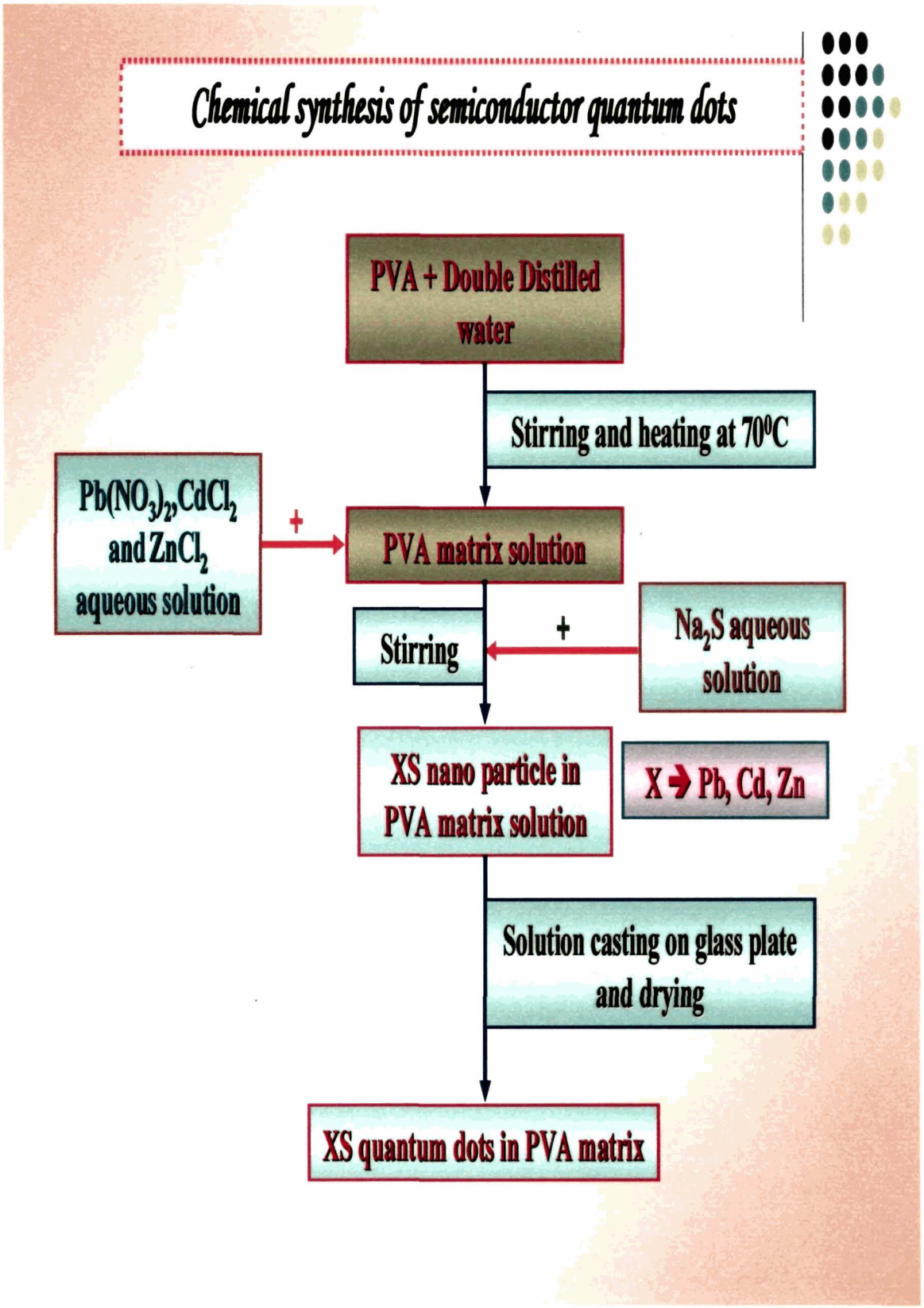

Figure 2.1: Schematic diagram for preparation of bare quantum dots

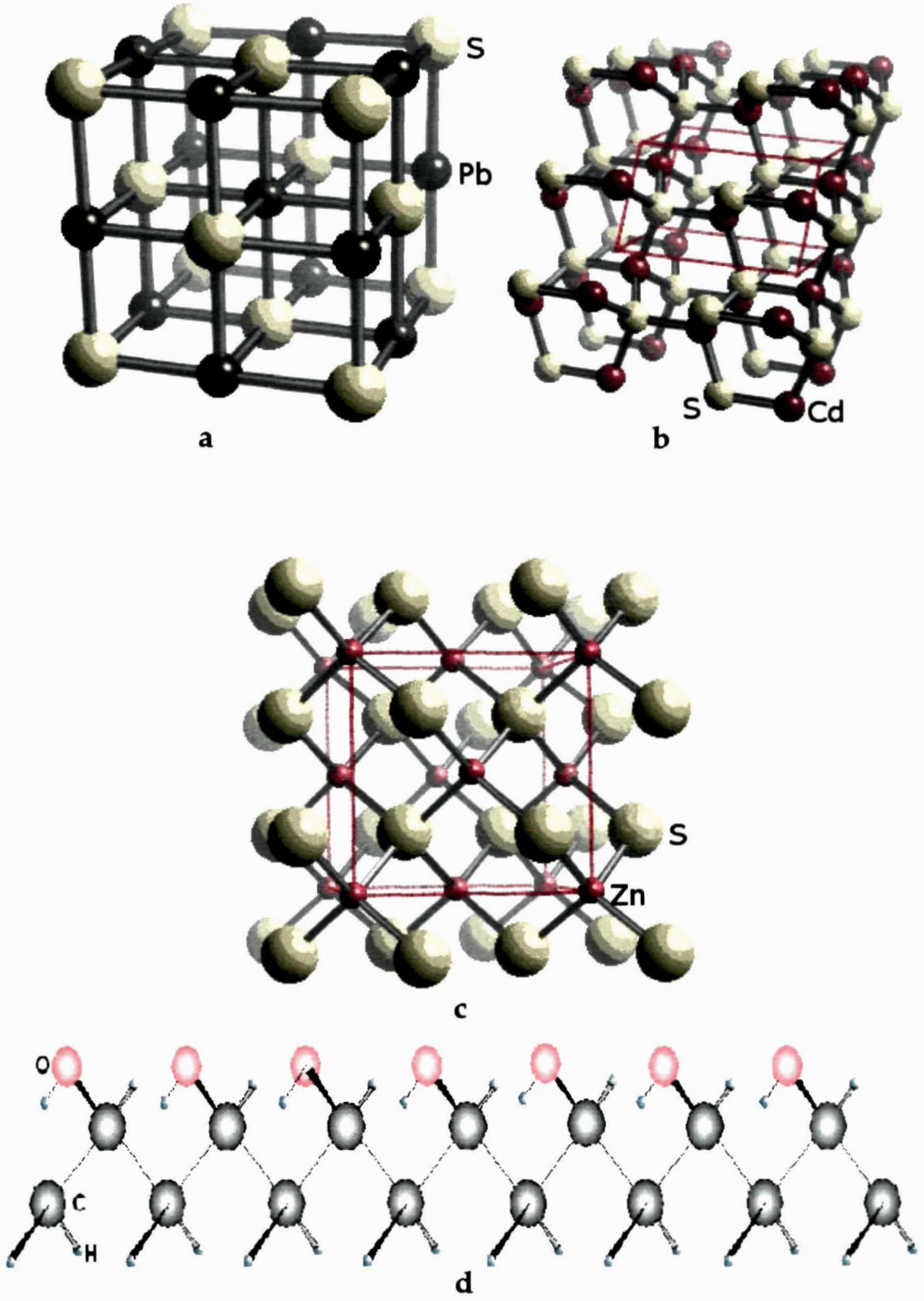

Figure 2.2: Atomic structure of (a) PbS, (b) CdS, (c) ZnS and (d) small part of polyvinyl alcohol (PVA) chain

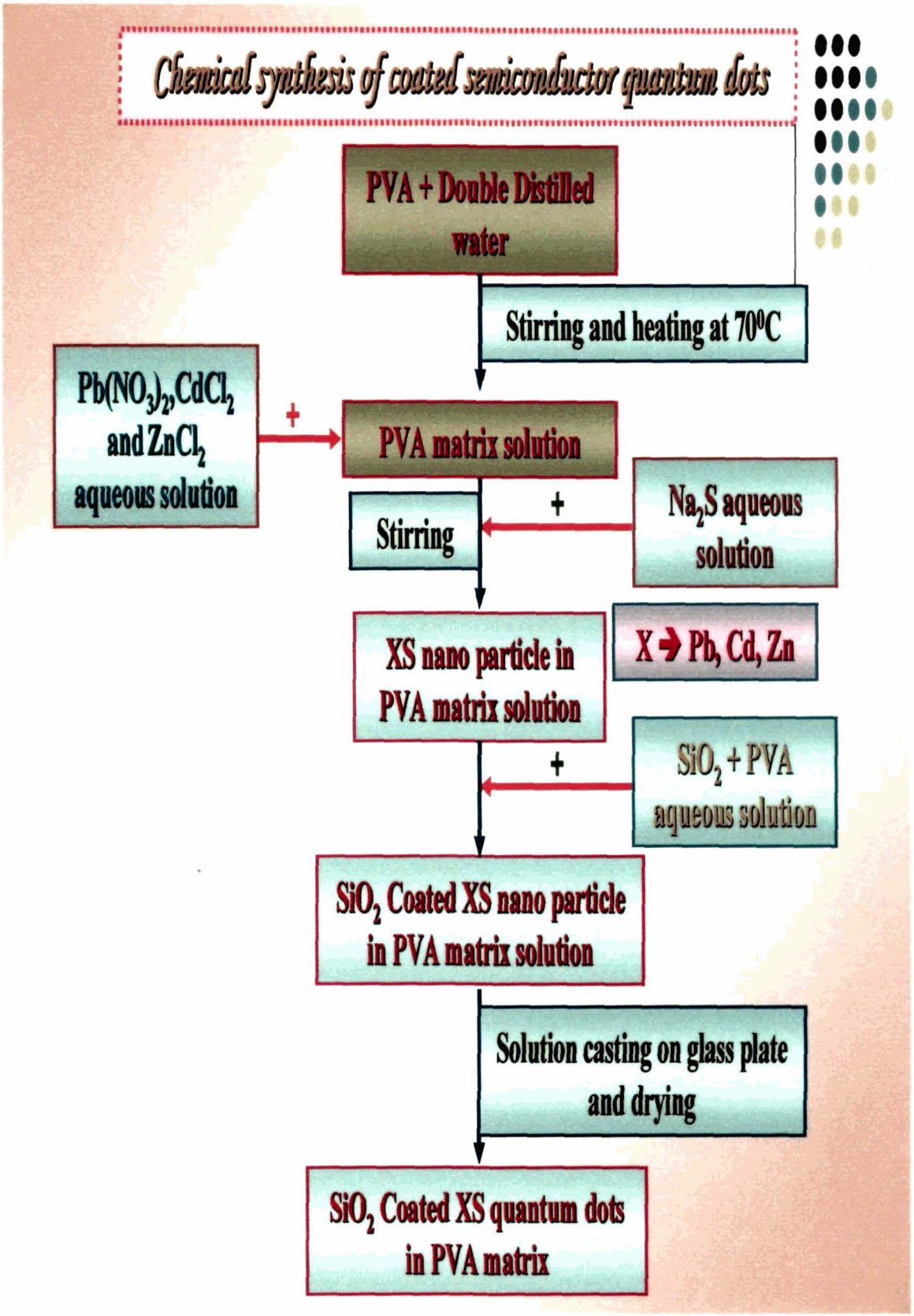

Figure 2.3: Schematic diagram for preparation of coated quantum dots

2.1.4 Synthesis of PVA/silica hybrid composite:

For the synthesis of PVA/silica hybrid composite [1] 6wt% sodium silicate solution was mixed with 8wt% PVA solution in the volume ratio1:5 with stirring to form a homogeneous mixture. Then the acid catalyst (0.5N HCl) was added slowly with stirring at a temperature of 60 ^{0}C. Stirring was continued for 30 minutes to carry out the in situ acid hydrolysis of sodium silicate within PVA.

2.1.5 Synthesis of Coated quantum dots:

To coat the PbS quantum dots with PVA/silica hybrid composite first the colloidal solution of PbS was prepared as described in section 2.1.To 10ml of this solution 2 ml of the PVA/silica solution was added with stirring at a constant temperature of 60 ^{0} C. The stirring was continued for ½ an hour. Then the mixture is kept undisturbed for 48 hrs.

Following the same procedure CdS and ZnS quantum dots are also coated with PVA/silica hybrid composite. The schematic diagram for synthesis of coated quantum dots is presented in figure 2.3.

2.2 Properties of polymer matrix (PVA):

Polyvinyl Alcohol (PVA) (Fig. 2.2 d) is water-soluble and is produced by the hydrolysis of polyvinylacetate which is made by the polymerization of vinyl acetate monomer. PVA as an environmentally sensitive water soluble polymer and is widely used for textile warp sizing, adhesive, paper sizing agent, ceramic binder and also used in cosmetics, emulsion stabilizer, civil engineering, pharmaceutical and electronic industries. Some of the physical parameters are enlisted in Table 2.1

Table2.1: Physical properties of PVA

Physical properties	
Glass transition temperature (^{0}K)	343
Melting temperature (^{0}K)	483
Refractive index	1.55
Specific gravity	1.55
Specific heat (J/gm K)	1.66
Thermal conductivity (W m^{-1} K^{-1})	2.0
Molar mass of single structure unit (g)	58.2
Dielectric constant	2.0

2.3 Theoretical model used for size estimation:

The description of the quantum confinement within the framework of the effective mass approximation (EMA) is a good approach. In case of solids, the band dispersion describes a complicated dependence of energy on momentum that usually cannot be described analytically. However, in the case of a semiconductor, the dispersion relations at the top of the valence band (TVB) and at the bottom of the conduction band (BCB) can often be described approximately as parabolic. Therefore, near the band edges, the delocalized electrons or holes follow a quadratic equation of the form

$$E(k) = \frac{\hbar^2 k^2}{2m^*} \qquad (2.1)$$

where, m* is the effective mass of the charge carrier (electron or hole). To use the effective mass approximation for describing the band gap variation with size for nanocrystals, one needs to solve the Schrödinger equation for the envelope function ψ

$$\left[-\frac{\hbar^2 \nabla_e^2}{2m_e} - \frac{\hbar^2 \nabla_h^2}{2m_h} - \frac{e^2}{4\pi \epsilon_0 \epsilon r_{eh}} + V_0 \right] \Psi(r_e, r_h) = E\Psi(r_e, r_h) \qquad (2.2)$$

where the subscripts e and h refer to the electron and the hole with m and r being the mass and position vector, respectively, and $r_{eh} = |r_e - r_h|$. ϵ_0 and ϵ_r are the permittivity in vacuum and the relative dielectric constant of the material. Using a trial wave function the above equation can be solved by approximate methods.

Brus and Kayanuma [2-4] proposed the following equation for the band gap, E_{gn}, of a quantum dot of radius R, considering an infinite potential outside the nanocrystals and zero potential inside,

$$E_{gn} = E_{gb} + \left(\frac{\hbar^2\pi^2}{2R^2}\right)\left[\frac{1}{m_e} + \frac{1}{m_h}\right] - 1.786\frac{e^2}{\varepsilon R} - 0.248E^*_{RY} \qquad (2.3)$$

where ε is the dielectric constant and m_e and m_h are the electron and hole effective mass, respectively. The first term on the right hand side of equation (2.3) is the band gap of the bulk semiconductor of the particular material, the second term represents the localization energy and has a $1/R^2$ dependence, the third term represents the Coulomb energy with $1/R$ dependence which is usually small for semiconductors with large dielectric constant and the last term is a result of spatial correlation. E^*_{Ry} is the effective Rydberg energy and is defined as [5]:

$$E^*_{Ry} = \frac{e^4}{2\varepsilon^2\hbar^2}\left(\frac{1}{m_e} + \frac{1}{m_h}\right) \qquad (2.4)$$

The energy of the nanocrystallite (E_{gn}) can be calculated from the UV-Vis absorption spectra using the relation hc/λ, λ being the corresponding absorption edge.

Kayanuma [3] defined confinement regimes, depending on the ratio of the radius of the quantum dot to the Bohr exciton radius, a_B of the bulk solid. For strong confinement regime $R/a_B >> 1$, while for weak confinement $R/a_B << 1$. However, he found that strong confinement effect were observable upto $R \sim 2a_B$ [6].This is the regime where the effective mass approximation is relatively more valid.

2.4 Characterization Techniques:

2.4.1 X-Ray diffraction (XRD) study:

X-ray diffraction is a versatile, non-destructive technique used for identifying the crystalline phases present in solid materials and powders and for analyzing structural properties (such as stress, grain size, phase composition, crystal orientation, and defects) of the phases. It probes a large number of crystallites that are statistically oriented. The method uses a beam of X-rays to bombard a specimen from various angles. The X-rays are diffracted (according to Bragg's law) as they are reflected from successive planes formed by the crystal lattice of the material. By varying the angle of incidence, a diffraction pattern emerges which is characteristic of the sample. The pattern is identified by comparing it with an internationally recognized data base containing tens of thousands of reference patterns.

In the field of quantum dot research, XRD is commonly used for identification of the sample and also for estimating the particle size. For sample identification, the diffraction angles obtained from the diffractogram is compared with the standard values of diffraction angles. A match between these two values helps to identify the particular element.

The lines observed at subsequent peaks in the XRD of bulk material for a particular structure, (normally, assessed from hkl parameters) are found to be broaden with reduction of particle size. Figure 2.4 shows the XRD pattern of CdSe nanocrystallites of different sizes (a-g) and of bulk (h). The reference is taken from the contribution of Murray et al [7]. The line broadening can be clearly understood from the figure.

The size of the nanocrystallites can be estimated by using Scherrer formula [8]:

$$d=0.9\lambda/w\cos\theta$$

where d is the diameter of the particle, λ is the wavelength of the X-ray used , w is the full width at half maximum (FWHM) of the diffraction peak and θ is the Bragg's angle.

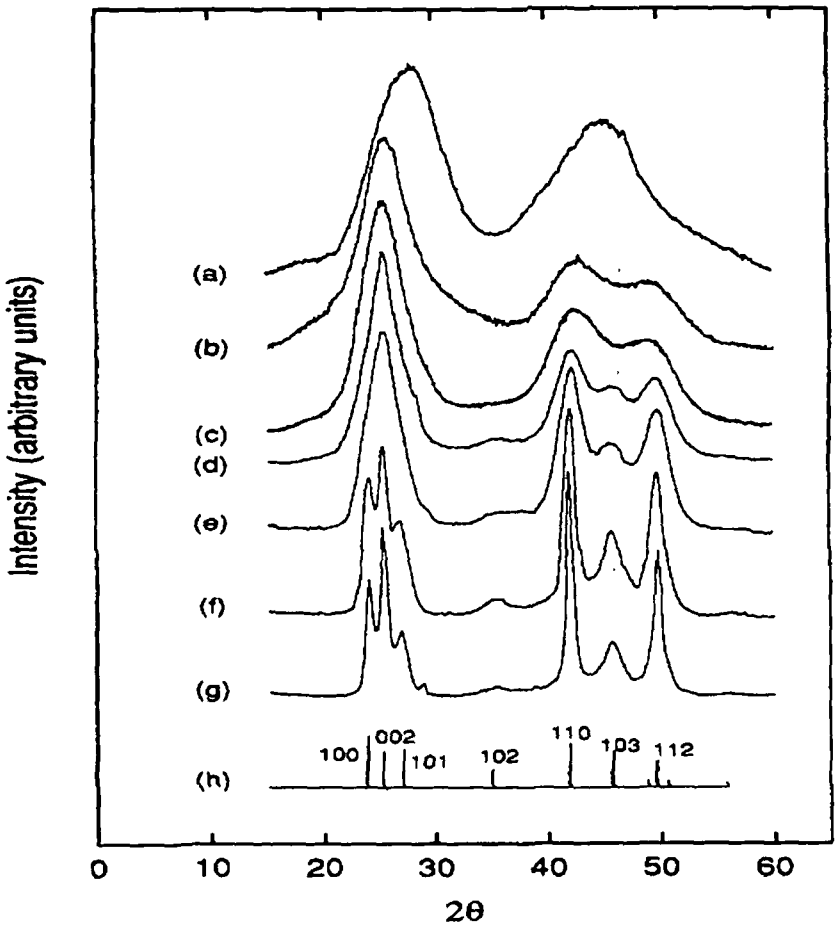

Figure 2.4: XRD pattern of (a) 12, (b) 18, (c) 20,(d) 37, (e) 42, (f) 83, and (g) 115 Å diameter CdSe nanocrystallites compared with the bulk wurtzite peak positions (h).

2.4.2 Ultraviolet-visible (UV-Vis) spectroscopy:

UV-Vis absorption spectroscopy is the easiest tool available to characterize semiconducting nanocrystals. Quantum dots generally exhibit threshold energy in the optical absorption measurements, due to the size specific band structure [9], which is observed by the blue shifting of the absorption edge, with decreasing particle size. Thus the blue-shift in the band gap reveals the formation of nanocrystals. In conjunction with more accurate approaches to calculate the band gap as a function of the size available these

days, it is possible to obtain reliable estimates of the size from the measure of the band gap shift.

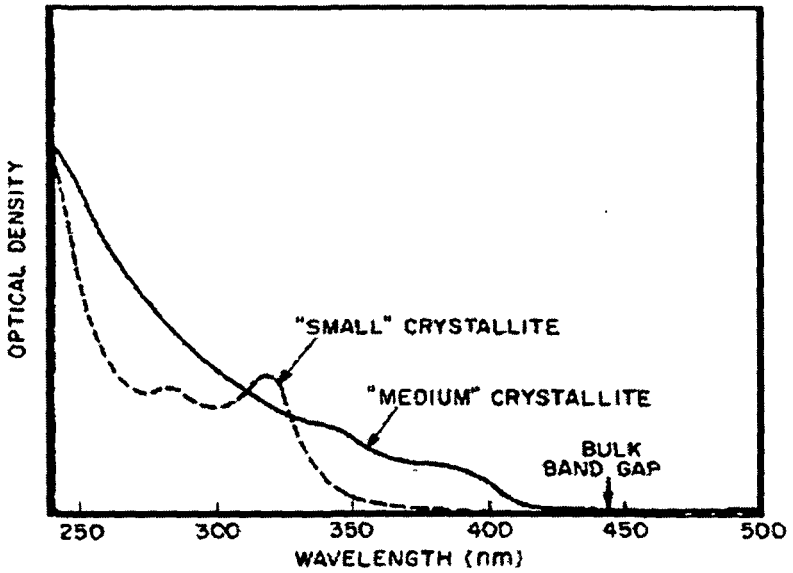

Figure 2.5: Size dependent optical absorption spectra for colloidal ZnSe nanocrystallite

Also, one can get an estimate of the size distribution from the sharpness of the absorption peak. Figure 2.5 shows the size dependent optical absorption spectra for colloidal ZnSe nanocrystallite [10]. The sharp excitonic peaks in the spectra indicate narrow size distribution in the prepared samples while featureless absorption spectra are indicative of broad size distribution and large particle size. This is because, if there exists broad size distribution in the sample, there would be a number of exciton peaks appearing at different energies corresponding to different sized nanocrystals and they overlap with each other yielding broad and featureless absorption spectra.

2.4.3 Transmission Electron Microscopy (TEM) study:

Transmission electron microscopy is one of the most vital non-destructive testing methods in nanoparticle research which can probe the particles down to < 1 nm. The size and shape of the particles can be directly estimated from the TEM study. Additionally, when a reaction behaves in an

odd fashion or produces precursors that emit broadly in the visible spectrum, TEM provides a method for discerning whether or not quantum dot material was actually produced. One can "see" and photograph the material, or rather its shadow. In TEM, an electron beam is focused on a monolayer of dried out quantum dots on a 200 mesh copper grid coated in carbon (i.e. the quantum dots are no longer a colloidal suspension). Electrons pass through these quantum dots at a slower rate than through the plain carbon grid, and hence, a shadow is detected by the film when it is exposed for the purpose of taking a photograph.

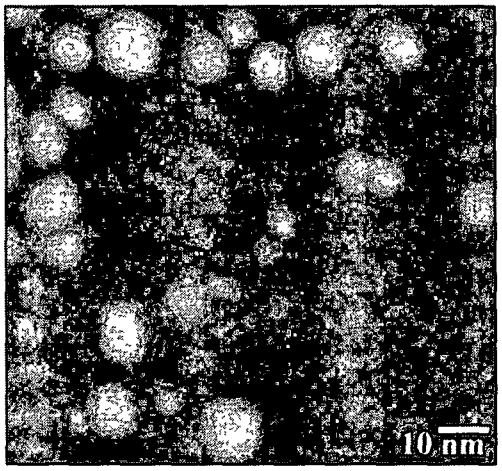

Figure 2.6: TEM image of spherical CdS quantum dots

Unfortunately, at the high magnifications necessary for observation of very small quantum dots, the resolution is often not very good, but does at least indicate that a certain kind of material was produced, such as dots, rods, or other shapes. Additionally, the pictures taken through TEM provide a good means of ascertaining aspect ratios and comparing samples. Figure 2.6 shows a TEM image of spherical CdS quantum dot with an average size of 5.3 nm.

2.4.4 Photoluminescence (PL) spectroscopy:

Photoluminescence spectroscopy is another important method for characterization of quantum dots. The emission characteristic of most of the

quantum dots consists of a single-broad emission band, which is symmetric and comes from states that fall in the quantum dot's band gap. These states are not detectable in absorption spectra. The luminescence characteristics depend upon the nature of the semiconductors, the physical dimension as well as the chemical environment and the luminescence property can be manipulated in useful ways [11].

Luminescence is the general term used to describe the emission of radiation from a solid when it is excited with some form of energy. When excitation arises from the absorption of photons, the phenomenon is known as photoluminescence. Whatever be the form of energy input, the final stage in the process is an electronic transition between two energy states E_1 and E_2 ($E_2 > E_1$), with the emission of radiation of wavelength λ where,

$$hc/\lambda = E_2 - E_1$$

h and c being the Planck's constant and velocity of light respectively.

According to Stoke's law, the first law in the history of luminescence, the wavelength of emitted light is generally equal to or longer than that of the exciting light (i.e., of equal or less energy). This difference in wavelength is caused by a transformation of the exciting light, to a greater or lesser extent, to non-radiating vibration energy of atoms or ions. In rare instances e.g. when intense irradiation of laser beam is used or when sufficient thermal energy contributes to the electron excitation process—the emitted light can be of shorter wavelength than the exciting light (anti-Stokes radiation).

Depending on the duration of the emission, one can distinguish between two general classes of luminescence--fluorescence and phosphorescence. The fluorescence is an instantaneous process whereas in phosphorescence, the presence of vacant lattice sites or other impurities, lattice defects, and/or irregularities in the host lattice, provide unoccupied states (traps) and delay the luminescence by detaining (trapping) the charge carriers (electrons/holes) before their radiative recombination with the luminescent centers.

In photoluminescence spectroscopy, photons with energy greater than the band gap of the semiconductor material studied are directed onto the surface of the material. The incident monochromatic photon beam is partially reflected, absorbed, and transmitted by the material being probed. The absorbed photons create electron-hole pairs in the semiconductor. The electrons are excited to the conduction band, or to the energy states within the gap. In

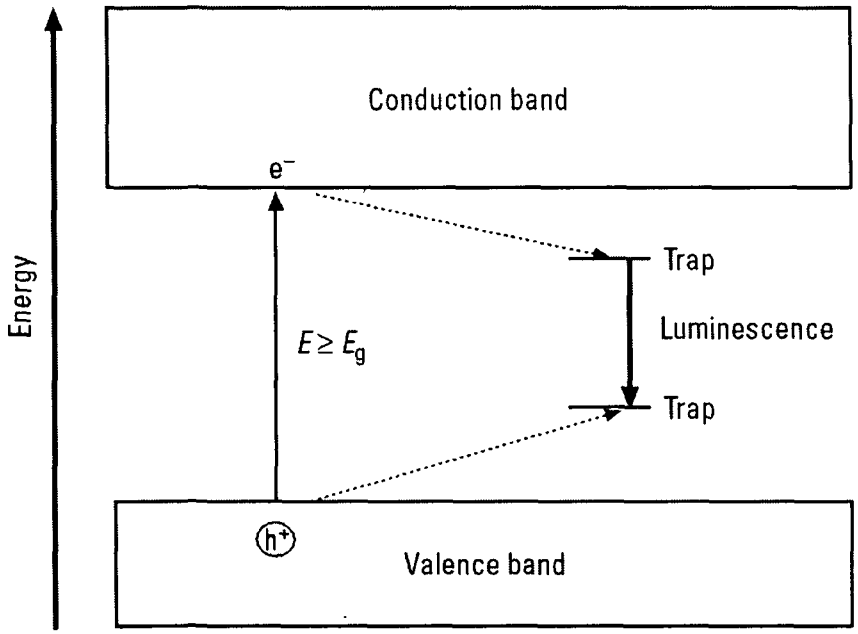

Figure 2.7: PL mechanism in quantum dots

addition, electrons can lose part of their energy and transfer from the conduction band to energy levels within the gap. Photons produced as a result of the various recombinations of electrons and holes are emitted from the sample surface and it is the resulting photon emission spectrum that is studied in photoluminescence (PL). The photon energies reflect the variety of energy states that are present in the semiconductor. A direct conduction band-to-valence band recombination is rarely observed in PL spectra. Even if direct band-to-band recombinations occur, the crystal will strongly reabsorb the photons emitted. Therefore, in PL spectra, recombination processes are observed with emission energies less than E_g. These processes include excitonic

recombinations and indirect transitions, which involve the trapping of electrons (or holes) by impurities.

The nature of the quantum dot surface is critical for photoluminescence experiments. The influence of the surface on photoluminescence can be understood in terms of the trap states described in figure 2.7 [12]. The created electron-hole pair may recombine immediately to produce light (radiative recombination).

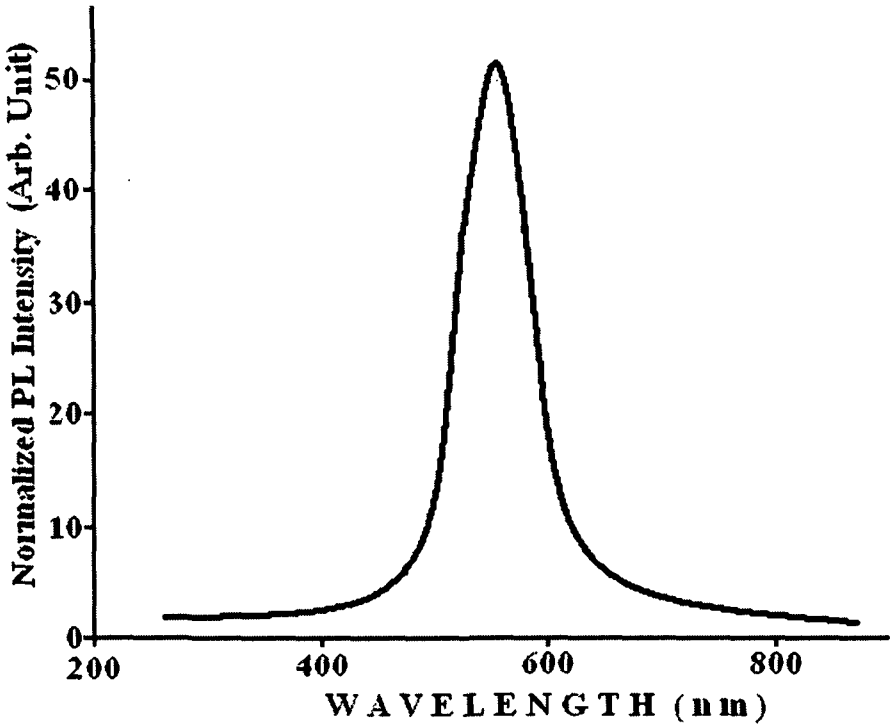

Figure 2.8: PL spectra of CdS quantum dots

These trap states are caused by defects, such as vacancies, local lattice mismatches, dangling bonds, or adsorbents at the surface. The excited electron or hole can be trapped by these local energy minima states and become less available for the radiative recombination of luminescence. Radiative recombination of the trapped charge carriers then produces luminescence that is substantially redshifted from the absorbed light. Surface passivation is a well-known phenomenon that decreases the possibility of charge carriers residing in traps.

Figure 2.8 shows the PL spectra of CdS quantum dots with FWHM of ~ 80 nm. The excitation wavelength is 325 nm (3.8 eV). The PL spectra exhibit a red shifted emission peak around 591 nm.

In this chapter the method of fabricating PbS, CdS, and ZnS quantum dots (both bare and silica coated) have been discussed. For fabricating the samples a series of experiments were carried out with different experimental parameters like concentration of the chemicals, stirring rate and temperature and then the best composition was followed. In that sense this work is original and the use of PVA and silica composite for coating the nanoparticle surface is a novel work.

References:

1. Kataky T .and Dolui S. K., *J. Sol-Gel Sci. and Tech.*, **29** (2004)107.
2. Brus L.E., *J.Chem.Phys.*, **80** (1984) 4403.
3. Kayanuma Y., *Phys. Rev. B*, **38** (1988) 9797.
4. Wang Y., Suna A., Maher W., and Kasowski R., *J. Chem. Phys.*, **87** (1987) 7315.
5. Wang Y. and Herron N., *J. Phys. Chem.*, **95** (1991) 525.
6. *The Chemistry of Nanomaterials* Published Online: 05 Jan 2005 Editor(s): Rao C.N.R., Müller h.c. A. and Cheetham A. K., Print ISBN: 3527306862 Online ISBN: 352760247X Copyright © 2004 Wiley-VCH Verlag GmbH & Co. KGaA.
7. Murray C.B., Norris D.J. and Bawendi M.G., *J. Am. Chem. Soc.*, **115** (1993) 8706.
8. Dijken A .V., Janssen A.H., Smitsmans M.H.P., Vanmaekelbergh D. and Meijerink A., *Chem. Mater.*, **10** (1998) 3513.
9. Chen S., Truax L.A. and Sommers J. M., *Chem.Mater.*, **12** (2000) 3864.
10. Brus L., *J. Phys. Chem.*, **90** (1986) 2555.
11. Alivisatos A.P., *J. Phys. Chem.*, **100** (1996) 13226.
12. Murphy C.J., *Anal. Chem. A*, **74** (2002) 520.

CHAPTER III

In this chapter the results of various characterizations viz XRD, UV-Vis absorption, TEM and Photoluminescence (PL) on quantum dots are presented and discussed in detail. Also the ageing effect on PL behavior of both bare and coated quantum dots have been discussed. The X-ray diffractogram are recorded using Rigaku (D-Max series) diffractometer mounted on a Rigaku x-ray generator. UV-Vis absorption spectra of the samples were taken with a double beam spectrophotometer (Hitachi U 2001) while PL study were recorded with Mechelle 900 spectrometer for recording PL with IK series KIMMON He-Cd laser. The 325nm line from He-Cd laser was used for the PL measurements.

3.1 Lead Sulphide (PbS) quantum dots:

Among semiconductor quantum dots, PbS is important due to their unique optical and electrical properties. PbS is a narrow gap IV-VI semiconductor with a band gap of 0.41 eV (3027nm) at room temperature. By varying the size and shape from bulk material to nanoparticle, it is possible to enhance the band gap as large as 2.8 or 5.2 eV [1].

The nanoparticles of PbS and other lead salts like PbTe and PbSe are better suited for strong confinement limit compared with other well-known II-VI semiconductor nanoparticles like CdS. The electron radius ($a_e = \varepsilon \hbar / m_e e^2$) and hole radius ($a_h = \varepsilon \hbar / m_h e^2$) of PbS are both ~10 nm which are much larger than a_e~3nm and a_h~1nm of CdSe [2, 3].The Bohr excitonic radius is~ 20 nm for PbS. Thus strong confinement effect of the carriers can be precisely achieved in these materials [4]. As the nonlinear optical properties of semiconductor quantum dots are expected to be greatly enhanced in the strong confinement regime, PbS would be a better candidate for exploiting non linear properties.

Earlier investigations into the fundamental limits of the performance of PbS nanoparticle based devices confirm their ability to become a versatile technological platform for the creation of better optoelectronic devices [5].

3.2 Cadmium sulphide (CdS) quantum dots:

CdS is an important II-VI semiconducting material that has attracted much interest owing to their unique electronic and optical properties, and their potential applications in solar energy conversion, photoconducting cells, nonlinear optics and heterogeneous photocatalysis [6]. CdS has a band gap of 2.42 eV (517nm) at room temperature and the Bohr excitonic radius of CdS is approximately 2.5 nm.

3.3 Zinc sulphide (ZnS) quantum dots:

ZnS is also an important II-VI semiconductor with a large band gap 3.68 eV (337 nm). ZnS, which in the bulk form absorbs in the UV region, is technologically important for electroluminescent displays. It can be also used as a host matrix for doping various ions. Tuning the band gap of ZnS in the nanometer regime allows us to achieve large quantum efficiencies of emission. Also, it can be used as a higher band gap material for passivating other semiconductor quantum dots, thereby increasing their quantum yields [7].

3.4 XRD study of quantum dots:

3.4.1 PbS quantum dots:

The XRD pattern of uncoated PbS quantum dots is shown in figure 3.1. The XRD of PVA is shown in the inset. For PbS, the XRD peaks at $2\theta = 25.9^0$, 30.1^0 and 43^0 corresponding to (111), (200) and (220) plans, suggest formation of fcc crystal. The diffraction peaks are indexed according to earlier published work [8, 9]. The peak around 20^0 corresponds to PVA crystalline phase [10]. The average size of the prepared PbS quantum dot samples calculated from XRD

pattern using Scherrer formula [chapter II, section 2.4.1] was ~12 nm corresponding to the FWHM of the most significant peak~0.116 radian.

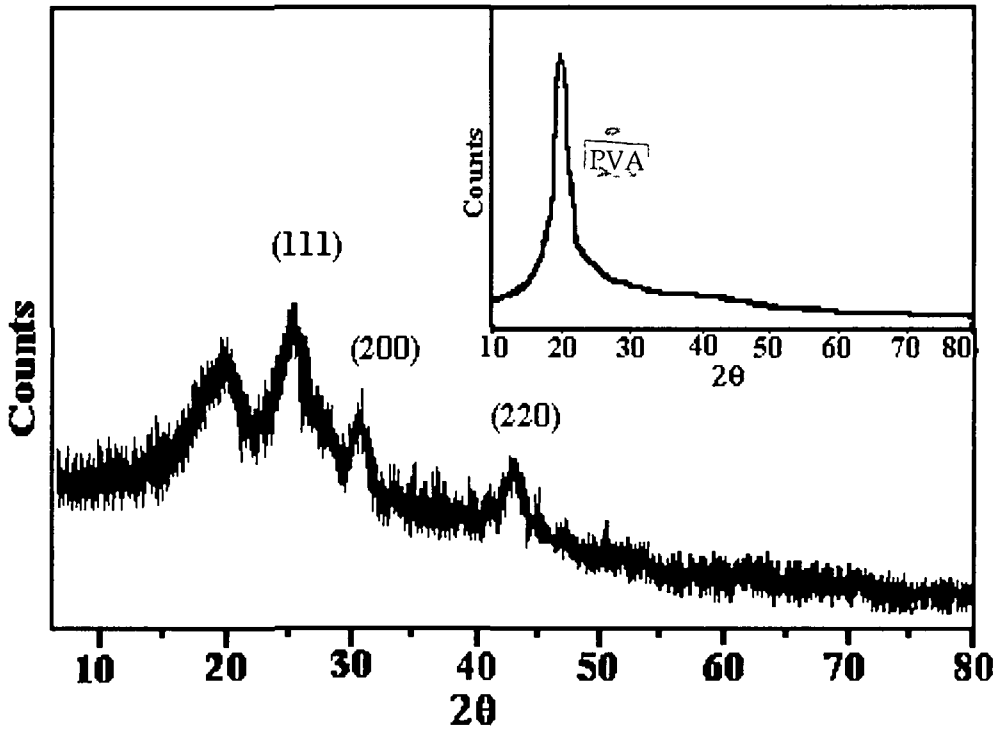

Figure 3.1: XRD pattern of bare PbS quantum dots

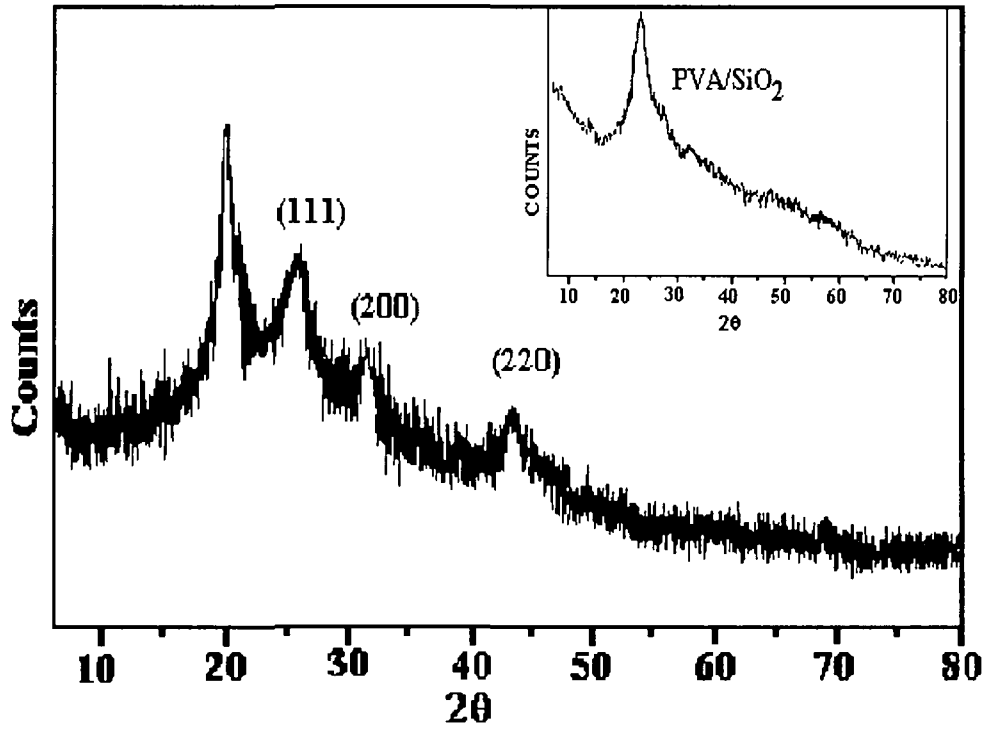

Figure 3.2: XRD pattern of coated PbS quantum dots

Figure 3.2 shows the XRD pattern of coated PbS quantum dots. It has been observed that the FWHM of the XRD peak have been broadened to a little extent compared to the bare samples indicating smaller size of the coated samples. This may be due to the coating effect of amorphous silica [11]. It has been reported that SiO_2 exhibits a hump around 22^0 [12, 13] which in our case might be overlapped by the PVA peak. Therefore it was not possible to locate the bump due to silica individually. However the peaks assigned to PbS appear in the same position which confirms the formation of PbS. The FWHM of the most significant peak measures ~0.127 radian. Thus the size of the silica coated PbS quantum dots estimated from XRD was 11 nm.

3.4.2 CdS quantum dots:

The XRD patterns of bare CdS quantum dots are shown in figure 3.3. The diffraction peaks at $2\theta = 27.1^0$, 44.8^0 and 53.4^0 which are assigned to (111), (220)

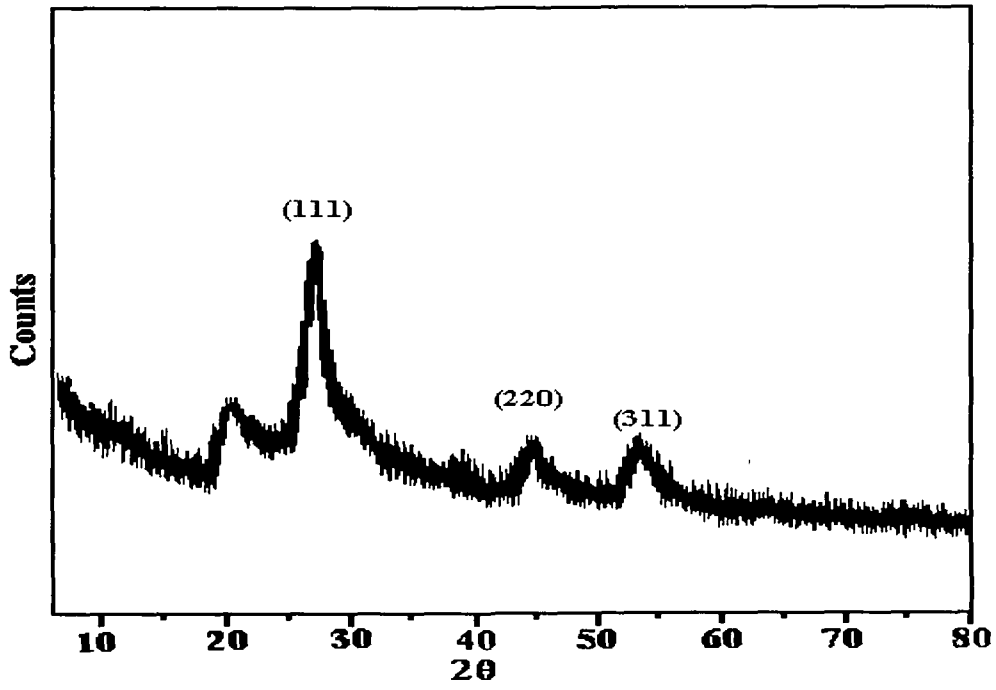

Figure 3.3: XRD pattern of bare CdS quantum dots

and (311) plans of CdS nanoparticles suggests cubic structure. The average size of the bare CdS quantum dots estimated using FWHM of the most prominent peak (~0.14 radian) were 10 nm.

Figure 3.4 shows the XRD pattern of silica coated CdS quantum dots. Since silica (SiO_2) has an amorphous network only, the XRD peaks of coated CdS particle retain the same pattern as that of the bare samples. However the peaks have been broadened to some extent in case of coated samples, which is caused by the coating effect. For coated samples, the average size estimated using Scherrer formula corresponding to FWHM value of 0.2 radian was 7 nm.

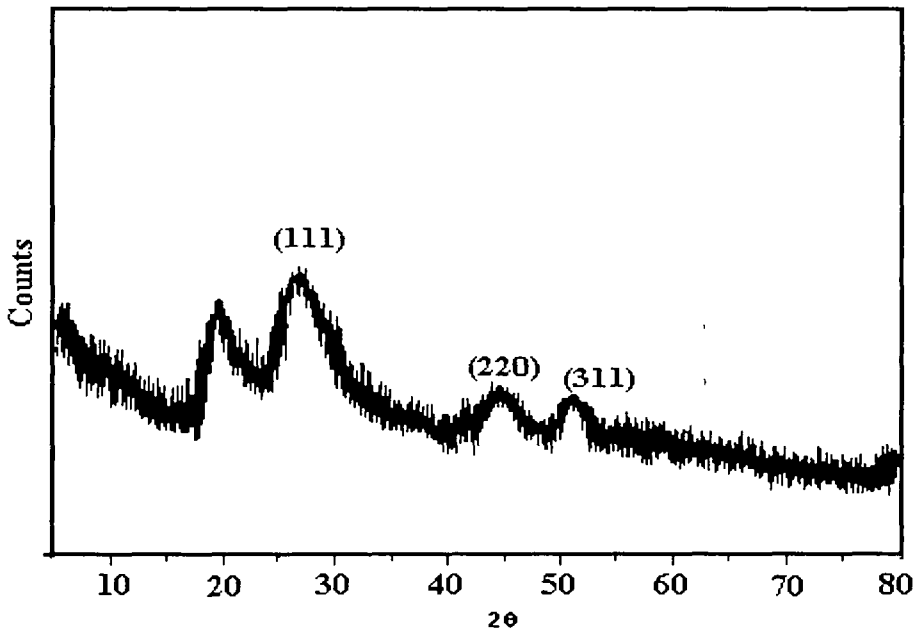

Figure 3.4: XRD pattern of coated CdS quantum dots

3.4.3 *ZnS quantum dots:*

The XRD pattern of bare ZnS quantum dots is shown in figure 3.5. For ZnS the diffraction peaks are recorded at $2\theta = 28.9^0$, 48.1^0 and 56.6^0. The peaks are assigned to (111), (220) and (311) plans of ZnS nanocrystal, exhibiting pure zinc blend structure [4]. The FWHM of the most significant peak measures ~ 0.15 radian. Substituting this value in Scherrer formula the average size of the uncoated ZnS quantum dots were found to be 9 nm.

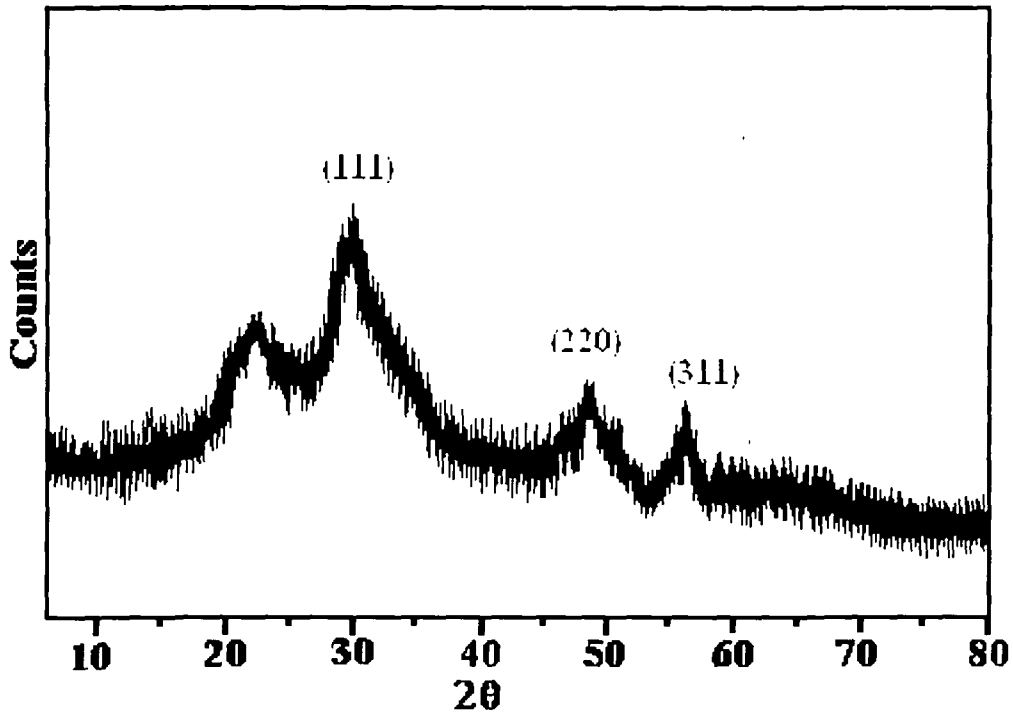

Figure 3.5: XRD pattern of bare ZnS quantum dots

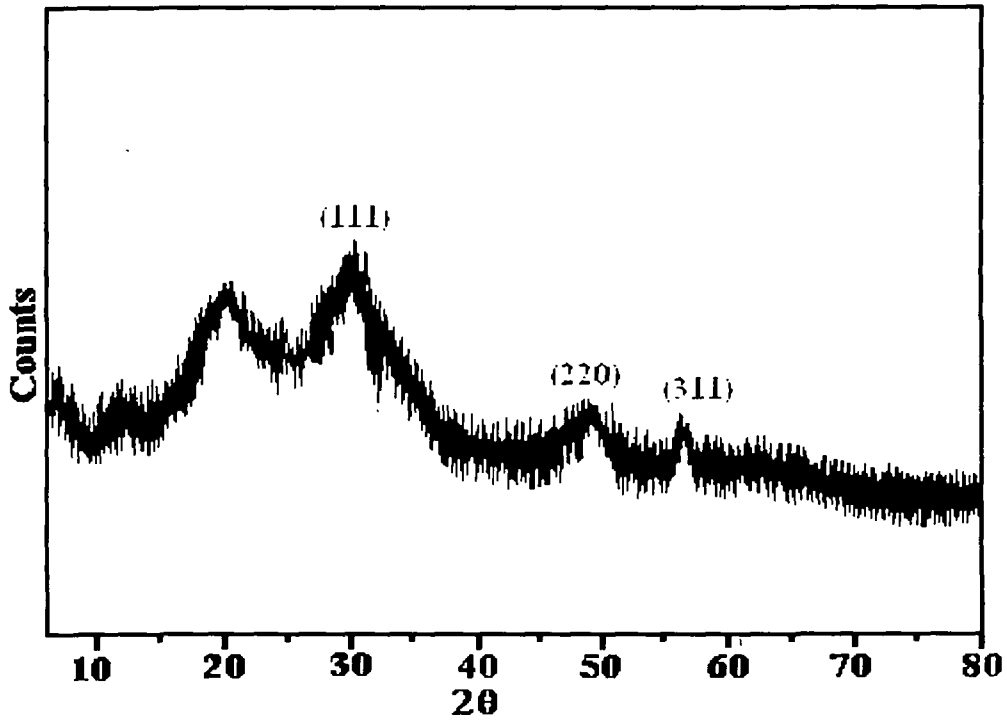

Figure 3.6: XRD pattern of coated ZnS quantum dots

Like PbS and CdS quantum dots, in case of silica coated ZnS quantum dots also, no appreciable change in XRD pattern is observed (Figure 3.6), apart from a slight broadening of the FWHM of the XRD peak. The average dot size estimated from XRD using Scherrer formula were 6 nm corresponding to FWHM value of 0.23radian. The results of the XRD analysis are summarized in table 3.1

Table 3.1: Size of the quantum dots estimated from XRD analysis

Sample	Diffraction plan	Peak positions (2θ)	Particle size (nm)	
			bare	coated
PbS	(111), (200), (220)	25.9^0,30.1^0, 43^0	12	11
CdS	(111), (220), (311)	27.1^0, 44.8^0, 53.4^0	10	7
ZnS	(111), (220), (311)	28.9^0, 48.1^0, 56.6^0	9	6

3.5 UV-Vis optical absorption study :

3.5.1 PbS quantum dots:

The UV-Vis absorption spectra of bare PbS and silica coated PbS quantum dots are shown in figure 3.7. In the inset the UV-Vis absorption spectra of PVA and PVA/SiO_2 have been shown.

For uncoated sample the absorption edge is found at ~511nm (2.42eV) which is largely blue shifted from the corresponding bulk value ~3027 nm (0.41 eV) indicating strong quantum confinement.

The absorption edge for coated sample is observed at ~506 nm. Table 3.2 records band gap enhancement for both bare and coated PbS quantum dots due to size quantization and the corresponding size, estimated from optical spectroscopy using EMA.

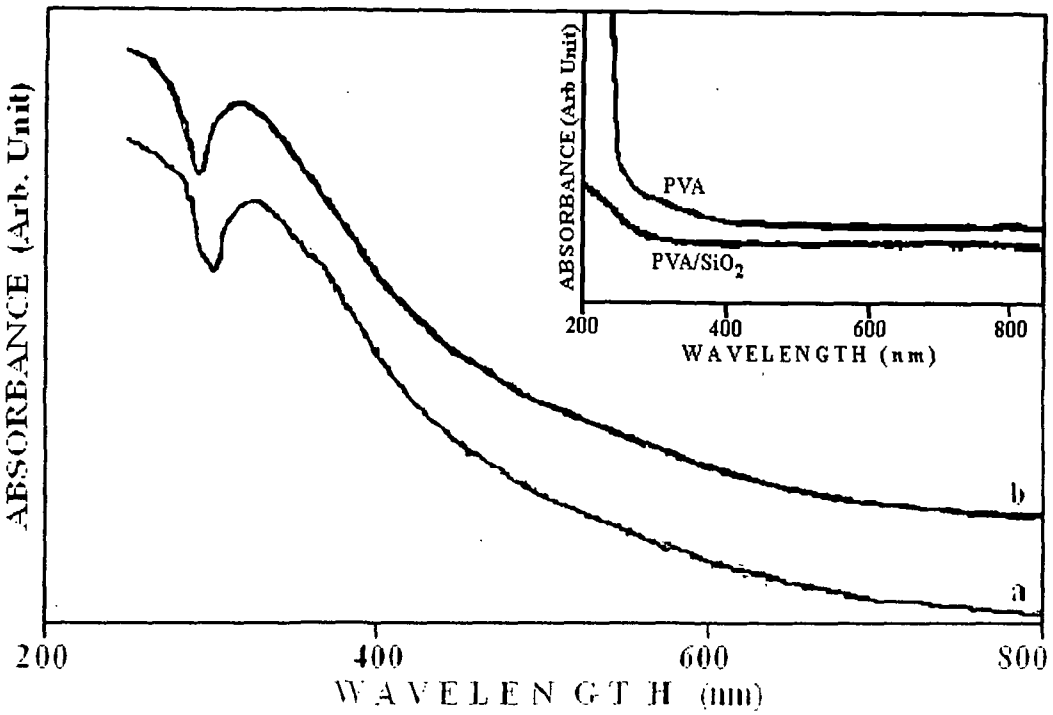

Figure 3.7: UV-Vis absorption spectra of (a) bare and (b) coated PbS quantum dots Inset UV-Vis absorption spectra of PVA and PVA/SiO_2

Table 3.2: Size of the quantum dots calculated using EMA

Samples	Absorption edge for quantum dots sample (nm)	E_{gn} (eV)	Blue shift energy (ΔE) (eV)	Average size estimated from EMA (nm)
PbS	511	2.42	2.01	3.6
PbS/SiO_2	506	2.45	2.04	3.56

3.5.2 CdS quantum dots:

The UV-Vis absorption spectra of bare and silica coated CdS quantum dots are shown in fig 3.8 (a) and (b).

The absorption spectra of uncoated sample have absorption edge at ~ 445 nm which is significantly blue shifted from the bulk value of 517 nm. We

note a slight blue shift in the onsets of absorption in case of coated samples (~ 439 nm) compared to the bare one (~445 nm). The data is presented in Table 3.3.

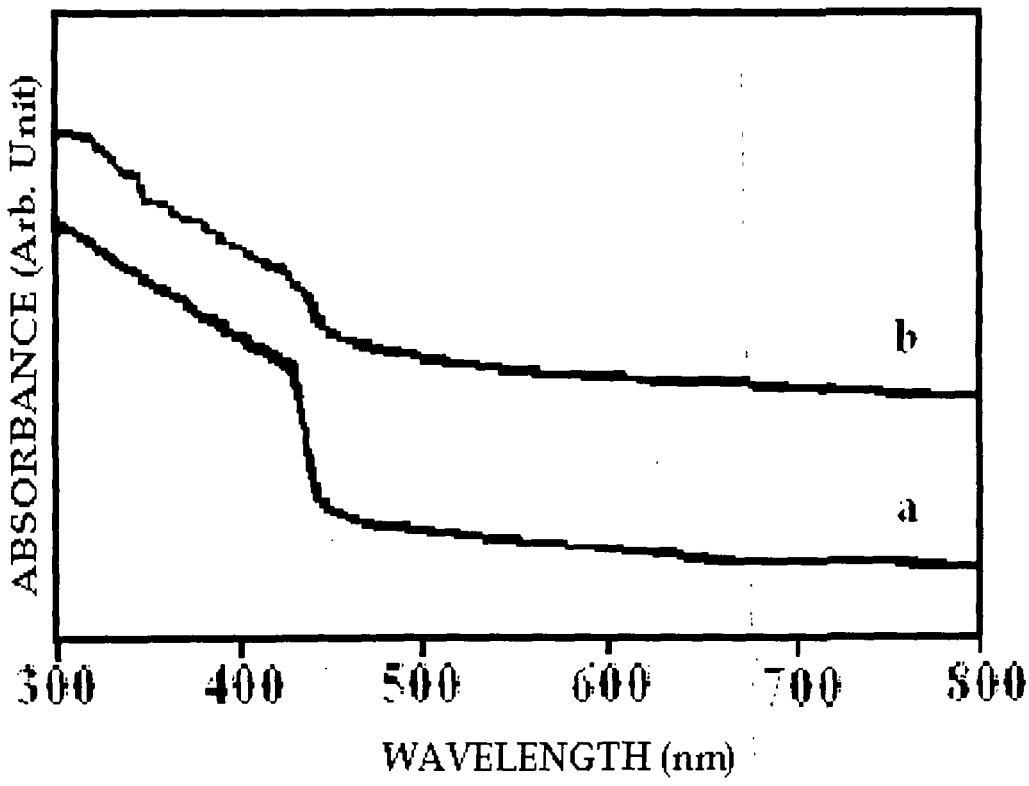

Figure 3.8: UV-Vis absorption spectra of (a) bare and (b) coated CdS quantum dots

Table 3.3 Size of the quantum dots calculated using EMA

Samples	Absorption edge for quantum dots sample (nm)	E_{gn} (eV)	Blue shift energy (ΔE) (eV)	Average size estimated from EMA (nm)
CdS	445	2.78	0.36	5.3
CdS / SiO_2	439	2.82	0.38	5.0

3.5.3 *ZnS quantum dots*:

The UV-Vis absorption spectra of bare and coated ZnS quantum dots are shown in figure 3.9 (a) and (b) respectively.

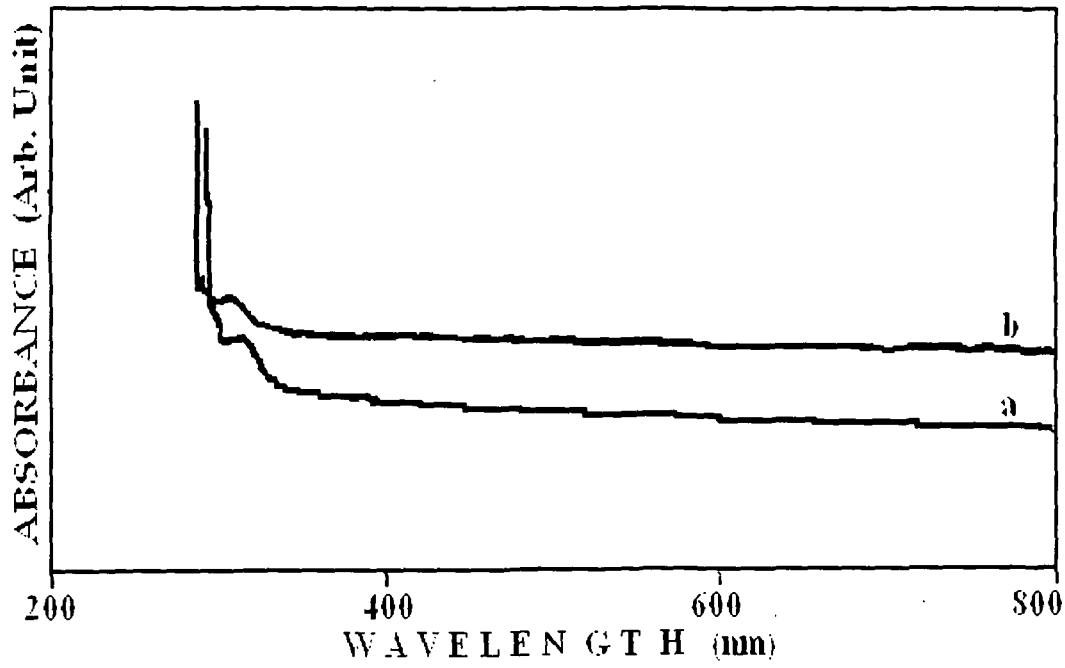

Figure 3.9: UV-Vis absorption spectra of (a) bare and (b) coated ZnS quantum dots

The absorption edge for uncoated samples is observed at ~327 nm which is blue shifted from the corresponding bulk value (337 nm).The coated samples have the absorption edge at ~320 nm . The different data obtained from UV-Vis absorption spectra is presented in Table 3.4.

Table 3.4: Size of the quantum dots calculated using EMA

Samples	Absorption edge for quantum dots sample (nm)	E_{gn} (eV)	Blue shift energy (ΔE) (eV)	Average size estimated from EMA (nm)
ZnS	326	3.8	0.12	5.4
ZnS/ SiO_2	320	3.88	0.22	4.5

3.6 Transmission electron microscopy (TEM) study:

3.6.1 PbS quantum dots:

The TEM image of bare PbS quantum dots is shown in figure 3.10. It can be observed from the TEM image that the nanoparticles are almost spherical in shape. It also indicates size distribution in the sample. The average particle size estimated from TEM for bare PbS quantum dot is ~10 nm.

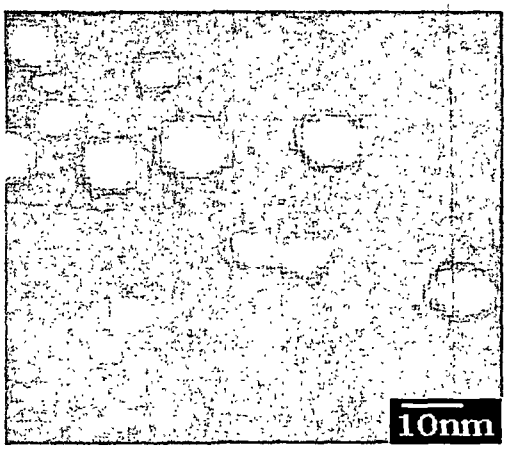

Figure 3.10: TEM image of bare PbS quantum dots

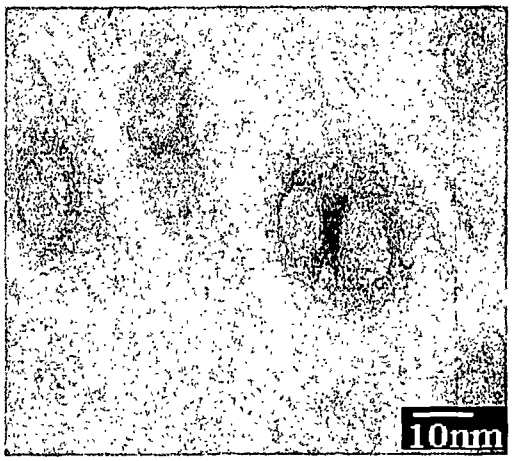

Figure 3.11: TEM image of coated PbS quantum dots

The TEM image of coated PbS quantum dots is shown in figure 3.11. The particles are almost spherical in shape but size distribution is still present in the sample. The particles measure an average diameter of 9 nm.

3.6.2 CdS quantum dots:

The TEM image of bare CdS quantum dots is shown in figure 3.12. As revealed from the TEM, the particles are spherical in shape and the size estimated from TEM is ~ 8 nm

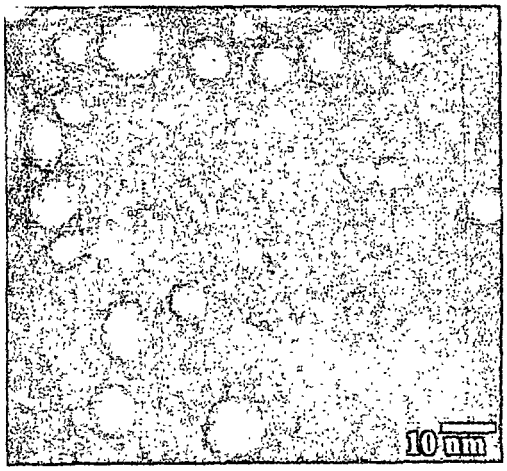

Figure 3.12: TEM of bare CdS quantum dots

Figure 3.13 shows the TEM image of coated CdS quantum dots. The particles are almost spherical in shape. From the TEM, the size estimated for CdS coated quantum dots is ~6 nm.

Figure 3.13: TEM of coated CdS quantum dots

3.6.3 ZnS quantum dots:

The TEM images of bare and coated ZnS quantum dots show (figure 3.14 and figure 3.15) the formation of spherical quantum dots with an average size of 5 and 4.8 nm respectively.

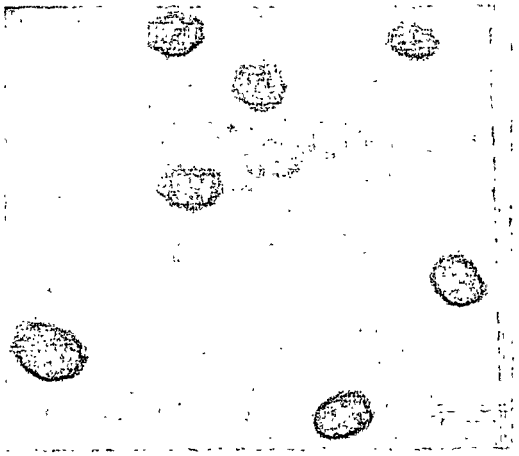

Figure 3.14: TEM of bare ZnS quantum dots

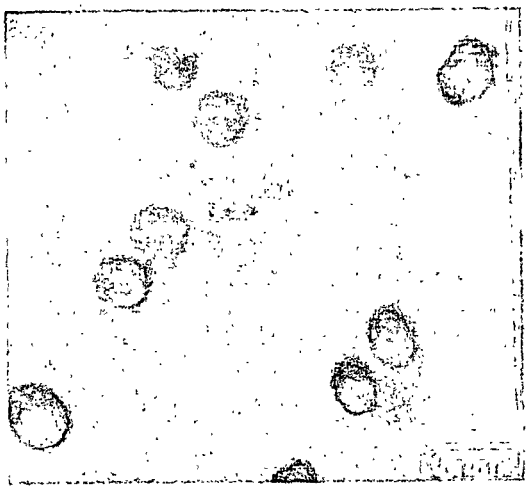

Fig 3.15: TEM of coated ZnS quantum dots

The result of TEM analysis regarding size and shape of all the quantum dots under investigation are summarized in Table 3.5.

Table 3.5 Size of the quantum dots estimated from TEM analysis

Quantum dot Sample	Shape	Size (nm)
PbS	Spherical	10
PbS/SiO_2	Spherical	9
CdS	Spherical	8
CdS/SiO_2	Spherical	6
ZnS	Spherical	5
ZnS/SiO_2	Spherical	4.8

It has been observed that there are discrepancies between theoretical and experimentally calculated particle size, being maximum for lowest band gap semiconductor under study (PbS) and minimum for semiconductor with highest band gap (ZnS). Such discrepancies may arise due to the non-parabolicity and anisotropy of the bulk band structure which result from the interaction between the conduction and valence bands in the narrow-gap materials and their couplings to nearby bands while in EMA, the parabolic band structure has been used for describing the band gap variation of quantum dots with size [14].

3.7 Photoluminescence (PL) study:

3.7.1 *PbS quantum dots:*

The PL spectra of bare and silica coated PbS quantum dots are shown in figure 3.16(a) and (b). For both the samples the PL peak is observed at 700 nm. A fluorescence peak for PbS nanoparticle at 700 nm has already been reported [15]. The low energy peak has been attributed to deep surface state as well as band edge emission in PbS [14]. However the peak intensity in case of coated samples increases significantly.

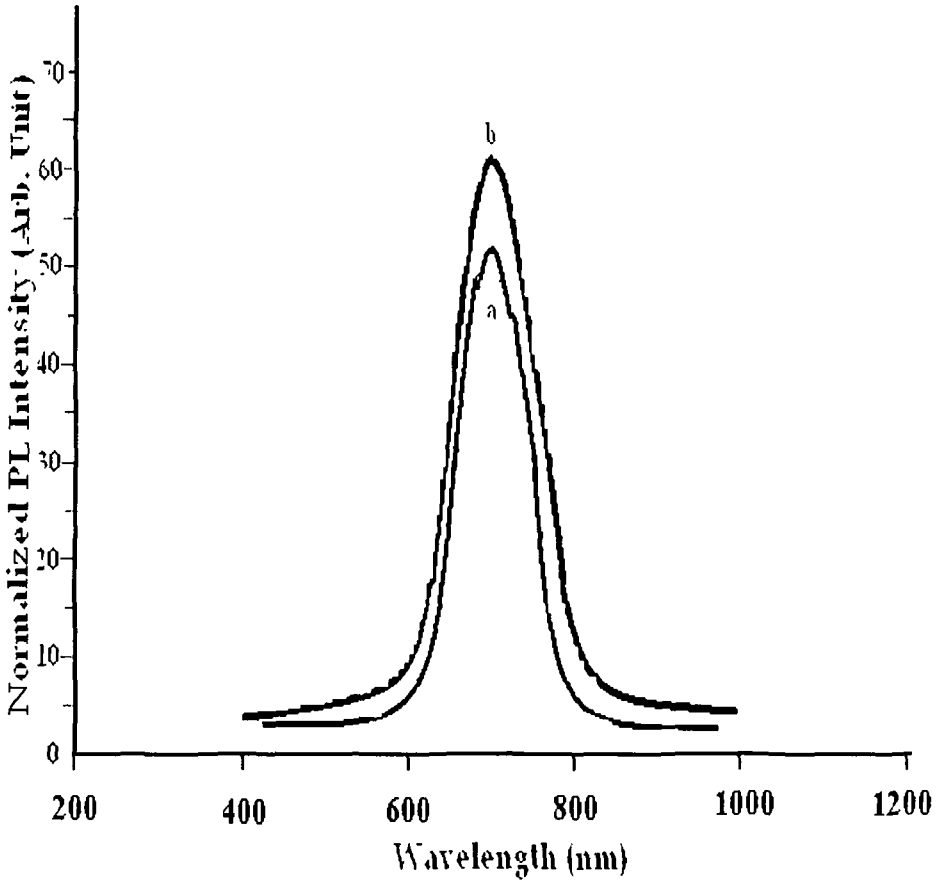

Figure 3.16 PL spectra of (a) bare and (b) coated PbS quantum dots

3.7.1.1 *Effect of ageing on photoluminescence:*

The PL spectra of both bare and coated PbS quantum dots were recorded after 30 days and 60 days, the corresponding spectra are shown in figure 3.17 and 3.18. In case of bare sample, it has been observed that the PL intensity increases with time. This may be due to the formation of an oxygen layer over nanoparticle surface as suggested by Myung *et al.* [16]. Table 3.6 presents the PL peak positions and corresponding intensities of freshly prepared and aged PbS quantum dots, both bare and coated.

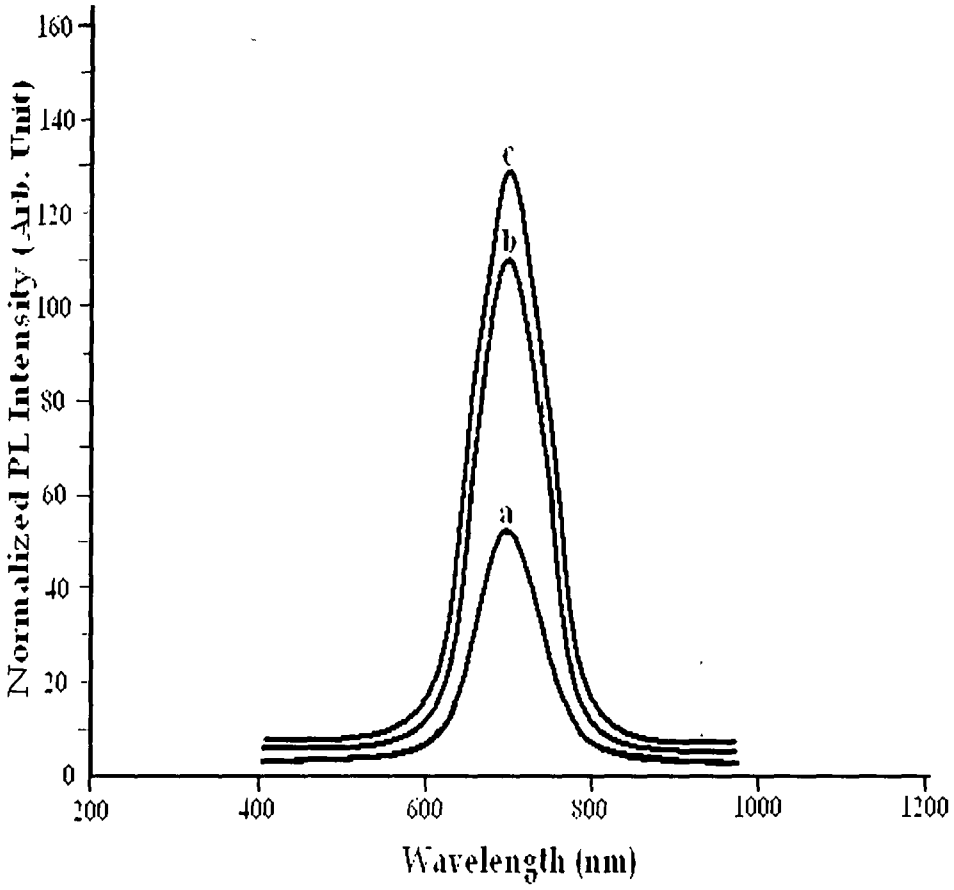

Figure 3.17: PL spectra of bare PbS quantum dots (a) freshly prepared (b) 30 days old and (c) 60 days old

Table 3.6: PL peak position and intensity of the freshly prepared and aged PbS quantum dots

	Sample	PL peak positions (nm)	PL intensity (Arb. Unit)
PbS	Freshly prepared	700	52.2
	30 days old	700	110.5
	60 days old	700	129.4
PbS/SiO_2	Freshly prepared	700	63.5
	30 days old	700	63.8
	60 days old	700	63.8

However no significant increase in intensity has been observed in case of coated samples. The positions of the peaks remain same in both coated and uncoated samples.

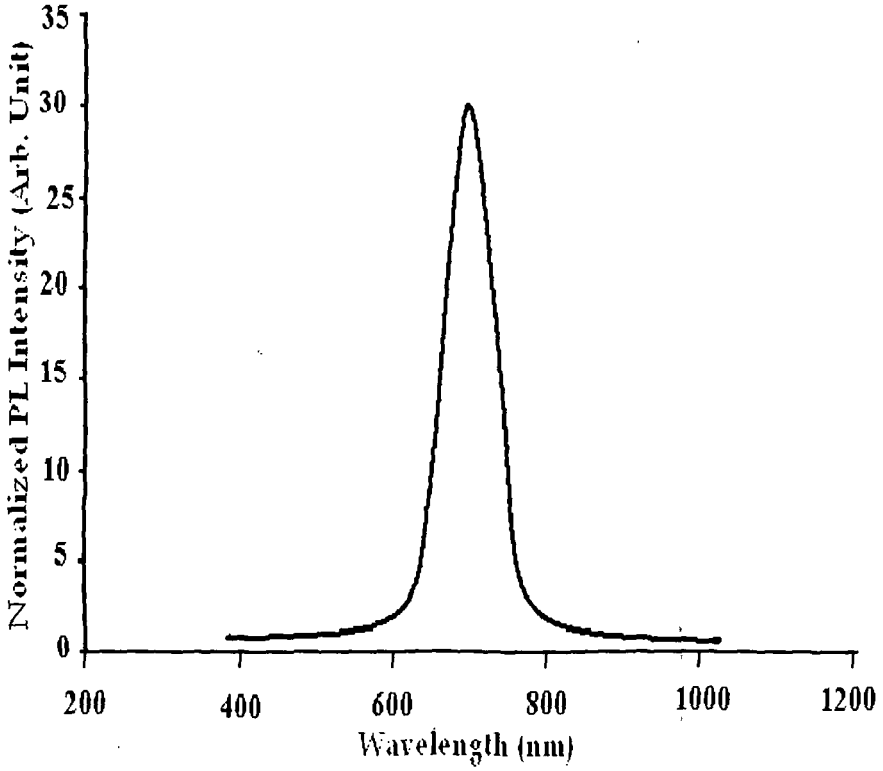

Figure 3.18: PL spectra of 60 days old coated PbS quantum dots

3.7.2 CdS quantum dots:

The PL spectra of uncoated CdS quantum dots [figure 3.19(a)] show that the sample possesses luminescence peak around 700 nm, corresponding to energy of 1.7 eV, which is less than the band gap energy. Therefore the transition involves donors, acceptors and surface traps. In case of chemical synthesis of CdS quantum dots, when they are exposed to atmosphere, the sulphur atoms at the surface oxidize to sulphate leaving a fresh surface with reduced Cd. This reduced Cd reacts with atmospheric oxygen to form Cd-O complex [7]. We assign the low energy peak in CdS quantum dot sample to the

transition associated with CdO. In case of silica coated CdS quantum dots, the PL spectra show a high energy peak around 570 nm [figure 3.19 (b)]. The absence of low energy peak may be due to the coating applied, which restricts the formation of Cd-O complex. We believe that the origin of this emission is electron hole recombination at the surface of the nanoparticle.

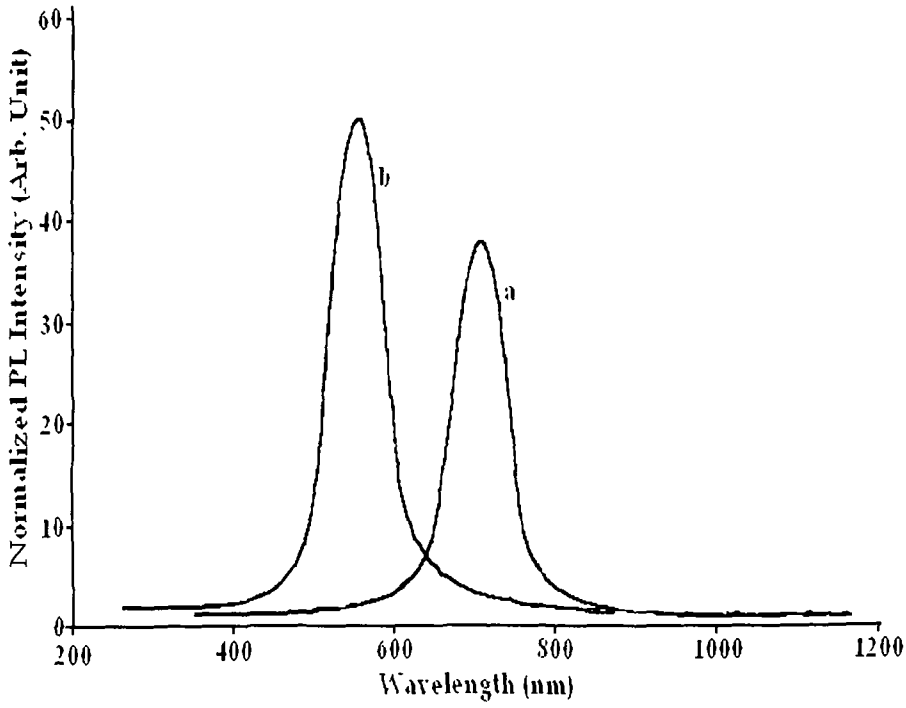

Figure 3.19: PL spectra of (a) bare and (b) coated CdS quantum dots

The occurrence of this peak in case of coated sample indicates that coating may enhance the possibility of electron hole recombination.

3.7.2.1 Effect of ageing on photoluminescence:

The bare CdS quantum dot samples were aged between 30 and 60 days and the PL (figure 3.20) were recorded. No shift in PL peaks positions are observed in either case. However, the intensity of 700 nm peak, observed in case of bare CdS sample increases significantly. This is obvious as the density of CdO increases with time.

The PL spectra of coated sample after ageing for 30 and 60 days are same in regards of PL peak position and intensity. Figure 3.21 shows the PL spectrum of 60 days old coated CdS quantum dots. Like coated PbS quantum dots the peak position and intensity remain almost unchanged for CdS quantum dots also.

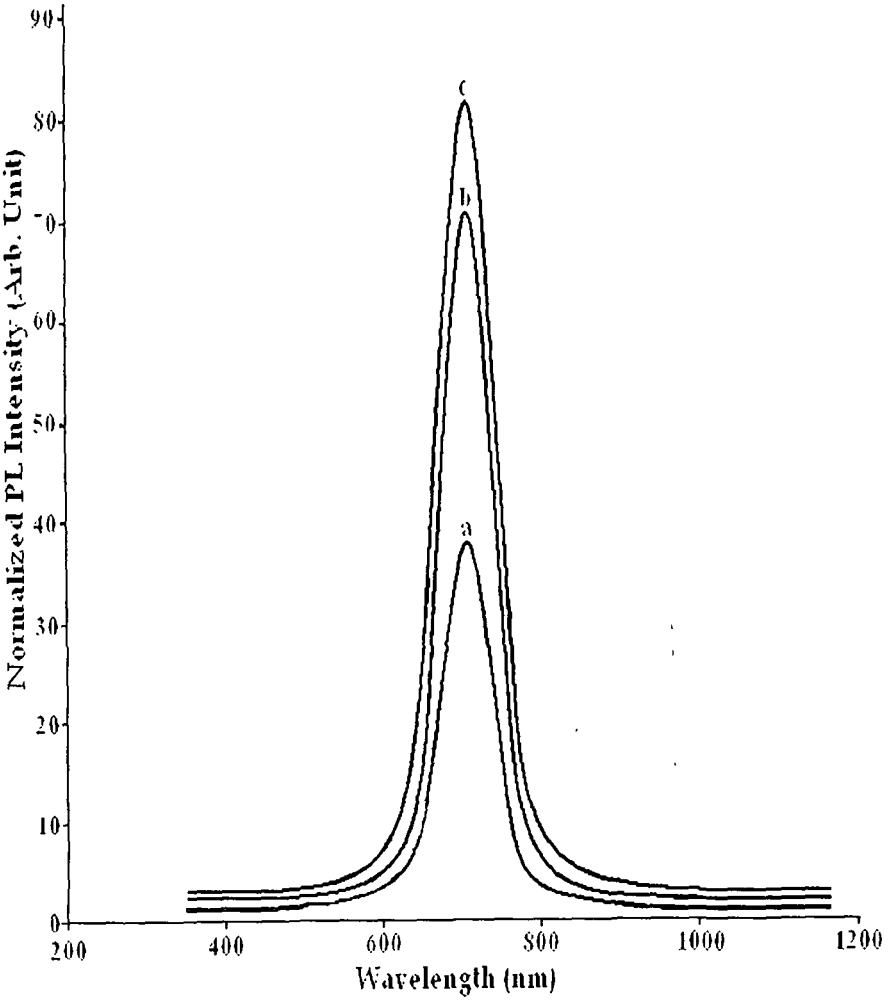

Figure 3.20 PL spectra of uncoated CdS quantum dots (a) freshly prepared b) 30 days old and (c) 60 days old

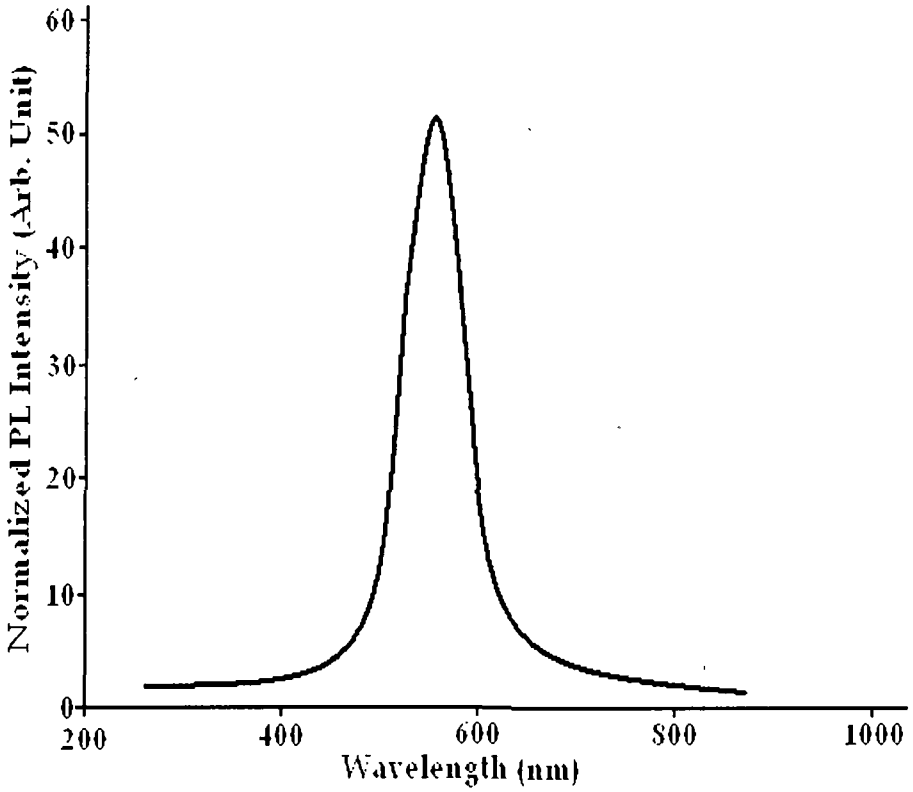

Fig 3.21: PL spectra of 60 days old coated CdS quantum dots

The position of the PL peaks of freshly prepared and aged CdS quantum dots along with the corresponding intensities have been presented in Table 3.7.

Table 3.7 PL peak position and intensity of the freshly prepared and aged CdS quantum dots

	Sample	PL peak positions (nm)	PL intensity (Arb. Unit)
CdS	Freshly prepared	700	37.9
	30 days old	700	71.3
	60 days old	700	81.9
CdS/SiO_2	Freshly prepared	570	50.8
	30 days old	570	50.9
	60 days old	570	50.9

3.7.3 *ZnS quantum dots:*

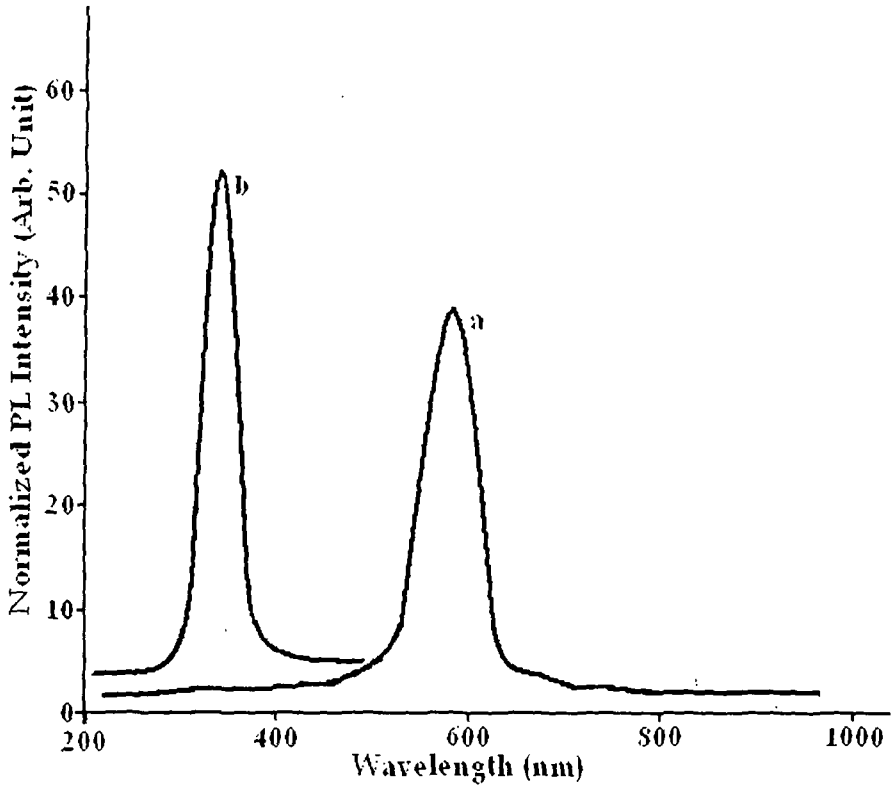

Figure 3.22: PL spectra of (a) bare and (b) coated ZnS quantum dots

The PL spectrum of bare ZnS quantum dots is shown in figure 3.22(a) which displays the luminescence peak at 591 nm. This emission is attributed to surface defects like dangling bonds and vacancies. The PL spectrum of coated ZnS quantum dots is shown in figure 3.22 (b). In this spectrum the peak is observed at 350 nm while the low energy peak is quenched. This emission may be attributed to band edge emission of ZnS quantum dots. From the PL study we observe that the surface state emission of ZnS quantum dots is quenched after coating, enhancing the band edge emission.

3.7.3.1 *Effect of ageing on photoluminescence:*

The PL spectra of bare ZnS quantum dots are recorded after 30 and 60 days and are presented in figure 3.23.

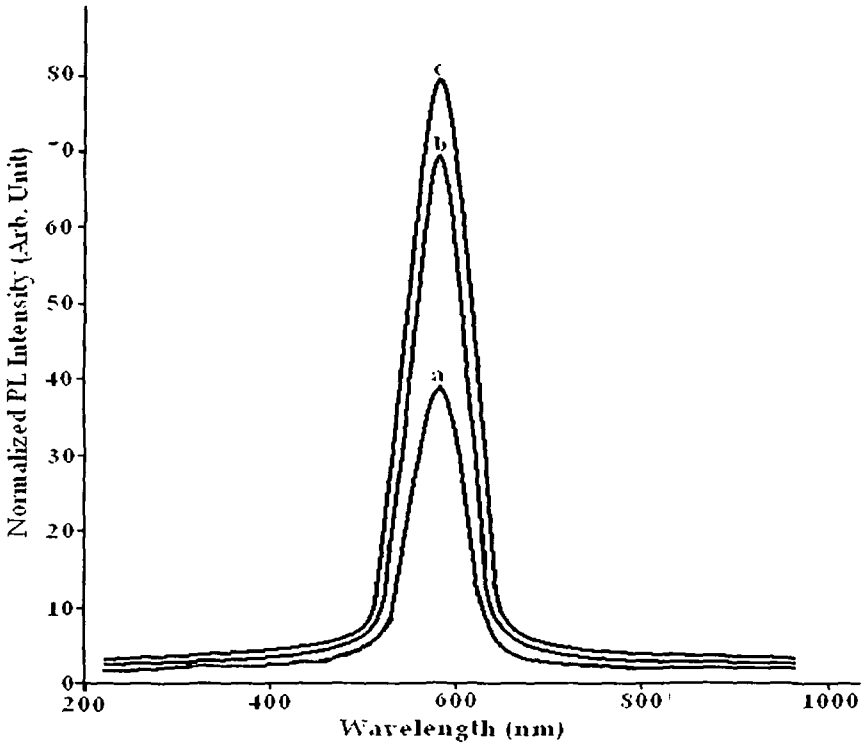

Figure 3.23: PL spectra of bare ZnS quantum dots (a) freshly prepared b) 30 days old and (c) 60 days old

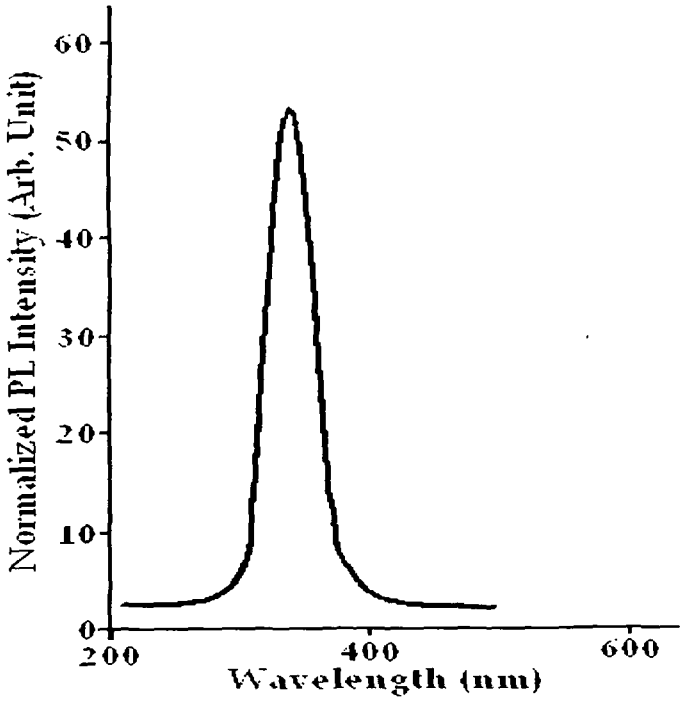

Figure 3.24: PL spectra of 60 days old coated ZnS quantum dots

Table 3.8: PL peak position and intensity of the freshly prepared and aged ZnS quantum dots

Sample		PL peak positions (nm)	PL intensity (Arb. Unit)
ZnS	Freshly prepared	591	39.1
	30 days old	591	69.9
	60 days old	591	80
ZnS/SiO_2	Freshly prepared	570	52.1
	30 days old	570	52.1
	60 days old	570	52.1

It has been observed that the PL peak occurs at the same wavelength for fresh and aged samples but there is significant increase in PL intensity with time.

The increase in PL intensity of the uncoated sample with time is attributed to the adsorption of atmospheric oxygen by the surface of the quantum dots, as discussed in case PbS quantum dots.

The observation for coated ZnS quantum dots indicates enhanced stability of the samples. The PL spectrum of coated ZnS quantum dots after ageing for 60 days is shown in figure 3.24. No change either in PL position or intensity has been observed for coated ZnS quantum dots as in case of bare ones. The corresponding data for bare and coated ZnS quantum dots are presented in Table 3.8.

In this chapter the results obtained from XRD, UV-Vis optical absorption spectra, TEM and PL spectra of bare and silica coated quantum dots have been discussed. All these analysis confirm formation of crystalline semiconductor quantum dots. The nanoparticles coated with PVA/Silica hybrid composite show higher PL intensity and stability.

References:

1. Wise F. W., *Acc. Chem. Res.* **33** (2000) 773.
2. Kang I. and Wise F.W., *J. Opt. Soc. Am. B*, **14** (1997) 1632.
3. Patel A. A., Wu F., Zhang J. Z., Torres-Martinez C.L., Mehra R.K., Yang Y. and Risbud S. H., *J. Phys. Chem. B*, **104** (2000) 11598.
4. Fern´ee M.J., Warner J., Watt A., Cooper S., Heckenberg N.R. and Dunlop R.H., *Nanotechnology*, **15** (2004) 16.
5. Joshi R. K., Kanjilal A., Sehgal H.K., *Appl. Surf. Sc.*, **221** (2004) 43.
6. Liu S.H., Qian X.F., Yin J., Ma X.D., Yuan J.Y., Zhu Z.K., *J. Phys. and Chem.Solids*, **64** (2003) 455.
7. Nikesh V.V. and Mahamuni S., *Semicond. Sci. Technol.*, **16** (2001) 687.
8. Qadri S .B., Yang J.P, Skelton E.F., Ratna B.R., *Appl Phys. Lett.*, **70** (1997) 1020.
9. Yang S., Wang S. and Fung K.K., *Pure Appl. Chem.*, **72** (2000)119.
10. Ma Xiao-Dong, Qian Xue-Feng, Yin J. and Zi-Kang Zhu *J. Mater. Chem.*, **12** (2002) 663.
11. Mu J, Gu D and Xu Z, *Appl. Phys. A: Materials Science & Processing*, (2004).
12. He H., WangY. and Zou Y. *J.Phys. D: Appl. Phys.*, **36** (2003) 2972.
13. Haranath D., Chander H., Bhalla N., Sharma P., and Sood K.N., *Appl. Phys. Lett.*, **86** (2005) 201904.
14. Chowdhury S., Mohanta D., Ahmed G.A, Dolui S.K., Avasthi D.K. Choudhury A., *J. Luminescence*, **114** (2005) 95.
15. Chen S., Truax L.A., Sommers J.M., *Chem. Matter.*, **12** (2000) 3864.
16. Myung N., Bae Y. and Bard A. J., *Nano Lett.*, **3** (2003) 747.

CHAPTER IV

4.1 Swift Heavy Ion (SHI) Irradiation Effect:

Ion beams have become an integral part in the modification of solids and of numerous surface processing schemes [1]. Recently there has been a growth of interest in high energy ion irradiation of polymers and other materials [2-7]. Ions couple energy to the target atoms in a solid predominantly through electronic excitation and ionizations and through direct collision displacement of the target atoms. Effect of Swift Heavy Ion irradiation (SHI) on quantum dots is comparatively a new area in the field of nanomaterial research. However ion implantation technique was used for fabrication of quantum dots [8-10]. Prajacta *et al.* reported fabrication of Si nanoparticles on SiO_2 [11] with the help of SHI irradiation. Mohanta *et al.* observed enhancement in size of ZnS:Mn quantum dots [12] and ZnO quantum dots [13] while Berthelot *et al.* reported fragmentation of SnO_2 nanoparticles upon SHI irradiation [14].

In this chapter we have investigated SHI induced modified properties of quantum dots. Prior to discussion of experimental results, we shall review in brief the ion-matter interaction process.

4.1.1 Ion -Mater Interaction:

Due to the passage of swift heavy ions through a material, the free electrons available in its path get excited within a time scale ~ 10^{-15} sec. This electronic excitation leads to rise in temperature of the ion's track known as electronic temperature which is of the order of 10^5 ^{0}K. Next, the energy of the ions is relaxed into the lattice and phonons get excited within a time frame of 10^{-12} sec, giving rise to lattice temperature rise of the order of 10^3 ^{0}K. Thus the energy of the ion is quickly transferred into other parts of the specimen [15]. This energy is spent either in displacing atoms of the sample by elastic collision or exciting the atoms by inelastic collision. The energy lost in the former process

is known as nuclear energy loss while energy lost in the later case is known as electronic energy loss. In case of low energy ion (a few tens of KeV to a few MeV) nuclear energy loss is predominant. In case of heavy ions with energies from few tens of MeV and higher the electronic energy loss process dominates and they are referred to as swift heavy ions. In SHI irradiation the impinging ions do not get embedded in the sample due to their large range (typically a few tens of μm or larger) and effect of elastic collision can be neglected. Also the effect of embedded ions does not come into picture [16].

4.1.2 Parameters Related to SHI Irradiation:

4.1.2.1 Fluence (ϕ):

It is defined as the total number of irradiating ions incident per square centimeter (ions/ cm^2) of the sample. It varies from sample to sample depending upon its size and material.

Fluences are calculated using the following formula

$$\text{Fluence } (\phi) = \frac{\text{Time } (t) \times \text{Beam Current} \times \text{pnA}}{\text{Ch}\,arg\,\text{e State}}$$

Beam currents for ion irradiation experiments are usually taken in the range of 2-5 nA.

$$1\ \text{pnA (particle nano} - \text{ampere)} = \frac{10^{-9}\,\text{Coul} / sec}{1.6\text{x}10^{-19}\,\text{Coul}} = 6.25\text{x}10^{9}\,\text{particles} / sec$$

4.1.2.2 Count:

During ion irradiation process, fluences are recorded by using a counter. Following relation relates the counts and the fluences

$$\text{Counts} = \frac{\phi\, q\, e}{S}$$

where ϕ is the fluence,

q is the charge state of ion beam,

e is the electronic charge (1.6×10^{-19} coulomb),

S is the scale of the counter

4.1.3 The SHI irradiation experiment:

The irradiation experiment was carried out on each of the bare and coated quantum dots samples. The samples were mounted on a vacuum shielded vertical sliding ladder having six rectangular faces. They were irradiated in the GPSC chamber under high vacuum (5×10^{-6} Torr) by using the 160 MeV Ni^{12+} beam with approximate beam current of 1.0 pnA (particle nanoampere), available from the 15UD tandem Pelletron Accelerator at NSC, New Delhi [17, 18]. The samples were irradiated with fluences 10^{12}, $5x10^{12}$ and 10^{13} ions/cm^2 respectively. Using Monte Carlo simulation program SRIM the projectile range for PbS, CdS and ZnS sample were calculated as 42.38, 36.48 and 34.44 μm. Following the SRIM calculation, the sample thickness was kept ~20 μm so that the possibility for ion implantation can be ruled out.

4.2 XRD study:

4.2.1 PbS quantum dots:

Figure 4.1 displays the XRD pattern of bare PbS quantum dots after irradiation with the fluences 10^{12}, $5x10^{12}$ and 10^{13} ions/cm^2. It has been observed that the FWHM of the XRD peaks after irradiation has been gradually reduced indicating increase in particle size. The TEM image of bare PbS quantum dots embedded in polyvinyl alcohol (PVA) matrix (chapter III), reveals that the quantum dots are closely distributed with very small inter particle distances. During SHI irradiation enormous heat generates in the ion track and the polymer matrix starts melting and gets easily amorphized even at low energy. This can be confirmed by the XRD pattern which shows that the sharp peak around 20^0 which is attributed to PVA becomes a hump with increase in ion fluence. This is because of amorphization of PVA. The quantum particles thus loose their support in the polymeric matrix and they agglomerate to form bigger clusters. Practically, it has been found that higher the ion fluence more is the generated heat, and hence bigger is the particle size. Using Scherrer formula, (chapter II, section 2.4.1) the particle size of PbS quantum dots after

irradiation were found to be 70, 72 and 74 nm corresponding to FWHM values of 0.02, 0.019 and 0.189 radian at fluences of 10^{12}, $5x10^{12}$ and 10^{13} ions/cm^2 respectively.

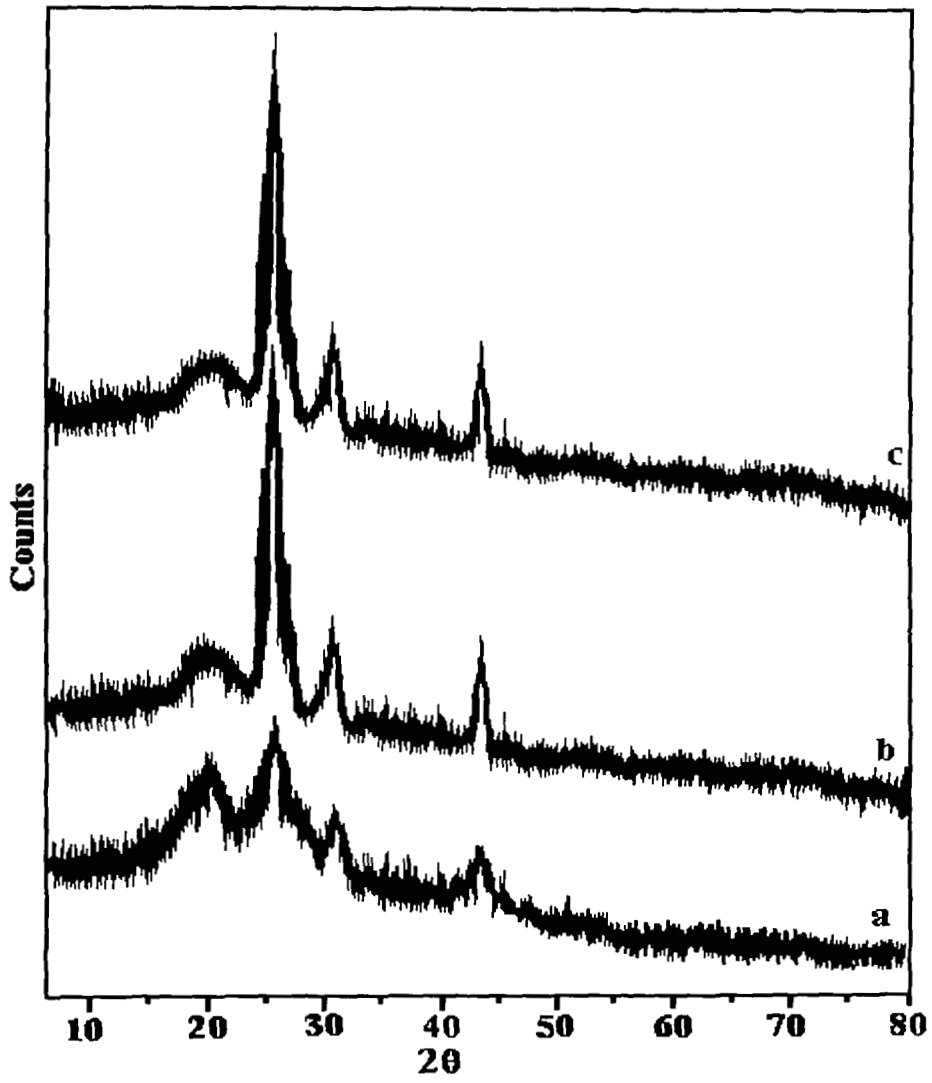

Figure 4.1 XRD patterns of bare PbS quantum dots after SHI irradiation at fluences (a) 10^{12} (b) $5x10^{12}$ and (c) 10^{13} ions/cm^2

In case of coated samples no significant difference is observed in the FWHM of the XRD pattern of unirradiated (chapter III) and irradiated samples as shown in the figure 4.2. This is because of the high melting point of SiO_2 (approximately 1000^{0}C) compared to PVA (483^{0}C). However it is interesting to note the appearance of a new peak around 54^0 which indicates the formation of PbO in the sample [19]. The formation of PbO is believed to be due to the

reaction of Pb atom with SiO_2 during SHI irradiation. The size of the bare and coated quantum dots after SHI at different fluences are presented in Table 4.1

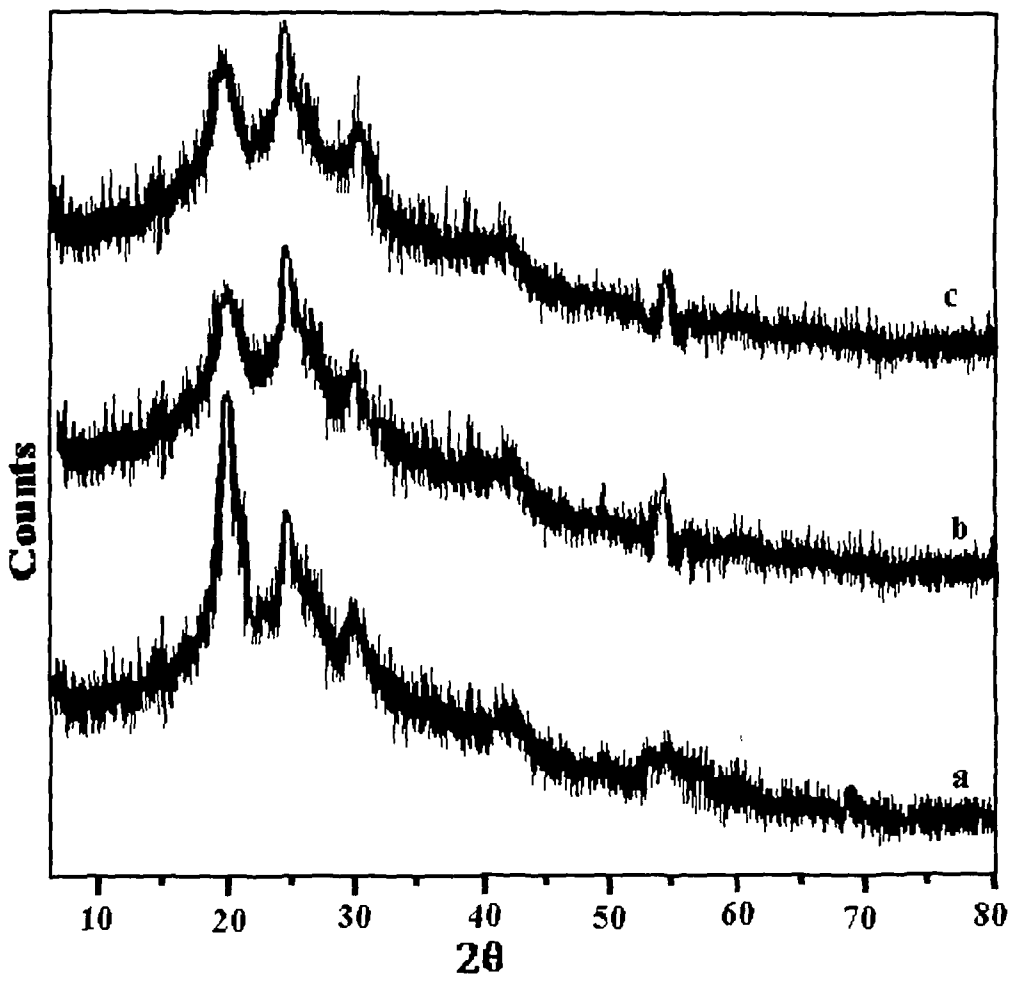

Figure 4.2 XRD patterns of coated PbS quantum dots after SHI irradiation at fluences (a) 10^{12} (b) $5x10^{12}$ and (c) 10^{13} ions/cm^2

Table 4.1 Size of the bare and coated PbS quantum dots after SHI irradiation calculated from XRD

Fluence (ions/cm^2)	Average size of bare PbS quantum dots (nm)	Average size of coated PbS quantum dots (nm)
10^{12}	70	12
5×10^{12}	72	12
10^{13}	74	12

4.2.2. *CdS quantum dots:*

The XRD patterns of uncoated CdS quantum dots after SHI irradiation at different fluences are displayed in figure 4.3. The increase in FWHM of the XRD peak after irradiation indicate the size enhancement of the quantum dots

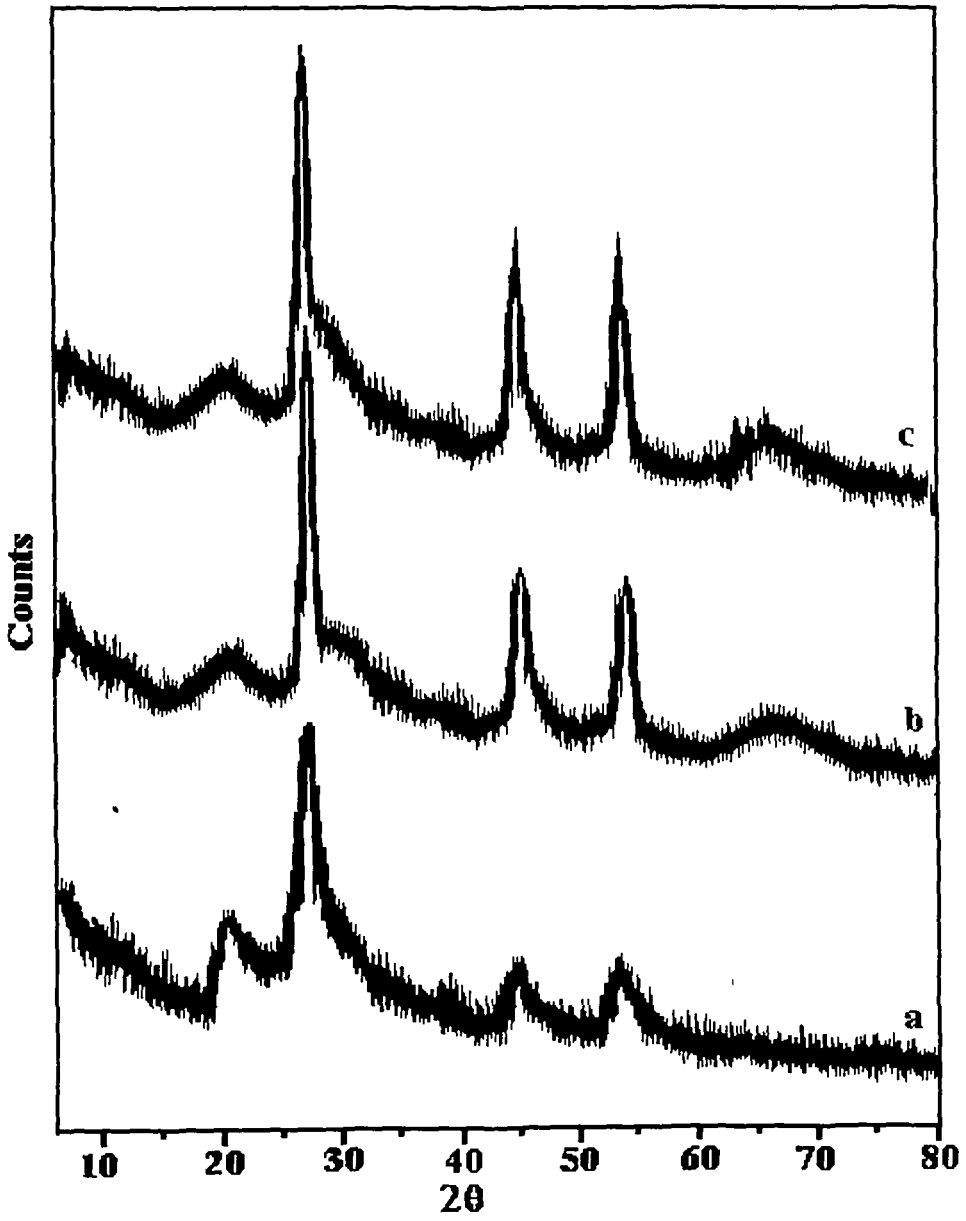

Figure 4.3 XRD patterns of bare CdS quantum dots after SHI irradiation at fluences (a) 10^{12} (b) $5x10^{12}$ and (c) 10^{13} ions/cm^2

after irradiation. Also the peak assigned to PVA seems to be amorphized after irradiation. Like PbS quantum dots, in case of CdS quantum dots also the size enhancement of the nano particles is believed to be due to melting of the

supporting matrix PVA so that the nano particles come out of the polymer cage and agglomerate to form bigger particles. The particle size estimated from Scherrer formula after irradiating with fluences 10^{12}, $5x10^{12}$ and 10^{13} ions/cm^2 were found to be 21, 37 and 50 nm respectively. The corresponding FWHM values were 0.07, 0.037 and 0.028 radian.

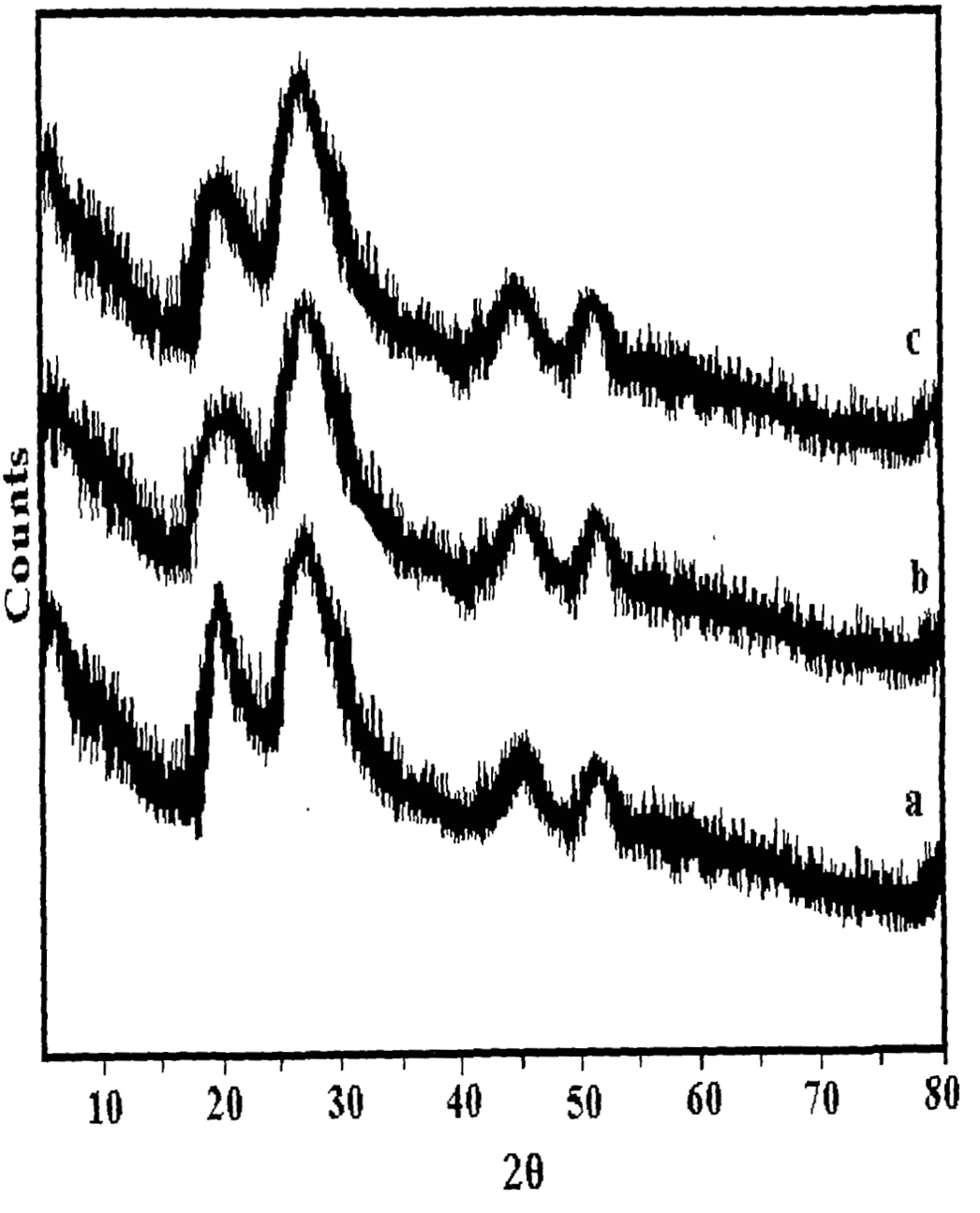

Figure 4.4 XRD patterns of coated CdS quantum dots after SHI irradiation at fluences (a) 10^{12} (b) $5x10^{12}$ and (c) 10^{13} ions/cm^2

The XRD patterns of coated CdS quantum dots after SHI at fluences 10^{12}, $5x10^{12}$ and 10^{13} ions/cm^2 are shown in figure 4.4. No significant change in XRD pattern of the coated CdS sample compared to the unirradiated sample (chapter III) imply that the size of the coated samples remain same after SHI irradiation. Thus silica coating can restrict particle growth under SHI irradiation.

The sizes of the bare and coated CdS quantum dots calculated from their XRD pattern after SHI irradiation is recorded in Table 4.2.

Table 4.2 Size of the bare and coated CdS quantum dots after SHI irradiation calculated from XRD

Fluence (ions/cm^2)	Average size of bare CdS quantum dots (nm)	Average size of coated CdS quantum dots (nm)
10^{12}	21	7
$5x10^{12}$	37	7
10^{13}	50	7

4.2.3 ZnS quantum dots:

The XRD patterns of uncoated ZnS quantum dot after irradiation with SHI at fluences 10^{12}, $5x10^{12}$ and 10^{13} ions/cm^2 are shown in figure 4.5. The XRD patterns reveal the same observations as in case of PbS and CdS quantum dot systems including reduction in FWHM of the XRD peak and change in PVA peak structure after SHI irradiation. The particle size was calculated with Scherrer formula and corresponding to the FWHM values of 0.07, 0.045 and 0.031 radian the sizes calculated were 20, 31 and 45 nm at fluences of 10^{12}, $5x10^{12}$ and 10^{13} ions/cm^2. Thus particle size enhancement of bare ZnS with increase in ion fluence has been confirmed from XRD study.

Figure 4.6 shows the XRD pattern of coated ZnS quantum dots after SHI irradiation with fluences 10^{12}, $5x10^{12}$ and 10^{13} ions/cm^2

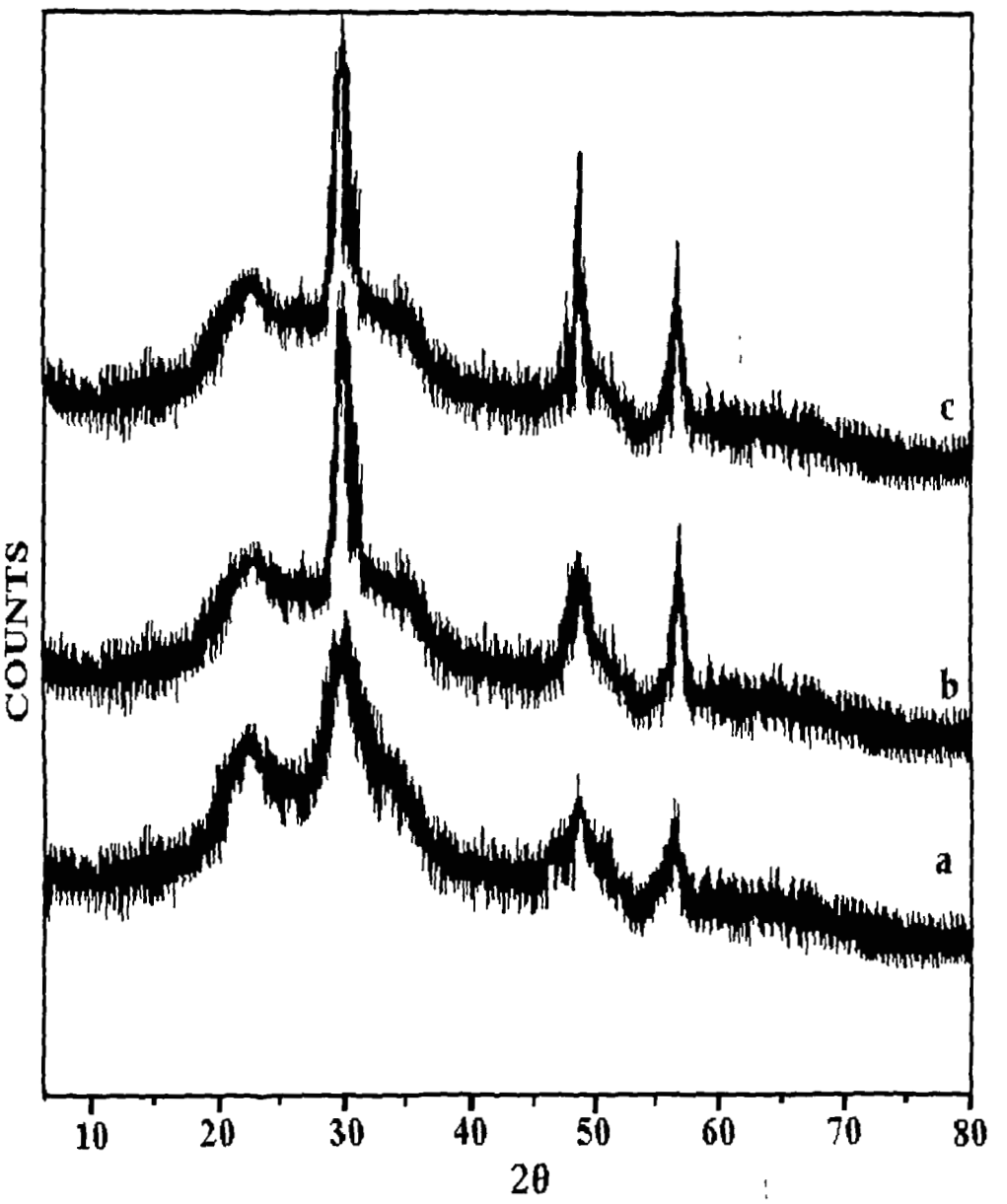

Figure 4.5 XRD patterns of bare ZnS quantum dots after SHI irradiation at fluences (a) 10^{12} (b) $5x10^{12}$ and (c) 10^{13} ions/cm^2

There is no any significant change either in position of the XRD peaks or in FWHM of the peaks compared to the unirradiated coated ZnS sample (chapter III). Thus XRD results indicate stability of the particles after SHI irradiation. The sizes of bare and coated ZnS quantum dot calculated from corresponding XRD pattern are given in Table 4.3.

From the XRD studies it has been observed that the size enhancement is maximum in case of PbS as compared to CdS and ZnS quantum dots. This may

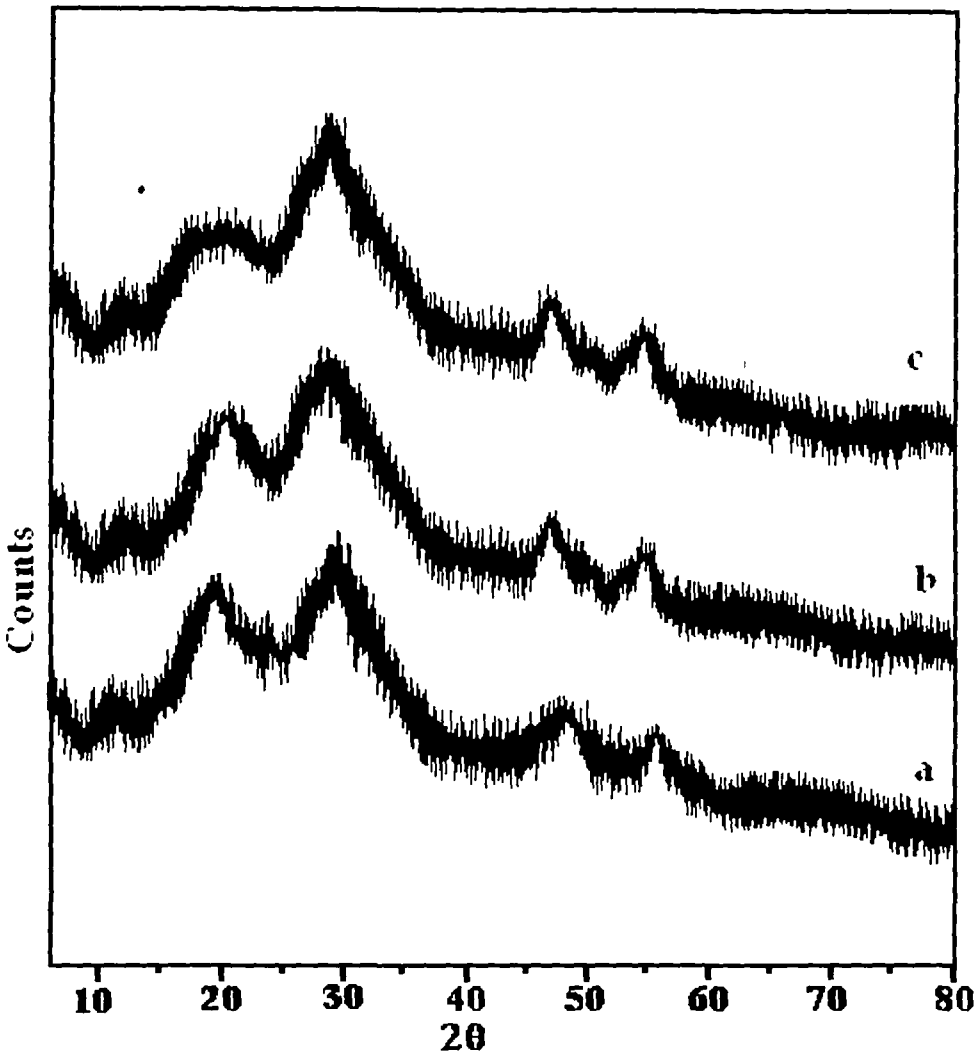

Figure 4.6: XRD patterns of coated ZnS quantum dots after SHI irradiation at fluences (a) 10^{12} (b) $5x10^{12}$ and (c) 10^{13} ions/cm^2

Table 4.3 : Size of the bare and coated ZnS quantum dots after SHI irradiation calculated from XRD

Fluence (ions/cm^2)	Average size of CdS quantum dots (nm)	
	Bare	Coated
10^{12}	20	6
$5x10^{12}$	31	6
10^{13}	45	6

be due to low melting point (1118 ^{0}C) of PbS than CdS (1750 ^{0}C) and ZnS (1700 ^{0}C). Also, as revealed from the TEM images of bare quantum dots, (chapter III, section 3.6), the CdS quantum dots are more closely packed so that many near by particles can agglomerate. But in ZnS the inter particle distances are more and therefore less number of particles will be available for coalescence.

4.3 UV-Vis optical absorption study:

4.3.1 PbS quantum dots:

The UV-Vis absorption spectra of bare PbS quantum dots after SHI irradiation at different fluences is shown in figure 4.7.

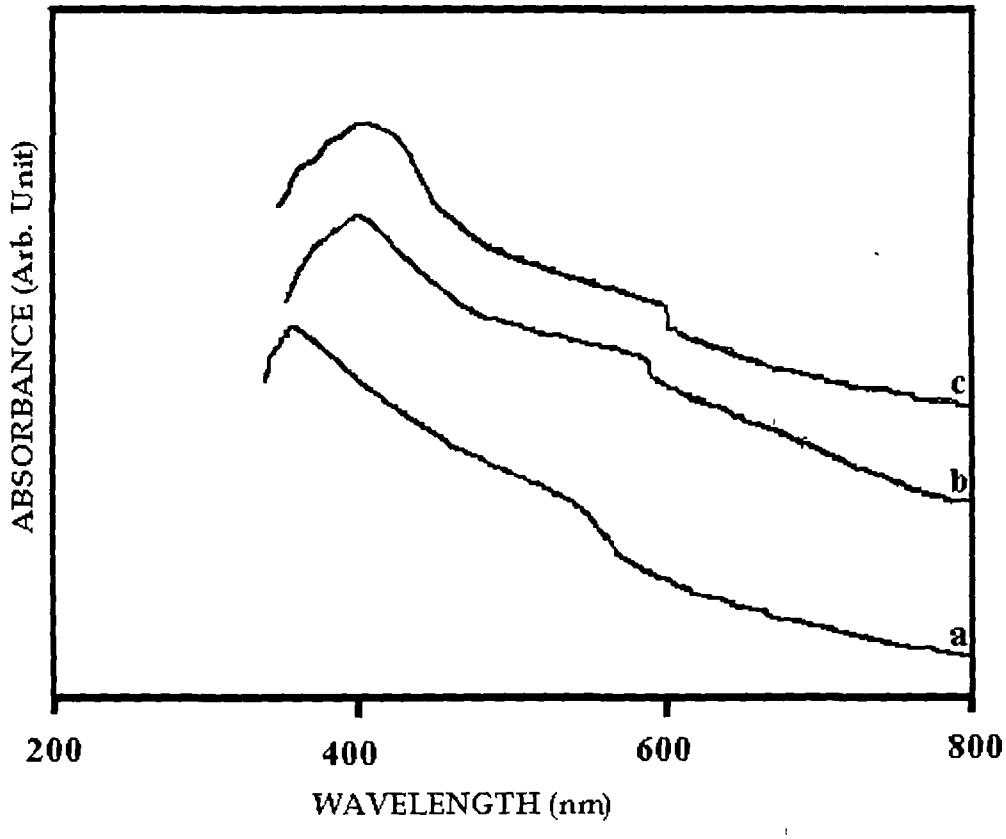

Figure 4.7: UV-Vis absorption spectra of bare PbS quantum dots after irradiating with fluences (a) 10^{12} (b) $5x10^{12}$ and (c) 10^{13} ions/cm^2

The spectra show red shift of absorption peaks compared to the corresponding spectra for unirradiated sample (chapter III) indicating formation of bigger particles during irradiation. The result is consistent with previous work [2

The shift in the onset of absorption and corresponding band gap enhancement at respective fluences is shown in Table 4.4. The calculated particle size using EMA is also given.

Table 4.4: Size of the bare PbS quantum dots calculated using EMA after SHI irradiation

Fluence (ions/cm^2)	Absorption edge from UV-Vis absorption spectra (nm)	Band gap of the nanoparticles (eV)	Calculated particle size (nm)
10^{12}	567	2.18	13.3
$5x10^{12}$	590	2.10	13.84
10^{13}	596	2.09	14.52

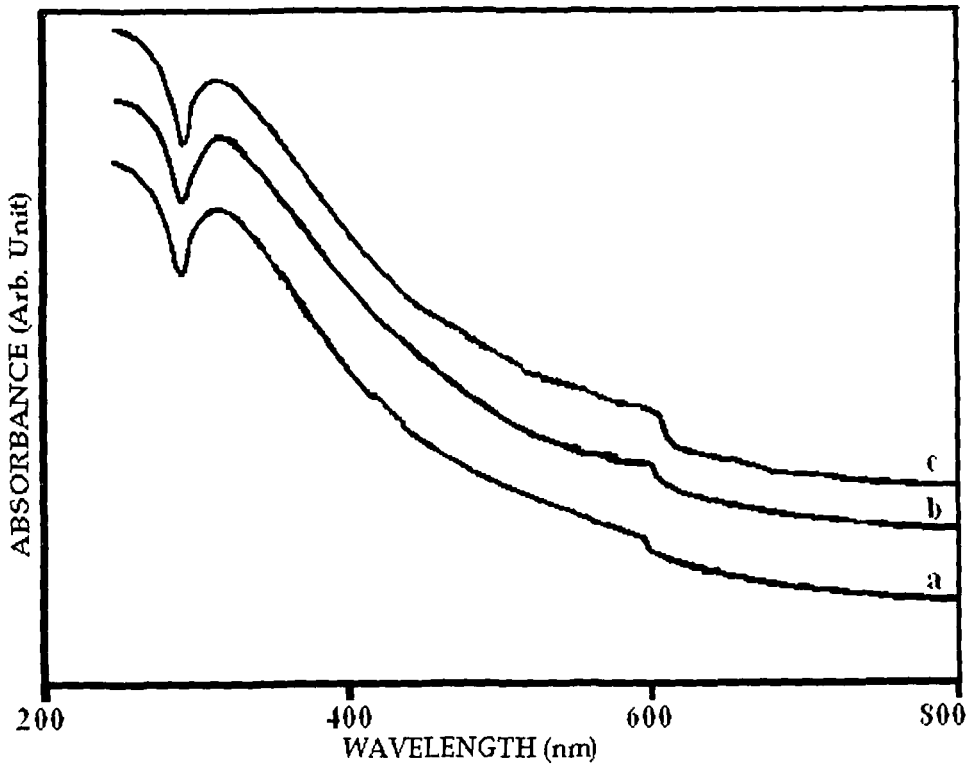

Figure 4.8: UV-Vis absorption spectra of coated PbS quantum dots after irradiating with fluences (a) 10^{12} (b) $5x10^{12}$ and (c) 10^{13} ions/cm^2

The UV-Vis absorption spectra of coated PbS quantum dots irradiated with different fluences 10^{12}, $5x10^{12}$ and 10^{13} ions/cm^2 are shown in figure 4.8.

The absorption edge is observed at around 510 nm without any significant shift from the corresponding position of the unirradiated sample (chapter III), indicating size consistency of the coated samples after SHI irradiation.

4.3.2 CdS quantum dots:

Figure 4.9 shows the UV-Vis absorption spectra of bare CdS quantum dots after SHI irradiation with fluences 10^{12}, $5x10^{12}$ and 10^{13} ions/cm^2 respectively.

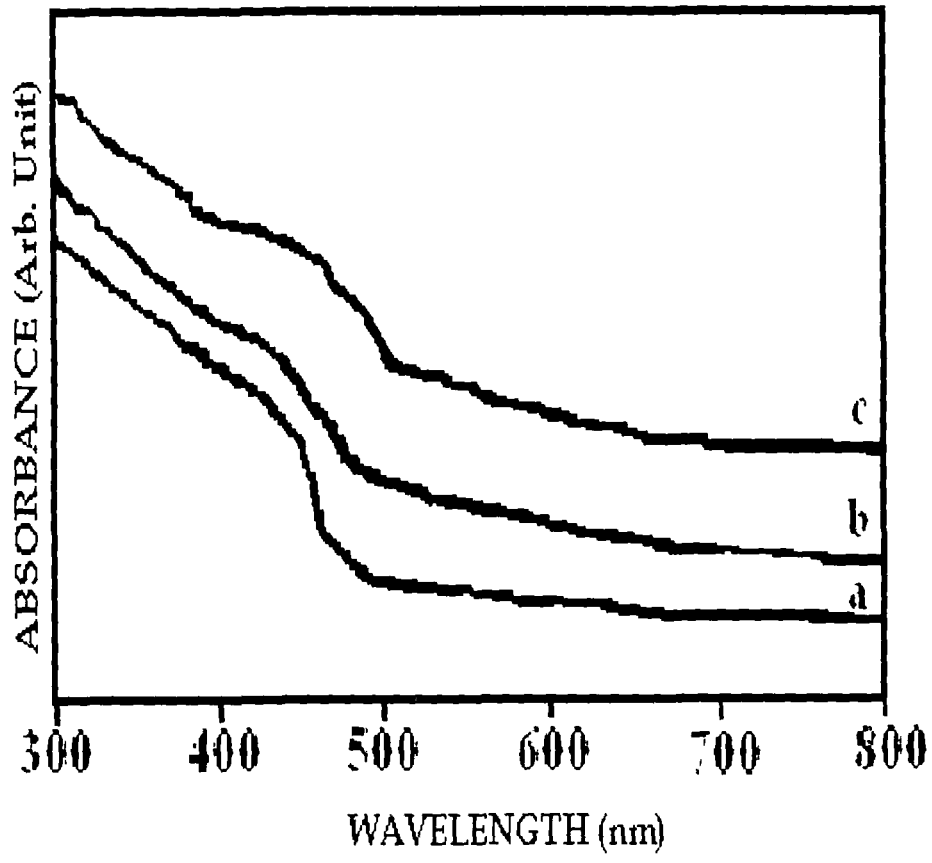

Figure 4.9: UV-Vis absorption spectra of bare CdS quantum dots after irradiating with fluences (a) 10^{12} (b) $5x10^{12}$ and (c) 10^{13} ions/cm^2

For bare CdS quantum dots, like PbS quantum dots clear red shift of the absorption edge compared to unirradiated samples (chapter III) is observed with increasing fluences. This indicates the size enhancement of the quantum

particles. The shifts in the onsets of absorption and corresponding band gap enhancement at respective fluences are shown in Table 4.5. The calculated particle size using EMA is also given.

Table 4.5: Size of the bare CdS quantum dots calculated using EMA after SHI irradiation

Fluence (ions/cm^2)	Absorption edge from UV-Vis absorption spectra (nm)	Band gap of the nanoparticles (eV)	Calculated particle size (nm)
10^{12}	475	2.61	7.3
$5x10^{12}$	481	2.58	7.8
10^{13}	500	2.48	11.9

The UV-Vis absorption spectra of coated CdS quantum dots after irradiating with fluences 10^{12}, $5x10^{12}$ and 10^{13} ions/cm^2 are shown in figure 4.10.

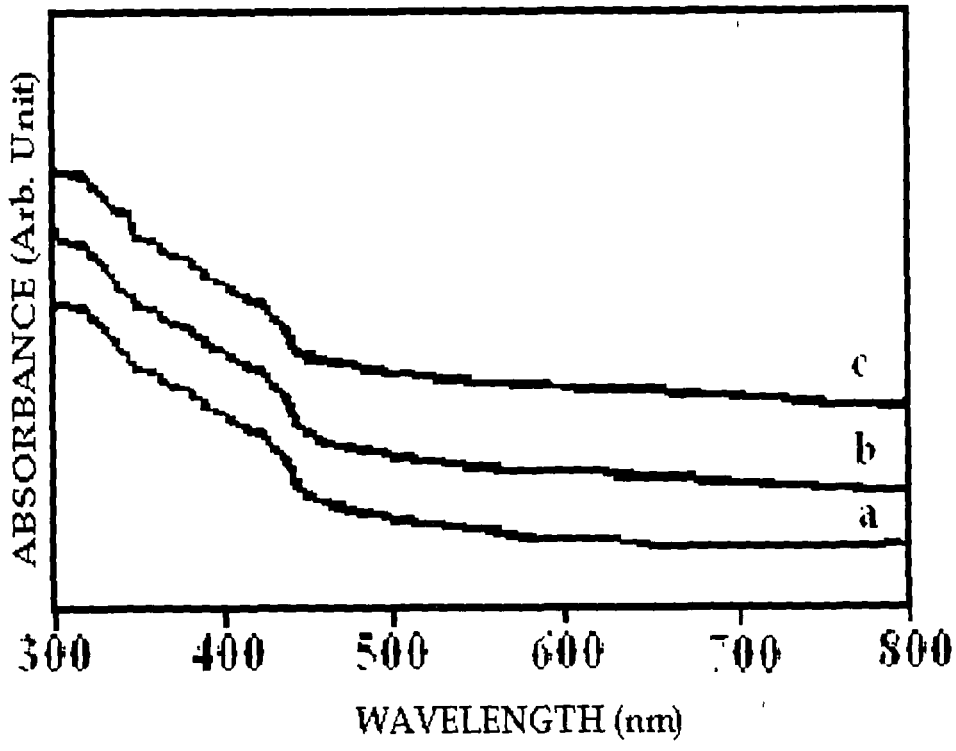

Figure 4.10: UV-Vis absorption spectra of coated CdS quantum dots after irradiating with fluences (a) 10^{12} (b) $5x10^{12}$ and (c) 10^{13} ions/cm^2

The onsets of absorption are occurring ~ 439 nm which is same as in case of unirradiated sample. Thus the UV-Vis spectra of coated CdS quantum dots samples reveal the size consistency of the particles after SHI irradiation.

4.3.3 ZnS quantum dots:

The UV-Vis absorption spectra of bare ZnS quantum dot after SHI irradiation with fluences 10^{12}, $5x10^{12}$ and 10^{13} ions/cm^2 are shown in figure 4.11. After irradiating the samples with the lowest fluence the onset of absorption is observed at ~ 327 nm which is just 1nm red shifted from the corresponding value for unirradiated sample (326 nm). However the extent of red shift increases with increase in ion fluence.

The blue shifted energy and calculated particle size of bare ZnS quantum dot is presented in Table 4.6.

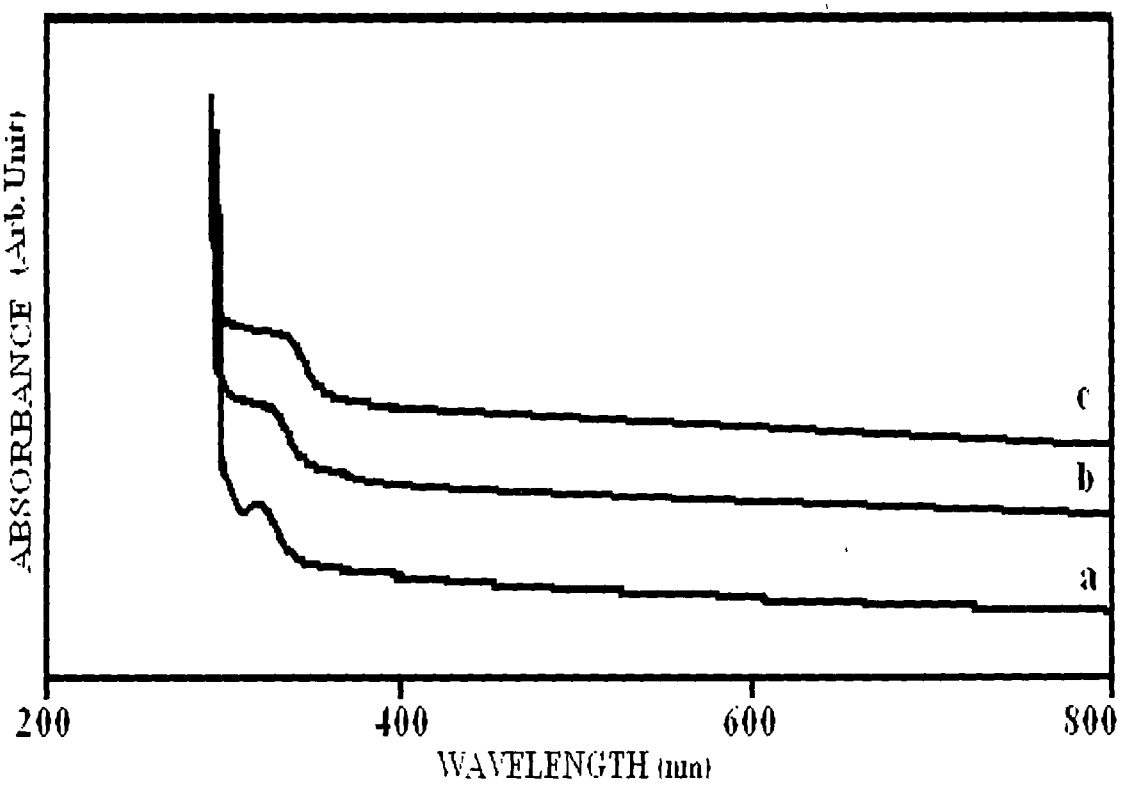

Figure 4.11: UV-Vis absorption spectra of bare ZnS quantum dots after irradiating with fluences (a) 10^{12} (b) $5x10^{12}$ and (c) 10^{13}ions/cm^2

Table 4.6: Size of the bare ZnS quantum dots calculated using EMA after SHI irradiation

Fluence (ions/cm^2)	Absorption edge from UV-Vis absorption spectra (nm)	Band gap of the nanoparticles (eV)	Calculated particle size (nm)
10^{12}	327	3.79	6.8
$5x10^{12}$	331.8	3.75	7.2
10^{13}	336	3.69	7.4

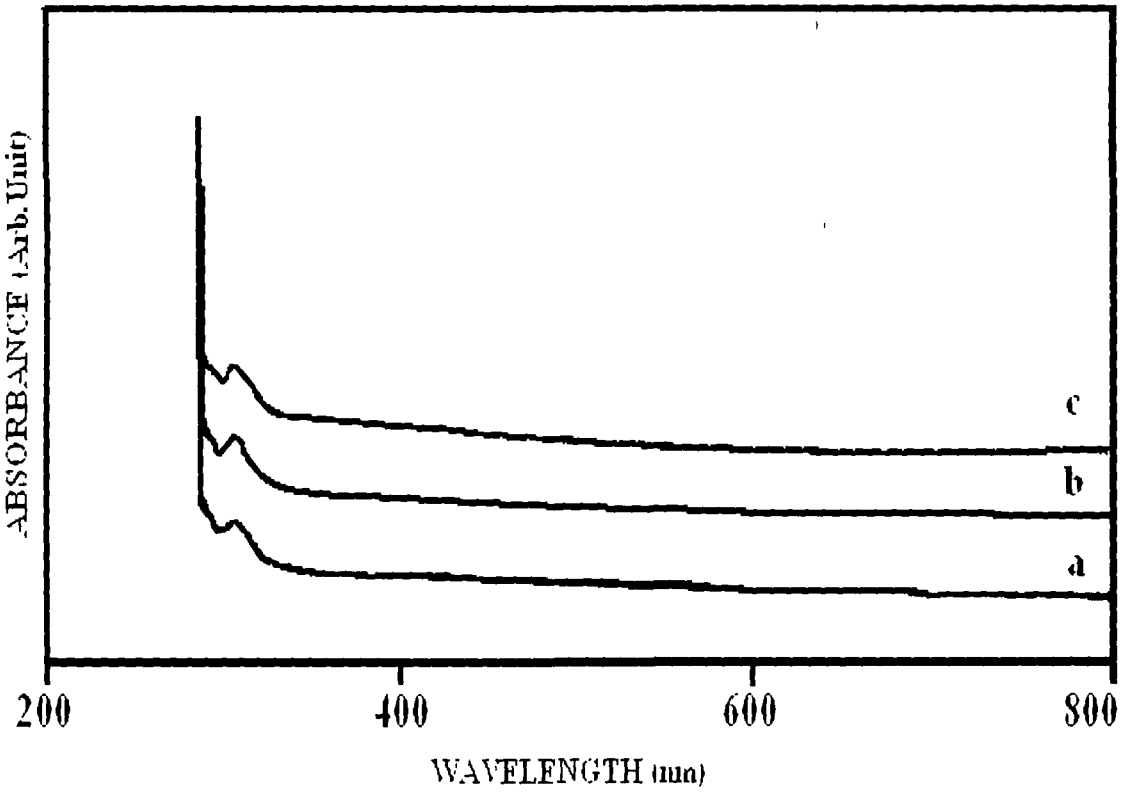

Figure 4.12: UV-Vis absorption spectra of coated ZnS quantum dots after irradiating with fluences (a) 10^{12} (b) $5x10^{12}$ and (c) 10^{13} ions/cm^2

The UV-Vis absorption spectra of silica coated ZnS quantum dots after irradiating with fluences 10^{12}, $5x10^{12}$ and 10^{13} ions/cm^2 are shown in figure 4.12.

Unlike bare samples no red shift was detected in case of coated ZnS quantum dots. Thus like silica coated PbS and ZnS quantum dots the result of

UV-Vis spectroscopy for ZnS quantum dots also indicates the size consistency of the coated particles under SHI irradiation.

4.4 Transmission Electron Micrograph (TEM) study:

4.4.1 PbS quantum dots:

TEM study of the quantum dots after SHI irradiation were carried out to

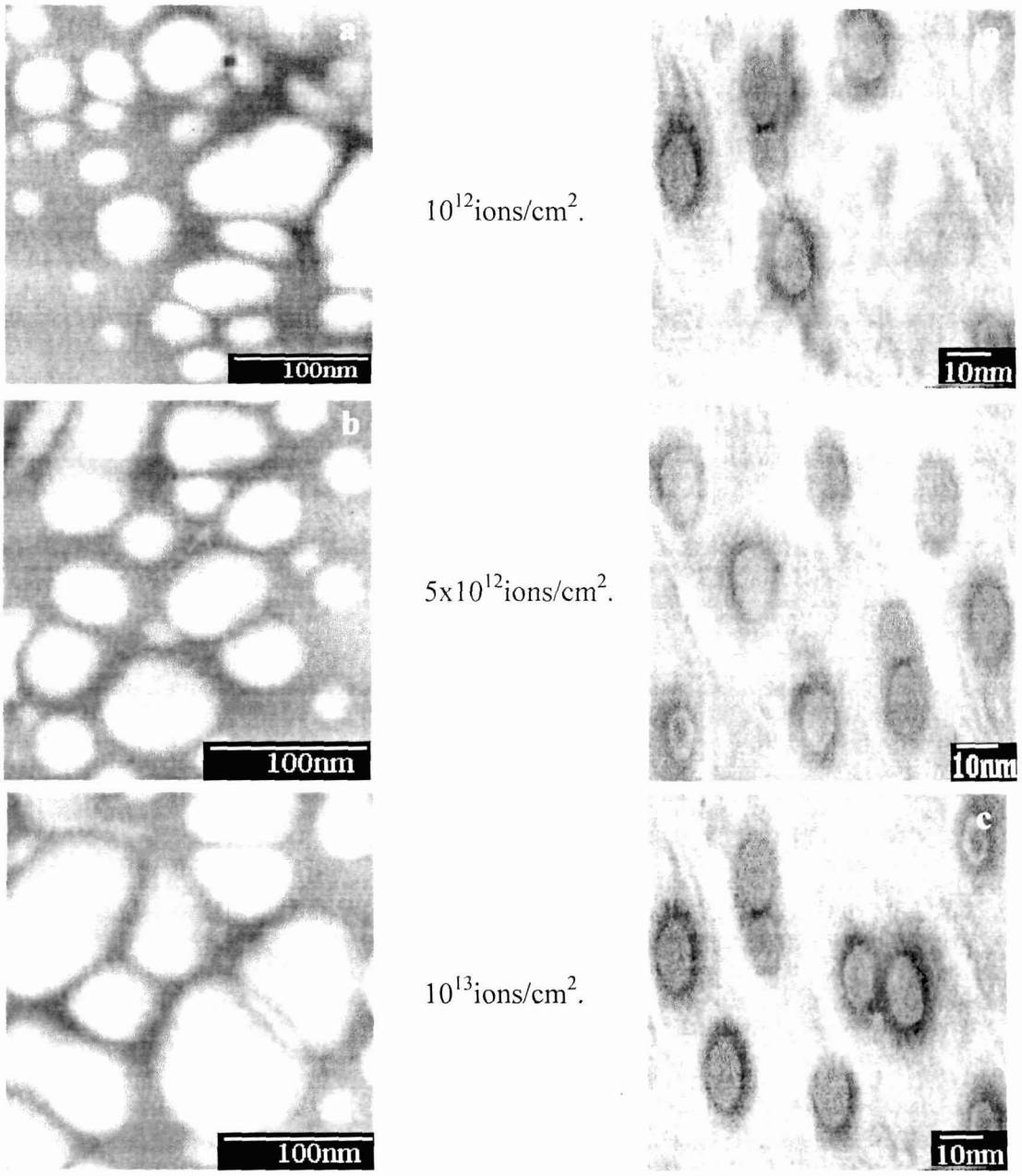

Figure 4.13: TEM images of bare (left) and coated (right) PbS quantum dots after irradiating with fluences 10^{12}, 5x10^{12} and 10^{13} ions/cm^2

calculate the actual size of the quantum particles and to investigate the structural changes of the samples.

The TEM images of bare and coated PbS quantum dots after SHI irradiation with different fluences are shown in figure 4.13. The agglomeration of bare nanoparticles after SHI irradiation can be observed clearly from the respective TEM images. The average size calculated from TEM after irradiating the samples with fluences 10^{12}, $5x10^{12}$ and 10^{13} ions/cm^2, were 80 nm, 96 nm and 120 nm respectively. Also there is change in shape of the particles after irradiation and most of them are no longer spherical as in case of unirradiated particles. As discussed in section 4.2 the heat produced in the ion track during SHI irradiation may amorphize the matrix such that closely placed nanoparticles agglomerate to form bigger particles.

The TEM images of the coated PbS quantum dots indicate no particle growth under SHI irradiation. The shape of the quantum dots also remains almost spherical. Thus SiO_2 coating can prevent the agglomeration of nano particles under SHI irradiation.

4.4.2 CdS quantum dots:

The TEM images of bare and coated CdS quantum dot samples after irradiating with different fluences (10^{12}, $5x10^{12}$ and 10^{13} ions/cm^2) are shown in figure 4.14.

The particle growth and also deviation from spherical shape has been observed in case of bare samples. The average size calculated from TEM after irradiation with fluences 10^{12}, 5 x 10^{12} and 10^{13} ions/cm^2 were 20, 35and 48 nm respectively.

In case of coated samples it is observed that the particles remain almost stable both in size and shape after SHI irradiation.

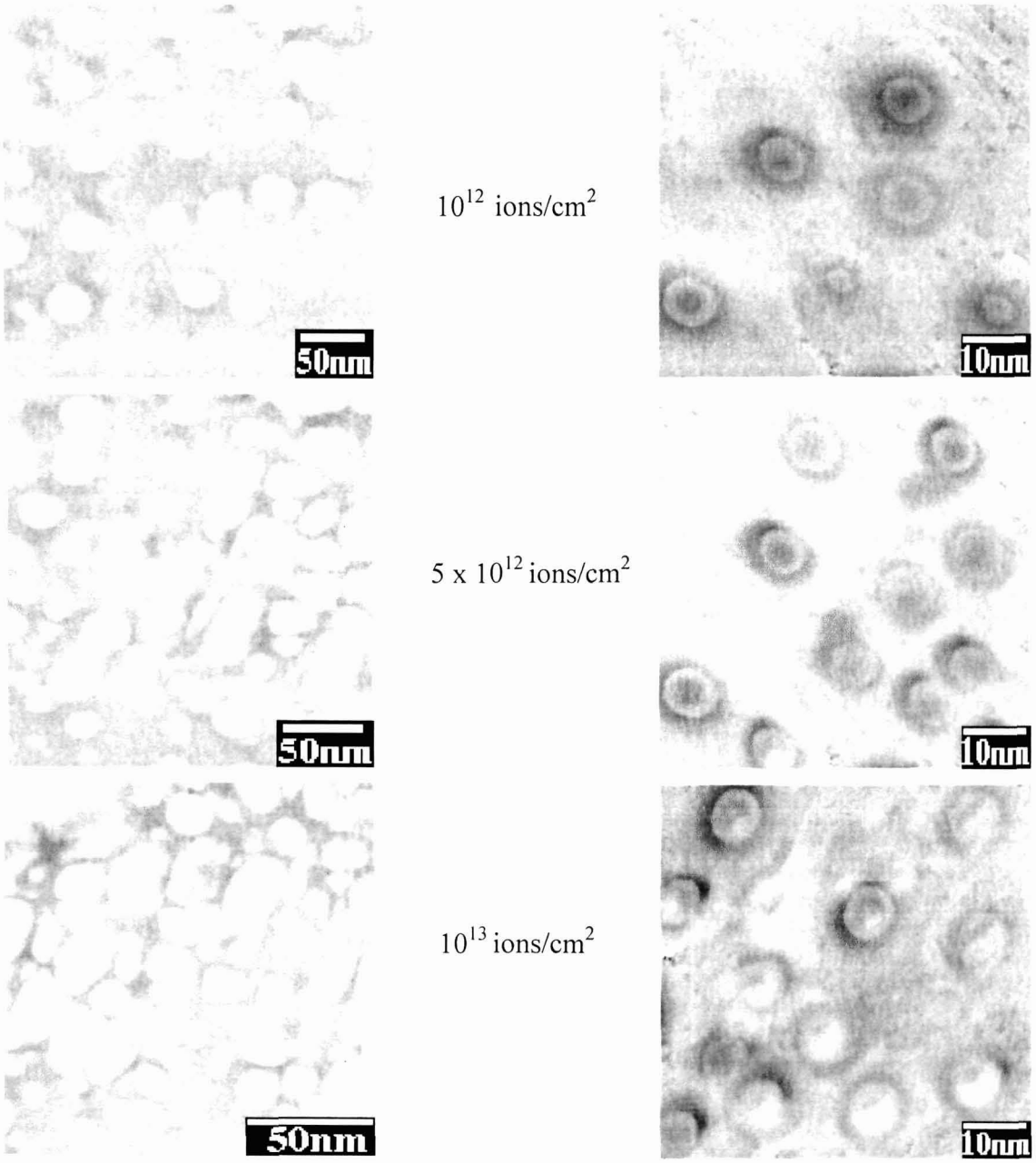

Figure 4.14: TEM images of bare (left) and coated (right) CdS quantum dots after irradiating with fluences 10^{12}, 5x10^{12} and 10^{13} ions/cm^2.

4.4.3 ZnS quantum dots:

The TEM images of uncoated and coated ZnS quantum dots after SHI irradiation at fluences10^{12}, 5x10^{12} and 10^{13} ions/cm^2 are shown in the figure 4.15. For uncoated particles, the size calculated from TEM, after irradiating with

fluences 10^{12}, $5x10^{12}$ and 10^{13} ions/cm^2 were18, 30 and 43 nm respectively. Thus the particle size enhances considerably after irradiation.

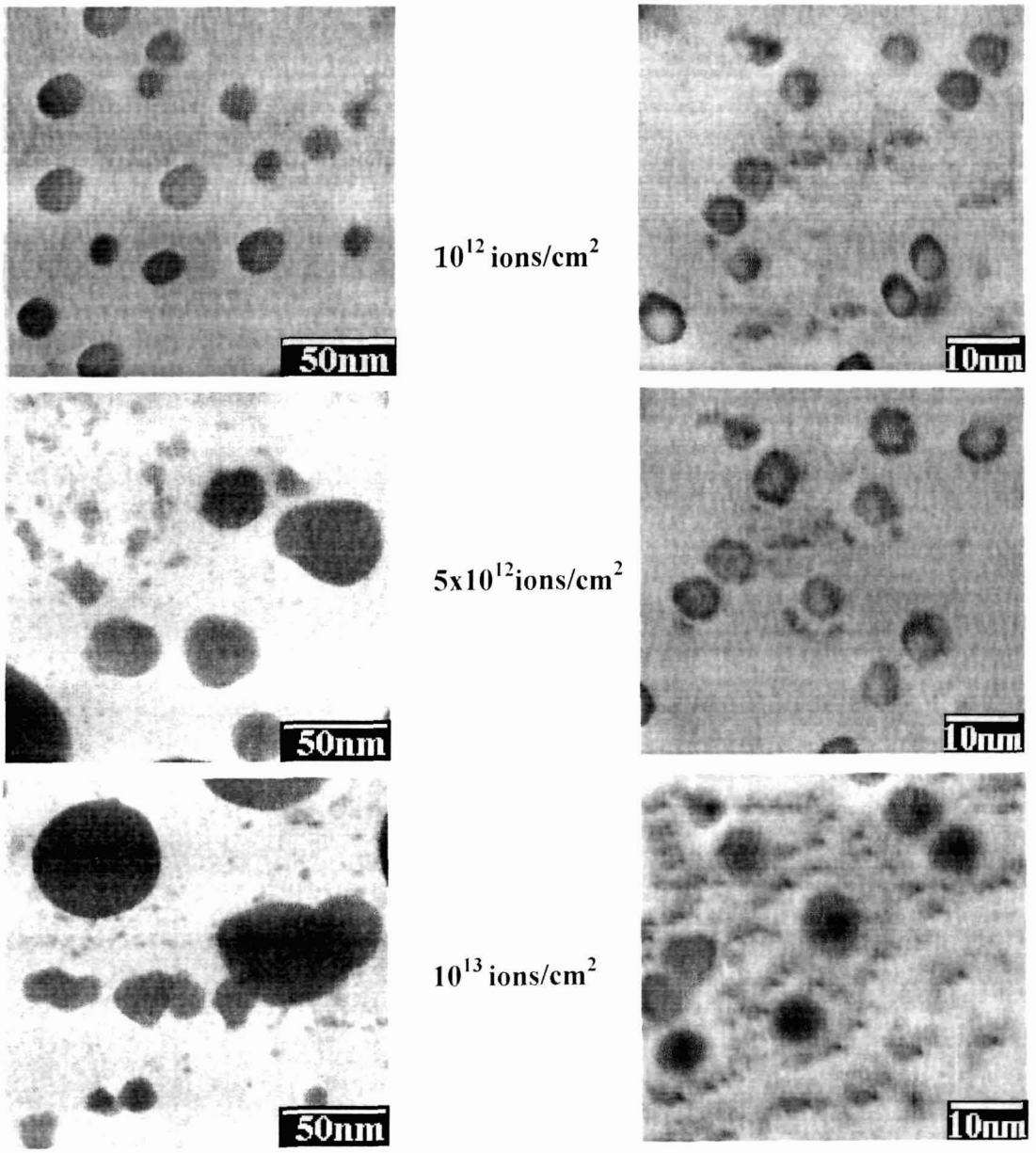

Figure 4.15: TEM images of bare (left) and coated (right) ZnS quantum dots after irradiating with fluences 10^{12}, $5x10^{12}$ and 10^{13} ions/cm^2.

But coated samples were found almost consistent with there size measuring ~ 6 nm, which is same as before irradiation. Thus, like PbS and CdS quantum dots, ZnS quantum dots also show greater stability under SHI

irradiation after coating. Thus SiO_2 can prevent particle agglomeration after SHI irradiation.

The results so far described in this chapter shows that the bare nanoparticles are affected by SHI irradiation and their size and shape changes considerably. Though the theoretical results showed size enhancement of the particles corresponding to red shifted absorption edges, the results were much lower than that determined experimentally from XRD and TEM. We believe that the absorption recorded in the UV-Vis absorption spectra are due to the particles which are less affected by SHI irradiation. It is obvious because all the particles in the sample will not be equally affected due to irradiation, those lying near the ion track will be affected more. It is also believed that the bigger particles, some of them being no longer spherical, contribute to the tail absorption of the UV-Vis absorption spectra. For PbS quantum dots the XRD and TEM results differ and the difference increases for particles irradiated with higher fluence. This indicates that Schrrer formula may not be accurate for determining the size of too large particles. However the size calculated by XRD and TEM are comparable in cases of CdS and ZnS quantum dots.

4.5 Photoluminescence Study:

4.5.1 PbS quantum dots:

Figure 4.16 shows the PL spectra of PbS quantum dots after SHI irradiation with fluences 10^{12}, $5x10^{12}$ and 10^{13} ions/cm^2. For the lowest fluence (10^{12} ions/cm^2) the PL peak appears at 700 nm. This low energy peak has already been observed in case of unirradiated sample (chapter III) and attributed to surface states emission. However the intensity is significantly increased in case of irradiated sample. The possible mechanism for the enhancement of PL intensity is the thermal detrapping of charge carriers from the shallow trap states. In a nanocrystalline material there will be many different trap levels, each with a slightly different trapping energy.

After the excitation of the nanocrystals an electron can be trapped in a shallow trap state from which it cannot escape. At higher temperatures the trapped electrons can have sufficient thermal energy to escape from the trap level into the conduction band and thereafter recombine with trapped holes giving intense luminescence.

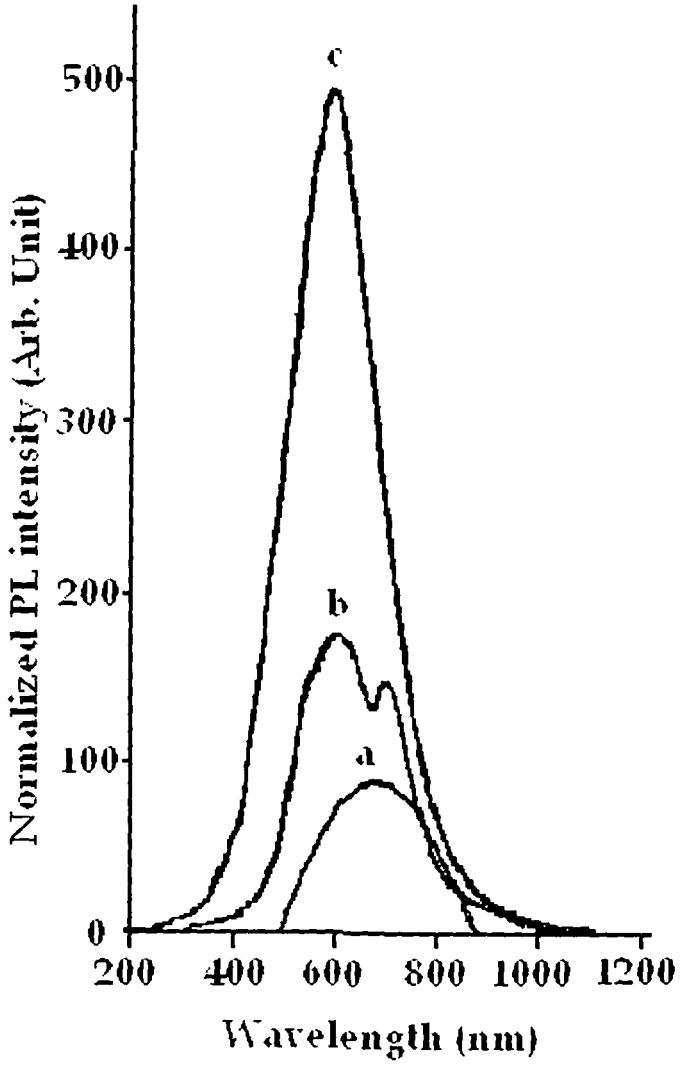

Figure 4.16: PL spectra of bare PbS quantum dots after irradiating with fluences (a) 10^{12} (b) $5x10^{12}$ and (c) 10^{13} ions/cm^2

No shift in position of this peak has been observed though the particles are growing in size upon ion irradiation, as confirmed from XRD, UV-Vis absorption spectra and TEM. Such size independent surface state emission has been reported earlier [21].

The increase in luminescence intensity may be due to the combined effect of surface state emission as well as emission from the large defects generated during SHI irradiation [22]. Similar observation has been reported earlier also [20].

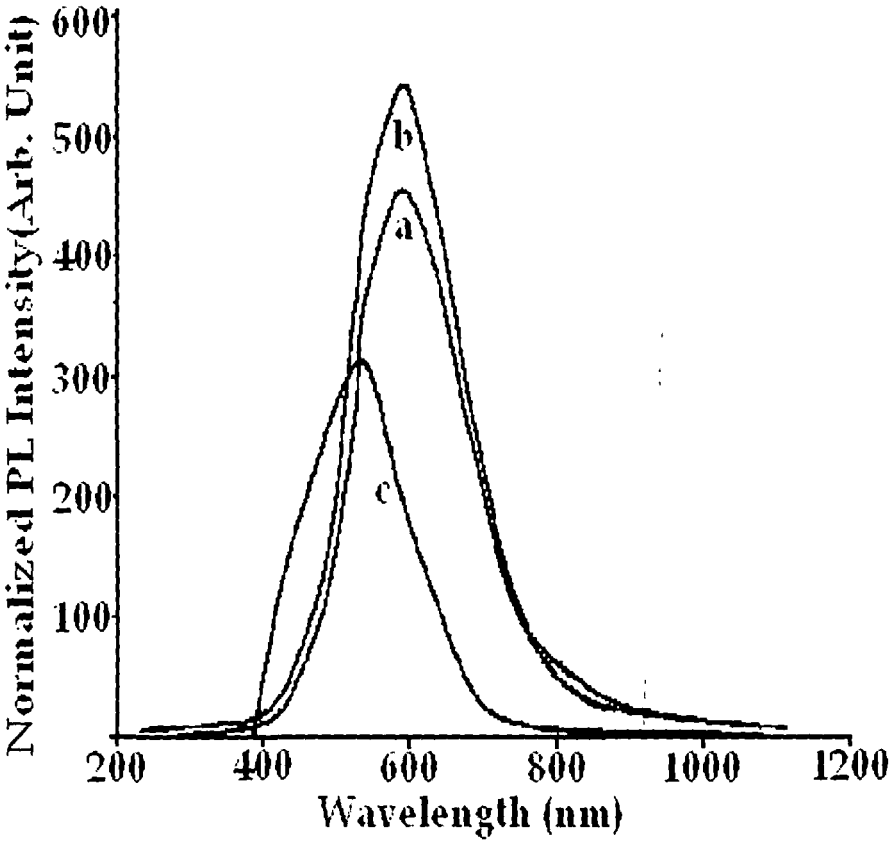

Figure 4.17: PL spectra of coated PbS quantum dots after irradiating with fluences (a) 10^{12} (b) $5x10^{12}$ and (c) 10^{13} ions/cm^2

It is interesting to note the PL peak at 600 nm appearing after irradiation with fluence $5x10^{12}$ ions/cm^2 along with the peak at 700 nm. The intensity of the peak increases when the sample is irradiated with fluence 10^{13} ions/cm^2, completely dominating the peak at 700 nm. The high energy peak indicates the involvement of excitons in luminescence process, after irradiating the sample with higher fluence. We believe that the excitonic recombination is possible due to thermal detrapping of charge carriers owing to the enormous heat generated during SHI irradiation [23]. The possibility of detrapping is expected to be

increased with ion fluence, thus enhancing luminescence intensity. In case of coated sample the intensity of the 700 nm peak increases with fluences up to $5x10^{12}$ions/cm^2. The enhancement of the luminescence intensity is believed to be due to thermal detrapping of charge carriers as well as more defect states generated after SHI irradiation. Another peak appears at around 550 nm after irradiating the sample with fluence 10^{13} ions/cm^2. It is believed that a PbO layer is formed due to the interaction of Pb with oxygen in SiO_2. The high band gap of PbO (2.75 eV) [24] also supports the probability of such low wavelength emission. Also the XRD peak around 53^0 [19] indicates the formation of PbO in the sample.

4.5.2 CdS quantum dots:

The PL spectra of uncoated CdS quantum dots after SHI irradiation at fluences 10^{12}, $5x10^{12}$ and 10^{13} ions/cm^2 are shown in figure 4.18.

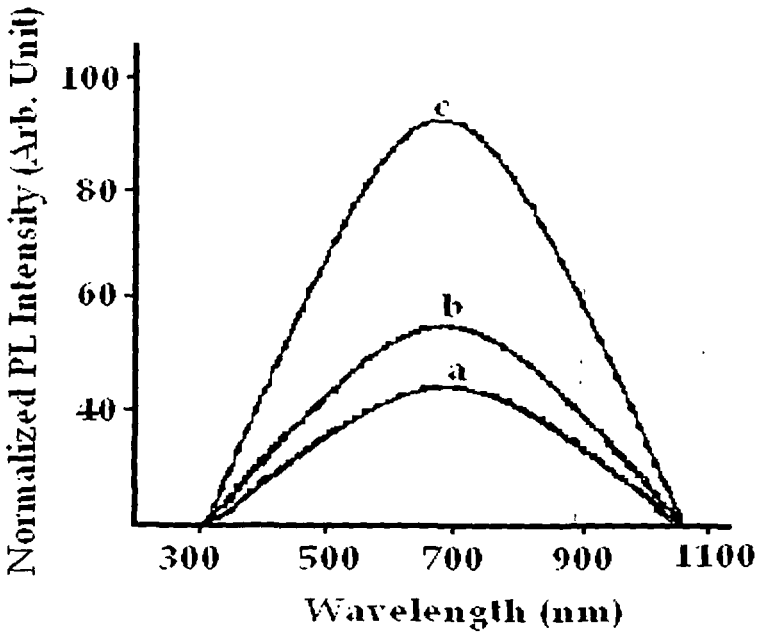

Figure 4.18: PL spectra of bare CdS quantum dots after irradiating with fluences (a) 10^{12} (b) $5x10^{12}$ and (c) 10^{13} ions/cm^2

As observed from the spectra, irrespective of the fluence applied, the PL peaks are appearing at 700 nm as in case of unirradiated samples. Thus there is no shift of PL peak position of the samples after SHI irradiation. Also the PL intensity significantly increases with fluence as observed in case of bare PbS quantum dot samples.

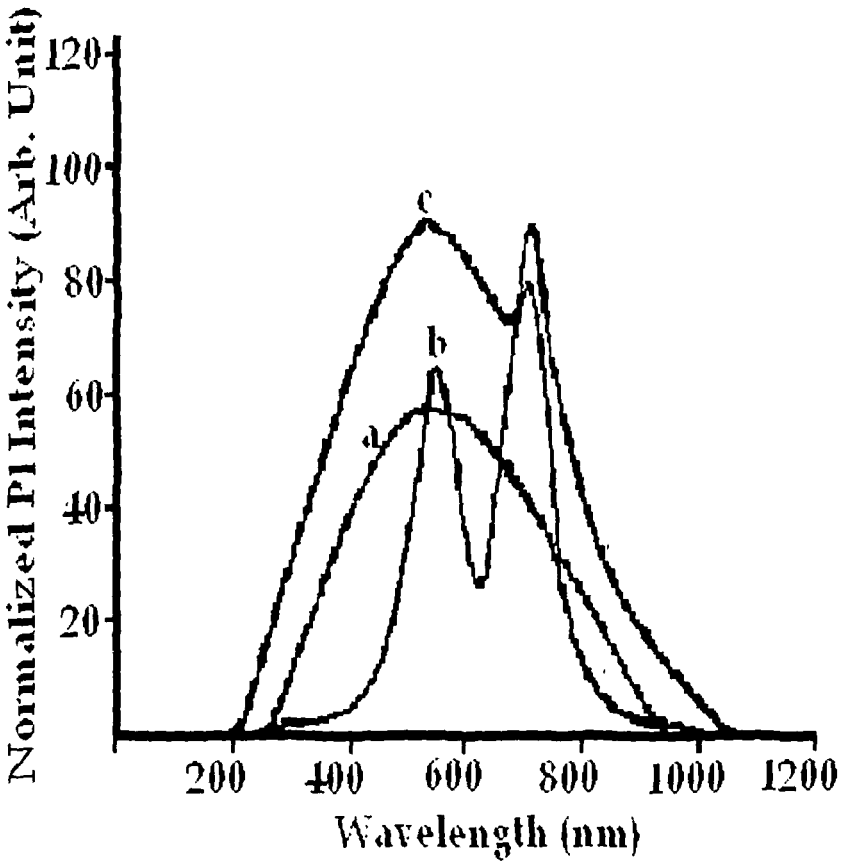

Figure 4.19: PL spectra of coated CdS quantum dots after irradiating with fluences (a) 10^{12} (b) $5x10^{12}$ and (c) 10^{13} ions/cm^2

In case of coated sample, the peak appears at 570 nm with significant increase in luminescence intensity after irradiating with fluence 10^{12} ions/ cm^2, as revealed from the PL spectra in figure 4.19. But after irradiating the sample with higher fluences the peak at 700 nm, which is assigned to CdO, appears along with the high energy peak. We believe that during SHI irradiation some Cd^{++} ions become free to react with oxygen atoms in SiO_2 to form CdO [25].

The intensity of both the peaks increases with ion fluence. The increase in intensity of the high energy peak may be due to the thermal detrapping of the charge carriers during SHI irradiation.

4.5.3 ZnS quantum dots:

The PL spectra of bare ZnS quantum dots after SHI irradiation with fluences 10^{12}, 5 x 10^{12} and 10^{13} ions/cm^2 are shown in the figure 4.20.

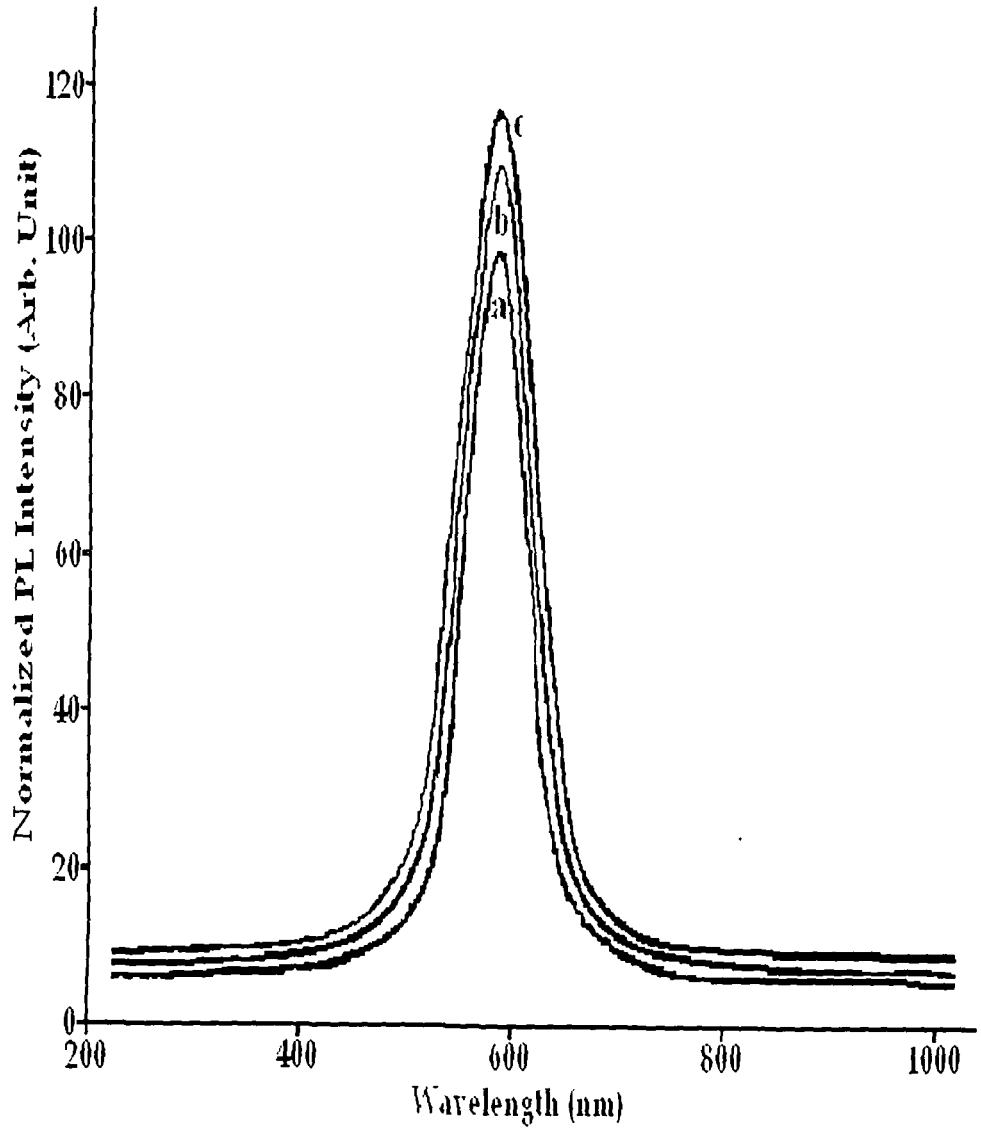

Figure 4.20: PL spectra of bare ZnS quantum dot after irradiating with fluences (a) 10^{12} (b) 5x10^{12} and (c) 10^{13} ions/cm^2

Like PbS and CdS quantum dots, in case of ZnS (bare) quantum dots also significant increase in PL intensity has been observed, which is supposed to be due to increase in defect concentration as well as thermal detrapping of charge carriers as discussed earlier. The PL peak position also does not change, appearing at 591 nm as in case of unirradiated sample.

Figure 4.21 shows the PL spectra of coated ZnS quantum dots after SHI irradiation. In case of coated samples, the PL peak appears at 350 nm as in case of unirradiated sample. This peak is already assigned to band edge emission. However the PL intensity increases considerably with increased fluences which is believed to be due to thermal detrapping of charge carriers.

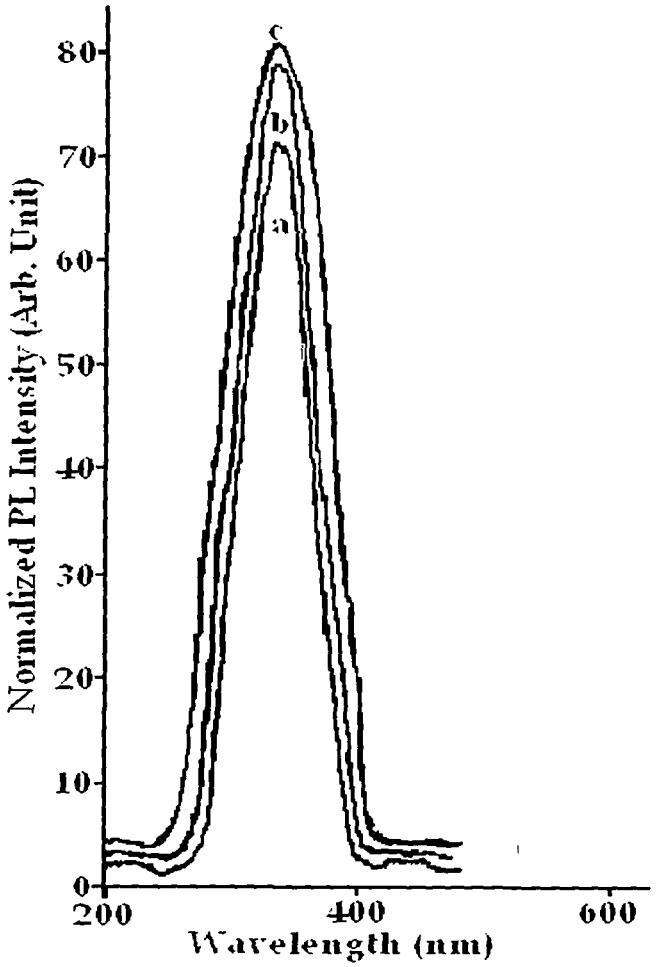

Figure 4.21: PL spectra of coated ZnS quantum dots after irradiating with fluences (a) 10^{12} (b) $5x10^{12}$ and (c) 10^{13} ions/cm^2

The FWHM of the PL peak in case of coated samples becomes narrower indicating low size distribution of the sample. Also the spectra reveal that e-h recombination plays the main role in case of luminescence of the coated ZnS particles overcoming contribution from the surface states.

In this chapter the SHI irradiation induced effects on PbS, CdS and ZnS quantum dots (both bare and coated) have been presented. The results from XRD, UV-Vis absorption spectra and TEM analysis show size enhancement of bare quantum dots upon SHI irradiation, whereas coated particles were found stable regarding size. The PL behavior has been modified in both bare and coated quantum dots. SHI irradiation effects on bare CdS and ZnS quantum dots using Cl^{+9} [15, 20] ion beam were reported earlier. To the best of my knowledge for the first time such studies have been carried out with silica coated quantum dots [25] along with bare PbS [23, 26] quantum dots. In that sense this work is novel and original.

References:

1. Rück D.M., *Nucl. Instr. and Meth. B,* **166/167** (2000) 602.
2. Venkatesan T., *Nucl. Instr. and Meth. B,* **7/8** (1985) 461.
3. Balanzat E., Bouffard S., Le Moël A. and Betz N., *Nucl. Instr. and Meth. B,* **91** (1994) 140.
4. Popok V.N., Odzhaev V.B., Kozlov I.P., Azarko I.I., Karpovich I.A. and Sviridov D.V., *Nucl. Instr. and Meth. B,* **129** (1997) 60.
5. Davenas J., Stevenson I., Celette N., Cambon S., Gardette J. L., Rivaton A. and Vignoud. L., *Nucl. Instr. and Meth. B,* **191** (2002) 653.
6. Laskarakis A., Gravalidis C., and Logothetidis S., *Nucl. Instr. and Meth. B,* **216** (2004) 131.
7. Guenther M., Gerlach G., Suchaneck G., Sahre K., Eichhorn K.J., Baturin V. and Duvanov S., *Nucl. Instr. and Meth. B,* **216** (2004) 143.
8. White C.W., Budai J.D., Withrow S.P., Zhu J.G., Pennycook S.J., Zuhr R.A., Hembree D.M. Jr., Henderson D.O., Magruder R.H., Yacaman M.J., Mondragon G., Prawer S., *Nucl. Instru. and Meth.* B, **127/128** (1997) 545.
9. Bonafos C., Garrido B., Lo´pez M., Romano-Rodriguez A., Gonza´lez-Varona O., Pe´ rez-Rodrı´guez A, and Morante J.R. *Appl. Phys. Lett.,* **72** (1998) 3488.
10. Tetelbaum D.I., Gorshkov O.N., Trushun S.A., Revin D.G., Gaponova D.M. and Eckstein W., *Nanotechnology,* **11** (2000) 295.
11. Chaudhari P.S. and Bhave T.M., *J. Appl. Phys.,* **93** (2003) 3486.
12. Mohanta D., Nath S.S., Mishra N.C. and Choudhury A., *Bull. Mat. Sci.,* **26** (2003) 289.
13. Mohanta D., Nath S.S., Bordoloi A., Choudhury A. Dolui S.K. and Mishra N.C., *J. Appl. Phys,* **92** (2002) 7149.
14. Berthelot A., Hemon S., Gourbilleau F., Dufour E., and Paumier E., *Nucl. Instr. Meth. B,* **146** (1998) 437.
15. Mohanta D., *'Synthesis of semiconductor quantum dots on polymer matrix and application in nonlinear optics/electronics'* Ph.D. Thesis, 2003

16. Avasthi D.K., *Current Sci.*, **78**, (2000) 1297.
17. Mehta G.K., Patro A.P., *Nucl. Instrum. Methods A*, **268** (1988) 334.
18. Kanjilal D., Chopra S., Narayanan M.M., Iyer I.S., Jha V., Joshi R. and Datta S.K., *Nucl. Instrum. Methods A*, **238** (1993) 97.
19. Li C.Y., Zeng J.D., Lang L. and Min L.J., *Chin. J. Chem.*, **22** (2004) 1288.
20. Nath S.S., *"Synthesis of semiconductor quantum dots on polymer matrix and their applications in Electronics, photonics, and nonlinear optics"*, PhD thesis, 2004.
21. Nanda J. and Sarma D.D., *J. Appl. Phys.*, **90** (2001) 2504.
22. Sehrawat K., Singh F., Singh B.P. and Mehra R.M., *J. Luminescence*, **106** (2004) 21.
23. Chowdhury S., Mohanta D., Ahmed G.A., Dolui S.K., Avasthi D.K. and Choudhury A., *J. Luminescence*, **114** (2005) 95.
24. Keezer R.C., Bowman D.L. and Beeker J.H., *J. Appl. Phys.*, **39** (1968) 2062.
25. Chowdhury S., Ahmed G.A., Mohanta D., Dolui S.K., Avasthi D.K. and Choudhury A., *Nucl. Instr. and Meth. B*, **240** (2005) 690.
26. Chowdhury S., Dolui S.K., Avasthi D.K. and Choudhury A., *Ind.J.Phys* (In Press).

CHAPTER V

5.1. Nonlinear Optics:

Nonlinear optics is a material phenomenon in which intense light induces a nonlinear response in the medium, and in return the medium modifies the optical fields in a nonlinear way. Any real, physical oscillating system will exhibit a nonlinear response when it is overdriven. In an optical system, a nonlinear response can occur when there is sufficiently intense illumination. In fact, all media are nonlinear to a certain degree.

The field of nonlinear optics was ushered in with the development of the first laser by Maimen [1] in 1960. Although nonlinear optical effects had been known as early as the nineteenth century (The Pockels and Kerr effects), only DC fields could be produced with enough intensity to reach the regime of nonlinear optical response. Due to this deficiency, nonlinear optics remained unexplored until the classic experiment by Franken and co-workers [2] in which second-harmonic generation was demonstrated in quartz with the use of a ruby laser. Soon after the first observations of optical nonlinearities were made, a theoretical explanation was provided based upon the nonlinear response of electron oscillators in the atomic Coulomb field. The field of nonlinear optics has continued to grow at a tremendous rate since its inception and has proven to be a nearly inexhaustible source of new phenomena and optical techniques.

For the typical light intensities encountered in everyday situations, the response of a medium to an applied optical field can, to a good approximation, be considered linear. In other words, the optical properties of the medium do not depend on the intensity of the incident field. But in presence of high intensity beams such as laser beam, the optical properties of the medium become dependent on the intensity of the applied field. Under such conditions the light waves can interact with the medium and with each other, resulting in a wide range of effects unseen at the lower everyday intensities. This is the realm

of non-linear optics. An extensive discussion of high-order nonlinearities can be found in literature [3 - 6].

When a material medium is subjected to one or more electromagnetic waves, the atoms and molecules of the medium oscillate not only at the frequencies of the electric fields applied, but also at different combinations of those frequencies, as a result of the nonlinear response of the medium. The particles of the medium are displaced from their equilibrium positions, so that positively charged particles move in the direction of the field, while the negatively charged particles move in the direction opposite to the direction of the applied electric fields. As a result of the displacement of these charged particles, dipole moments are created and the dipole moment per unit volume describes the induced polarization of the medium. When the applied electric fields are sufficiently small, the electric polarization is approximately linearly proportional with the applied electric field **E**

$$\mathbf{P} = \chi \mathbf{E} \qquad (5.1)$$

where χ is called the polarizability or dielectric susceptibility or electric susceptibility tensor of the medium and is constant only in the sense of being independent of **E**; its magnitude is a function of frequency. This is the case of linear optics. However, when the applied electric fields are high enough, the induced polarization has a nonlinear dependence on these electric fields and can be expressed as a power series with respect to the electric field:

$$\begin{aligned} \mathbf{P} &= \chi^{(1)}.\,\mathbf{E} + \chi^{(2)}.\,\mathbf{E}\,\mathbf{E} + \chi^{(3)}.\,\mathbf{E}\,\mathbf{E}\,\mathbf{E}..... \\ &= \mathbf{P}^{(1)} + \mathbf{P}^{(2)} + \mathbf{P}^{(3)} + ... \\ &= \mathbf{P}^{(1)} + \mathbf{P}^{NL} \end{aligned} \qquad (5.2)$$

where $\chi^{(1)}$ is the linear susceptibility, $\chi^{(2)}$ is the second order nonlinear susceptibility, and $\chi^{(3)}$ is the third order nonlinear susceptibility. The term $\chi^{(1)}$ is responsible for linear absorption and refraction, and is the only term that

reflects the linearity between the induced polarization and the incident electric field. The term $\chi^{(2)}$ is present only in noncentrosymmetric materials, i.e. materials that do not have inversion symmetry. $\chi^{(2)}$ is responsible for sum and difference frequency mixing, optical rectification, and the electro-optic effect. Third-order nonlinear optical interactions, which are described by the term $\chi^{(3)}$, can take place in any material. Equation 5.2 shows that the total polarization (**P**) can be expressed as sum of linear $\mathbf{P}^{(1)}$ and nonlinear contributions $\mathbf{P}^{NL}$. Third-order nonlinear optical materials can be useful for all optical switching and signal processing. The significance of the higher order terms increases with the increase in the intensity of the light source.

The third-order susceptibility, $\chi^{(3)}$, describes third harmonic generation, four-wave mixing, and the optical Kerr effect. Optical switching and image processing are some of the important technological applications of $\chi^{(3)}$ processes.

For a material possessing third-order optical nonlinearity the relation between its refractive index (n) and the intensity of incident light(I) , can be expressed as;

$$n = n_0 + n_2 I \qquad (5.3)$$

where n_o is the refractive index at the low-intensity limit, and n_2 is called the nonlinear refraction coefficient.

Such type of change in the refractive index can be induced by either a resonant or a nonresonant process [7]. In resonant process, the frequency of the incident light overlaps with an electronic absorption band. The sample absorbs the energy, and an excited-state population is generated. This induces a transient change in the absorption spectrum and of the material due to the bleaching of the ground-state absorption and/or the appearance of the excited-state absorption. The change in the absorption coefficient, gives rise to a change in the refractive index, since they are interdependent according to the Kramers-Kronig relations. Thus the resonant nonlinearity originates from a transient change in the absorption spectrum (and refractive index) of the material.

For non resonant process the wave length of the incident light is different from any electronic transitions of the sample. The optical nonlinearity basically originates from the anharmonicity of the electronic system. Traditionally, the nonresonant optical nonlinearity of a material is described by equation (5.3).

Third order nonlinearities can be determined by many different processes, the commonly used are the Z scan technique, third harmonic generation and a large number of three and four wave mixing processes, the most common among them being the degenerate four wave mixing (DFWM).

5.1.2 Principle of DFWM:

DFWM is a third order nonlinear optical process where two counter propagating pump waves and a probe wave, all with the same frequency ω, interfere in a medium having a third order nonlinearity resulting another wave with frequency $\omega = \omega+\omega-\omega$, counter propagating to the probe wave. The output of the mixing process can be interpreted in terms of induced gratings and diffraction. Two of the three input waves interfere and form either a spatially or temporally modulated grating; the third input wave is scattered by the grating to yield the output wave. Since the output is directly related to the nonlinear response of the medium, DFWM is often used to measure third-order nonlinearities.

Advantages of DFWM:

i) A single light source can be used because the frequencies involved are the same.

ii) Not only crystals, but also gases, liquids, semiconductors and organic materials can be used as media since third order nonlinear polarization exists for all media.

iii) Since the phase conjugate wave is automatically the reverse of the probe wave, the condition of phase matching is much less rigorous.

5.1.3 Theory of DFWM:

In order to find the wave equation for a beam that propagates through a nonlinear optical medium, one starts with Maxwell's equations (expressed here in Gaussian units):

$$\nabla.\mathbf{D} = 4\pi\rho \tag{5.4a}$$

$$\nabla.\mathbf{B} = 0 \tag{5.4b}$$

$$\nabla \times \mathbf{E} = -\frac{1}{c}\frac{\partial \mathbf{B}}{\partial t} \tag{5.4c}$$

$$\nabla \times \mathbf{H} = \frac{1}{c}\frac{\partial \mathbf{D}}{\partial t} + \frac{4\pi \mathbf{J}}{c} \tag{5.4d}$$

We assume nonmagnetic materials, with no free charges or currents, i.e.

$$\rho = 0 \tag{5.5a}$$

$$\mathbf{J} = 0 \tag{5.5b}$$

$$\mathbf{B} = \mathbf{H} \tag{5.5c}$$

$$\mathbf{D} = \mathbf{P} + 4\pi\mathbf{E} \tag{5.5d}$$

We can determine the wave equation, using the conditions above and Maxwell's equations:

$$\nabla\times\nabla\times E + \frac{1}{c^2}\frac{\partial^2 D}{\partial t^2} = 0 \tag{5.6}$$

which can be rewritten as:

$$-\nabla^2 E + \frac{1}{c^2}\frac{\partial^2 D}{\partial t^2} = -\frac{4\pi}{c}\frac{\partial^2 P}{\partial t^2} \tag{5.7}$$

Therefore, the nonlinear wave equation becomes

$$-\nabla^2 E + \frac{\varepsilon^{(1)}}{c^2}\frac{\partial^2 E}{\partial t^2} = \frac{4\pi}{c}\frac{\partial^2 P^{NL}}{\partial t^2} \tag{5.8}$$

The equation is inhomogeneous, and the nonlinear response of the medium represents the source term, which is included as the right-hand term.

5.1.4 DFWM and Phase conjugation:

Let us consider an electric field $E_1(\mathbf{r},t)=Re\{\psi(\mathbf{r})e^{i(kz-\omega t)}\}$ which has a spatial dependence $A_1(\mathbf{r})=\psi(\mathbf{r})e^{ikz}$. If we can produce in the material another electric field $E_2(\mathbf{r},t)=Re\{\psi^*(\mathbf{r})e^{i(-kz-\omega t)}\}$, with $A_2(\mathbf{r})=\psi^*(\mathbf{r})e^{-ikz}=A_1^*(\mathbf{r})$ at any z, we call this field E_2 the phase conjugate of E_1.Degenerate four-wave mixing (DFWM) can yield phase conjugation and is useful, for example, for correcting aberrations by using a phase conjugate mirror (PCM). It can be thought of as the complex conjugate of space but not time, or as a time-reversed wave front. Now consider light that passes through an aberrating medium and becomes distorted. By reflecting the distorted wave front off a phase-conjugate mirror, when the generated phase-conjugate wave front passes back through the distorting medium, the output wave would be, ideally, undistorted.

As a technique, DFWM is mostly used in characterizing third order nonlinear materials. There are several configurations that are used: folded boxcars, phase-conjugate or backward geometry, and two beam DFWM or forward geometry. The latter configuration is not phase matched. The working principle for all of these geometries is the following: two beams interfere to form some type of grating (e.g. intensity grating) and a third beam scatters off this grating, generating the fourth beam named the conjugate or signal beam.

The most frequently used DFWM configuration is the phase-conjugate geometry (fig. 5.1 (a)). In this configuration, two counter propagating pump beams, called backward (B) and forward (F), and a probe beam (P) are incident on the nonlinear material. Since beams B and F are collinear, $\mathbf{k}_F = -\mathbf{k}_B$. The probe beam is incident at a small angle to the direction of the forward beam. Due to the third order nonlinear polarization, a fourth beam is created and is referred to as the conjugate beam. This fourth beam is counter propagating to the probe beam, $\mathbf{k}_C = -\mathbf{k}_P$. The process can be understood using the grating diagram (Fig. 5.1(b) and (c)). The forward and the probe beams interfere to form a grating from which the backward beam scatters, generating the conjugate

beam. Similarly, the backward and probe beams create a grating from which the forward beam scatters and generates the conjugate beam.

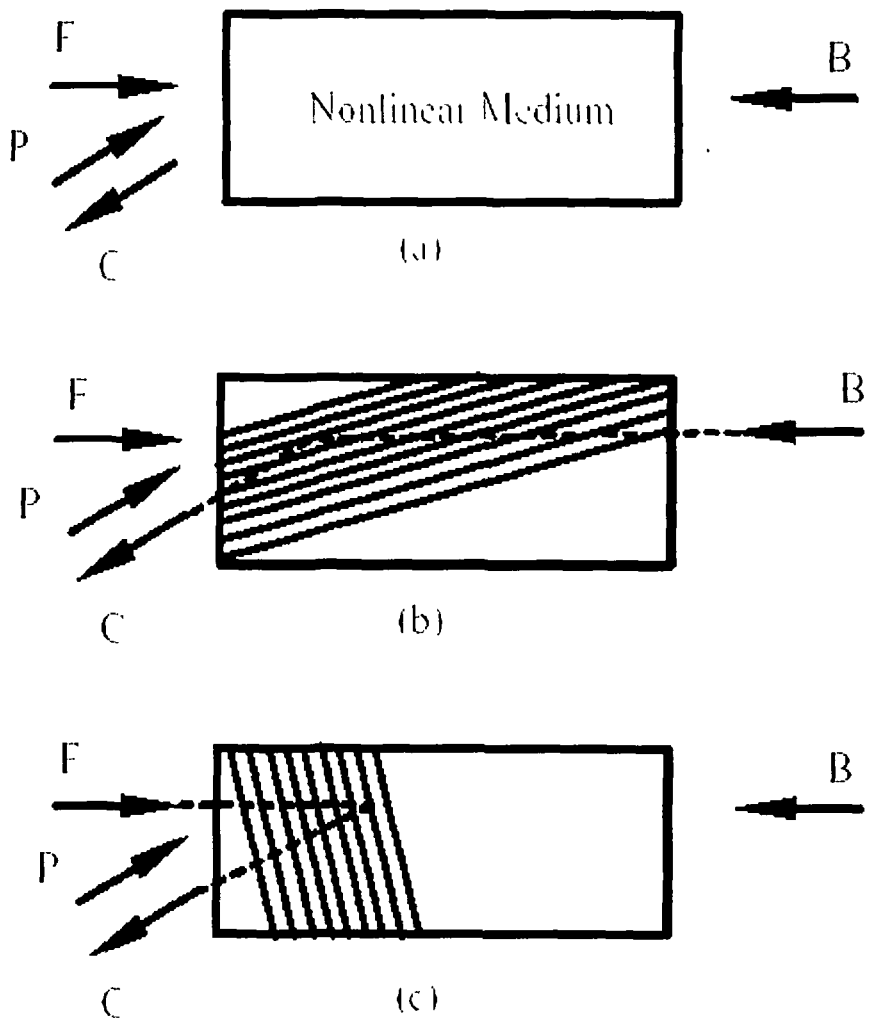

Figure 5.1: (a) Geometry and grating interpretation for phase-conjugation (b) Backward beam scattering off grating created by forward and probe beams c) Forward beam scattering off grating formed by backward and probe beams.

We express the input fields as:

$$E_i(\mathbf{r}, t) = A_i(\mathbf{r})e^{i(k_i \cdot r)} \qquad (5.9)$$

The nonlinear third-order polarization produced by the interaction of the three beams is oscillating at the same frequency ω as the input fields

$$P_i^{(3)} = 6\chi_{ijkl}^{(3)}(-\omega;\omega,\omega,-\omega)E_jE_kE_l^*$$
$$= 6\chi_{ijkl}^{(3)}(-\omega;\omega,\omega,-\omega)A_jA_kA_l^*e^{i(k_1+k_2+k_2).r} \quad (5.10)$$

and is propagating in the $\mathbf{k}_1+\mathbf{k}_2-\mathbf{k}_3$ direction, where $\mathbf{k}_1$and $\mathbf{k}_2$ correspond to the forward and backward beams and $\mathbf{k}_3$ corresponds to the probe beam. The subscripts j, k, and l correspond to the vector components of the forward, backward, and probe beams, respectively. Because the two pump waves are counter propagating, their wave vectors are related by

$$\mathbf{k}_1+\mathbf{k}_2=0 \quad (5.11)$$

The field amplitude of the wave generated by the nonlinear polarization is proportional to $A_jA_kA_l^*$and is the phase conjugate of A_l

5.1.5 Wave-equations for phase conjugation:

The third order polarization expressed in the previous section couples the four interacting waves. Let us consider the counter propagating pump beams as strong (undepleted), plane waves with slowly varying amplitudes A_i. Therefore, the second order derivative

d^2A_i/dz^2 may be neglected $\left(\left|\frac{d^2A_i}{dz^2}\right| << \left|k_4\frac{dA_i}{dz}\right|\right)$

This condition is valid as long as the fractional change in A_i over a distance of the order of the optical wavelength is much smaller than unity. The amplitude of the generated wave E_4 satisfies the wave equation:

$$\nabla^2E_4 - \frac{\varepsilon^{(1)}}{c^2}\frac{\partial^2E_i}{\partial t^2} = \frac{4\pi}{c}\frac{\partial^2P^{NL}}{\partial t^2} \quad (5.12)$$

$$\text{where, } P^{NL} = 6\chi^{(3)}(-\omega;\omega,\omega,\omega)E_1E_2E_3^*$$

is the nonlimear source term.

Let $E_3(\mathbf{r},t) = A_3(z)e^{i(kz-\omega t)}$ and try a solution of the term

$$E_4(\mathbf{r},t) = A_4(z)e^{i(-kz-\omega t)}. \tag{5.13}$$

Substituting E_4 in the wave equation

$$\nabla^2 E_4(r,t) = \frac{d^2 A_4}{dz^2} - 2ik^2 A_4 - A_4 k^2 \tag{5.14}$$

and using the slowly varying amplitude approximation, one can obtain:

$$\frac{dA_4}{dz} = -i\kappa A_3^* \tag{5.15}$$

$$\text{and } \frac{dA_3}{dz} = i\kappa A_4^* \tag{5.16}$$

$$\text{where } \kappa = \frac{12\pi\omega^3}{kc^2}\chi^{(3)}A_1A_2 \tag{5.17}$$

is called the coupling coefficient. To obtain the set of coupled equations above, it is assumed that, the angle between the probe and forward beam is very small. Otherwise, the left-hand sides of the equations should be multiplied by $\cos\theta$. Using the boundary conditions $A_3(0) \neq 0$ and $A_4(L) = 0$ we obtain the solutions to the coupled wave equations:

$$A_3(z) = \frac{\cos\left[|\kappa|(z-L)\right]}{\cos\left(|\kappa|L\right)}A_3(0) \tag{5.18}$$

$$A_4(z) = -\frac{i\kappa}{|\kappa|}\frac{\sin\left[|\kappa|(z-L)\right]}{\cos\left(|\kappa|L\right)}A_3^*(0) \tag{5.19}$$

The output amplitudes of the two waves are:

$$A_3(L) = \frac{1}{\cos(|\kappa|L)}A_3(0) \tag{5.20}$$

$$A_4(0) = \frac{i\kappa}{|\kappa|}\tan(|\kappa|L)A_3^*(0) \tag{5.21}$$

The generated wave is therefore seen to be proportional to the complex conjugate of the input probe beam $A_3(0)$.

5.1.6 Grating formation and types of gratings:

In terms of the intensity dependent refractive index, the DFWM process is considered as the interference of two input beams which results in a grating formation from which the third beam scatters generating the phase-conjugate wave. This is because the interference results in a spatially periodic light intensity or distribution of polarization. As a result, the optical properties of the material are changed, with the grating represented by the spatial modulation of these parameters. The type of grating created depends on the properties of the medium as well as the characteristics of the input beams.

For highly absorptive materials, for example, an incident laser beam populates the excited electronic states due to the absorption of light. Therefore, a population density grating is created. During the relaxation of the excited states, a space charge grating can form if there are excited, mobile charges. Space charge gratings are important in photorefractive materials. During the absorption process, heat is generated in regions of high optical intensities and therefore a temperature grating is formed. The material tends to expand in these regions generating stress, strain, and density gratings and in mixtures it can be accompanied by concentration gratings. Various time-dependent studies of the phase-conjugate signal can give information on the different relaxation mechanisms in the nonlinear medium and their characteristic parameters. These five gratings are included in one large category generally known as the thermal grating. The response time for the thermal grating is approximately 10^{-3}s. Another type of grating is the orientational grating, which forms on time scales of 10^{-12}s. It is a result of the alignment of anisotropic molecules to the electric field when an optical wave is applied.

Nonresonant electronic nonlinearities (resulting strictly from the redistribution of the electrons in the medium) are very fast, since they involve only virtual processes. The time necessary to form electronic grating is very short, $<10^{-15}$sec, which is the time required for an electron cloud to become distorted in response to an applied optical field. For this study we are

interested only in the electronic contribution to the nonlinear susceptibility $\chi^{(3)}$ because of its inherently fast response.

5.1.7 Optical nonlinearity in quantum dots:

In recent years, there are extensive studies on optical responses of semiconductor nanocrystals because of there size-dependent optical properties like optical absorption, photoluminescence (PL), and the nonlinear refractive index. By incorporating semiconductor nanoparticles into polymer, glass, or ceramic matrix materials, many of their interesting optical properties including absorption, fluorescence, luminescence, and nonlinearity may be studied. Such studies enhances the possibilities of there application in nonlinear optical devices [8, 9].

For the same reasons materials with large third order non linear susceptibility χ^3 have been an object of increasing interest in recent years. In particular, great effort has been devoted to the determination of the third-order

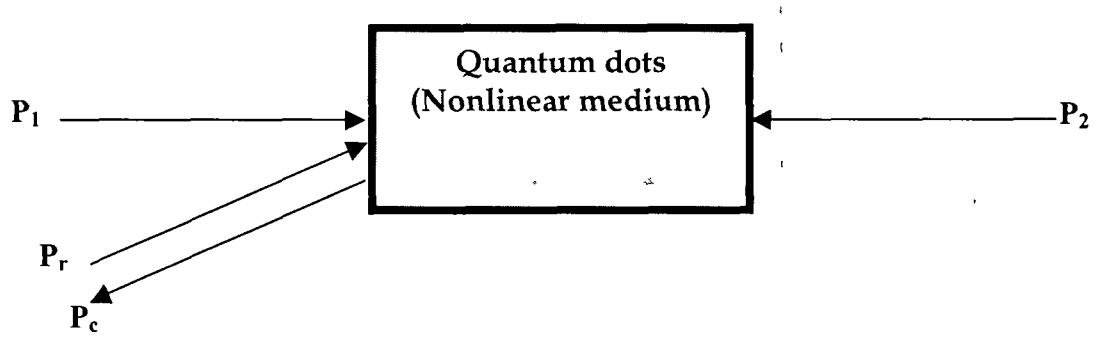

Figure 5.2 : Schematic diagram of DFWM. P_1 and P_2 are the counter propagating pump waves P_r is the probe wave and P_c is the phase conjugate output wave.

nonlinear optical susceptibility, χ^3, responsible for phenomena such as third harmonic generation or optical phase conjugation [10,11].

Whereas in bulk semiconductors the physical origin of nonlinear absorption and refraction is associated with the optically created high density many particle system causing screening, band gap renormalization and band

filling, the mechanism of nonlinearity in quantum dots is of a basically different kind. With decreasing size the optical nonlinearity is strongly influenced by quantum confinement.

Again like bulk semiconductor, semiconductor nanocrystal also exhibit resonant and non resonant nonlinearity.

5.1.8 Resonant Nonlinearity of Semiconductor Clusters:

For quantum dot with size comparable to that of the exciton, the laser excitation can generate an electron-hole (e-h) pair bounded by the cluster surface. Because of the large surface to volume ratio in quantum dots, the bound exciton may rapidly trapped by the surface states forming a trapped e-h pair. The presence of such trapped e-h pairs affects the cluster absorption spectrum and gives rise to the optical nonlinearity.

5.1.9 Nonresonant Nonlinearity of Semiconductor Clusters:

When the wavelength of the laser source is not in resonance with any electronic transitions of the quantum dot, the effects of excitons can be neglected. For semiconductor clusters embedded in a dielectric medium, the major factor to be considered is the local field effect. Inorganic semiconductors usually possess large refractive indices. When they are embedded in media with lower refractive indices such as glasses, polymers, or solvents, a boundary is established by the difference in the refractive indices. When illuminated by light, the local electric field experienced by the clusters can be enhanced compared to the incident field because of the presence of this boundary. The local field effect can also arise from the dipole-dipole interaction between the molecule and the surrounding medium. Significant increase in nonlinearity due to local field effects has been reported for CdS semiconductor clusters [7]

Though the enhanced nonlinear optical properties of quantum confined semiconductors, attracted many, Wang *et al.* have been the pioneers in making these measurements on polymeric systems. In 1987, Wang and Mahler reported

the first study of NLO properties in polymer stabilized CdS quantum dots using the degenerate four-wave mixing (DFWM) [12]. It has been reported [13] that the non-linear refractive index for the CdS nanoparticle in distilled water was measured to be 10^3 times lager than that of bulk CdS.

5.2 Third order nonlinear susceptibility measurement:

There are several research papers reporting third-order nonlinear optical susceptibilities of quantum dots. For CdS doped glasses Takada *et al.* [14]

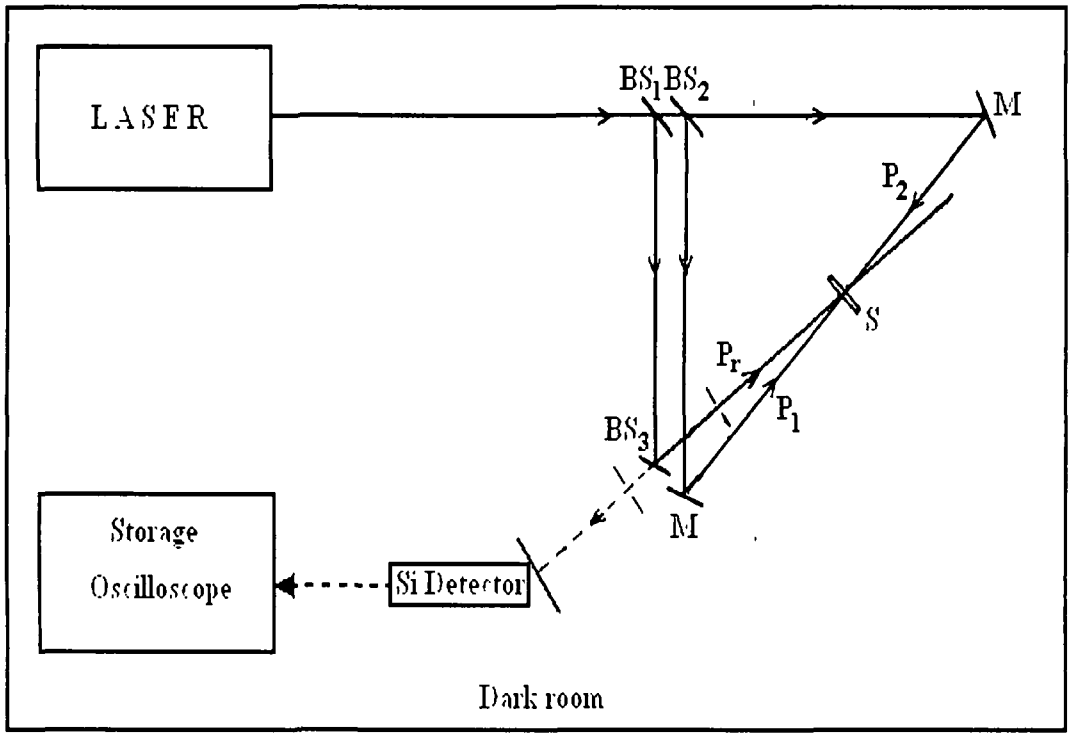

Figure 5.3: Experimental set up for DFWM

measured a χ^3 value of 1.1 x 10^{-6} esu (1.5 x 10^{-14} m^2/v^2) while Woggon [15] *et al.* reported χ^3 value of 3.2 x 10^{-8} esu for CdS quantum dots. For surface modified CdS nanoparticle Yamaki *et al.* [16] observed χ^3 value near ~ 10^{-7} esu. Significantly some bulk semiconductor like HgTe possesses χ^3 value as high as 1.6x 10^{-4} esu [17].

For PbS quantum dots in PVA coating Lu [18] *et al.* measured a χ^3 value of 1.06 × 10^{-5} esu. Fick *et al.* [19] reported a χ^3 value of 4x 10^{-18} m^2/v^2 for PbS nanocrystal prepared by sol-gel technique.

For DFWM experiment high power pulse laser like Nd:Yag or Ar ion laser are extensively used as the laser source [19]. Yang *et al.* [20] for the first time showed that a low-intensity cw laser can be used as the DFWM source. In their experiment they used an argon ion laser as the exciting light source. Earlier Kiessling *et al.* showed that Phase-conjugated signals are achievable with relatively low intensities of the interacting waves (in the range 1-100mW/cm^2) [21]. Recently Kurian *et al.* [22] studied optical nonlinearity induced in PbS nanoclusters by the z-scan method using low power continuous wave He-Ne laser.

5.2.1 DFWM Experiment:

In this work we report the first ever DFWM experiment using low power He-Ne (λ=32.8 nm) laser. The experimental set up and circuit diagram are shown in fig. 5.3 and 5.4 respectively.

This is the counter propagating-pump configuration. The wave from the laser source is divided into pump and probe waves by beam splitter BS_1 The pump wave is further separated into two wave paths by beam splitter BS_2, becoming pump waves P_1 and P_2. These two waves counterpropagate from both sides of the quantum dot sample (S) and are injected into it. The probe wave P_r reflected by the beam splitter BS_3 is also injected into the sample along with the pump waves. The resulting phase conjugate wave is guided to the observation system by the beam splitter BS_3. The amplified signal, detected with the help of a Si detector (TIL 81), is recorded with a storage oscilloscope

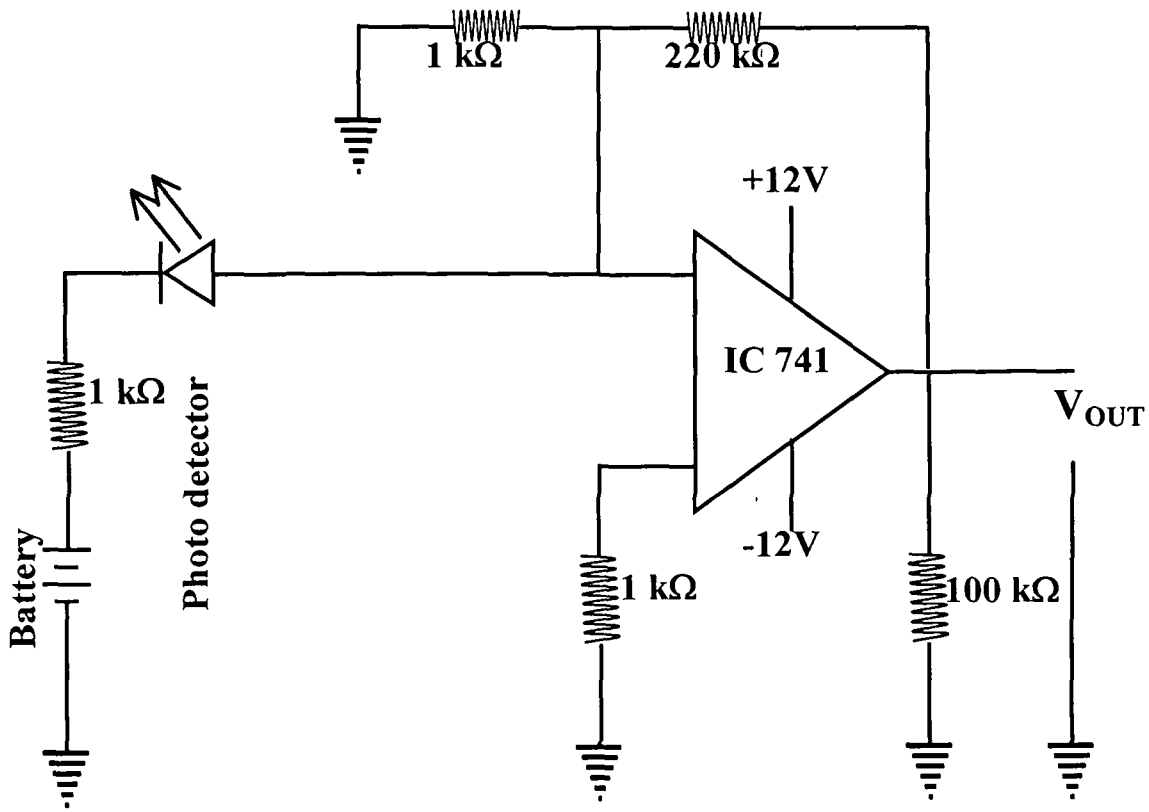

Figure 5.4: Circuit diagram for measuring χ^3 of PbS quantum dots

[HM1507-3, HAMEG Gmbh, Germany]. The sample was in the form of thin film measuring a thickness ~ 20 μm .The χ^3 value was calculated using the relation [18]

$$\chi^3 = \frac{4n^2 c\varepsilon_0 \lambda \alpha \sqrt{\eta}}{3\pi(1-T)I_p} \qquad (5.22)$$

where $\eta = I_1/I_0$ is the linear refractive index, c the velocity of light, λ the measurement wavelength, α the sample absorption coefficient at λ, I_p the pump intensity, T the transmission at I_p, ε_0 the dielectric constant of the material. Here, η is the diffraction efficiency, i.e., the intensity relation of the transmitted first-order (I_1) and zeroth order (I_0) of the diffraction pattern, which appears by self-diffraction of a laser induced grating.

Using experimental data, n =1.52 [19], c=3 x 10^8 m/s, ε_0 =17.2 for PbS [23] λ= 632.8 nm, I_p =1.7 x 10^6 watt/m^2, η= 0.05 and α= 6.65 x 10^6 [24] we calculate

value as 19.6×10^{-4} m^2/v^2. A comparison of this result with other published results could not be made because the discrepancy in the order of χ^3 arises due to the smaller value of I_p, appearing in equation 5.22. For a high power laser with $I_p \approx GW/m^2$, the order will automatically come down. Since we have recorded the absorption onset at around 511 nm, exciton resonance can not be the origin of the observed nonlinearity. Instead we believe that the surface states absorption is the right mechanism to be considered here. However the surface states are not detectable in the optical absorption spectra [25] may be due to lower content of the surface states in the samples synthesized in polymer matrix [26]. Here 'lower content' has only a relative meaning, the surface state in these nanoparticles is considerably higher than the bulk material. The PL spectra of the sample also confirm the presence of surface states in our sample as discussed in chapter III. Thus it is worth believing that the surface state absorption during intermixing of the laser beam on the sample may induce a transient change in the absorption coefficient resulting a change in refractive index which in turn gives rise to nonlinearity in the sample.

5.3 Application of quantum dots in optoelectronic devices:

Any device that operates as an electrical-to-optical or optical-to-electrical transducer is termed as optoelectronic device. Optoelectronic switching devices accept optical signals and yield electrical signals or vice versa. When the input is optical, the term "detector" switch is used; when the output is optical, the term is "transmitter switch" [27]. In the following section we discuss the application of quantum dots in optoelectronic switch (detector). It is experimentally found that up to a critical bias potential, the specimens function as detector switch while above the critical bias, the same specimen acts as electronic switch. Therefore the quantum dots samples are also tested for electronic switch. The details of the experiments and results are presented here.

5.3.1 Quantum dot as optoelectronic and electronic switch:

Current conduction in semiconductors occurs due to electronic transition between two energy states in the specimen. These transition and hence current generations are of two types. These are:

(i) Current generation takes place in semiconductor due to increase in electrical conductivity caused by biased voltage or photons of energy higher than or equal to the band gap. Under this condition, free electron-hole pairs are produced by applied bias or by absorption of incident photon while electrons and holes serve as the charge carriers in conduction band and valance band respectively producing current in the external circuit.

(ii) In another type, current conduction is not of this intrinsic kind where impurities and other imperfections plays significant role in producing out current with fast response peak, even with biased voltage or photons having energy below the threshold (band gap energy) for production of mobile electron/hole. In fact, in quantum dot we can not understand the experimental facts of conductivity, without invoking the presence of imperfection and impurities. Imperfections produce discrete energy level in the forbidden gap, which are called 'traps'. From this point of view, current conductivity is described as a process where by, electrons are trapped and detrapped by crystal imperfections (traps), excited by biased voltage or photons and produce current in the external circuit.

Trapping and detrapping of charge carriers are very fast in the order of 10^{-9} sec to 10^{-14} sec depending upon the types of traps.

To investigate quantum dots as electronic and optoelectronic switch we experimentally show that it produces electronic (current) output excited by biased voltage and optical signal of proper energy. The investigation is carried out on bare PbS, CdS and ZnS quantum dots. The optical operating range of the devices are revealed from photoluminescence studies, as the reason behind electronic and optoelectronic switching is the same as that of photoluminescence phenomena i.e., like luminescence process electronic and

optoelectronic switching are also caused by fast trapping and detrapping of charge carriers.

5.3.2 PL study to estimate optical operating range of quantum dots:

As mentioned above the optical operating range of optoelectronic device can be estimated from photoluminescence studies. For that we have carried out photoluminescence (PL) studies of the samples with different excitation wavelength. The results of PL studies for bare PbS, CdS and ZnS quantum dots are discussed below.

5.3.2.1 PbS quantum dots:

To carry out the PL study of PbS quantum dots the samples are excited with excitation sources of wavelengths 200 nm, 325 nm and 680 nm. The results with 325 nm excitation source has already been discussed in chapter III, therefore those PL plots are not displayed here. The PL spectra recorded with 200 and 680 nm excitation sources are shown in fig. 5.5 and 5.6.

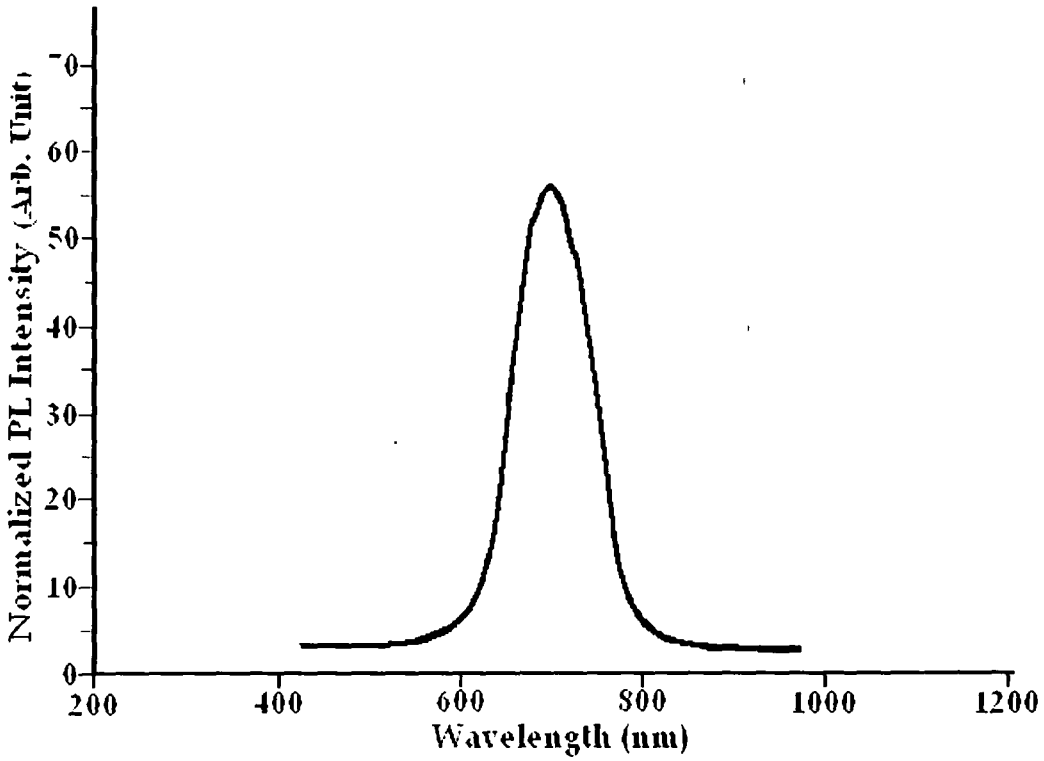

Figure 5.5: PL spectra of PbS quantum dots with excitation at 200 nm

It has been observed that irrespective of the wavelength used for excitation, the PL peaks occurred around 700 nm, which has been attributed to deep surface state as well as band edge emission in PbS [28].

No emission has been observed in PbS quantum dot samples with excitation sources of wavelength more than 680 nm as this energy may not be sufficient for band to band or surface states related excitation to cause luminescence.

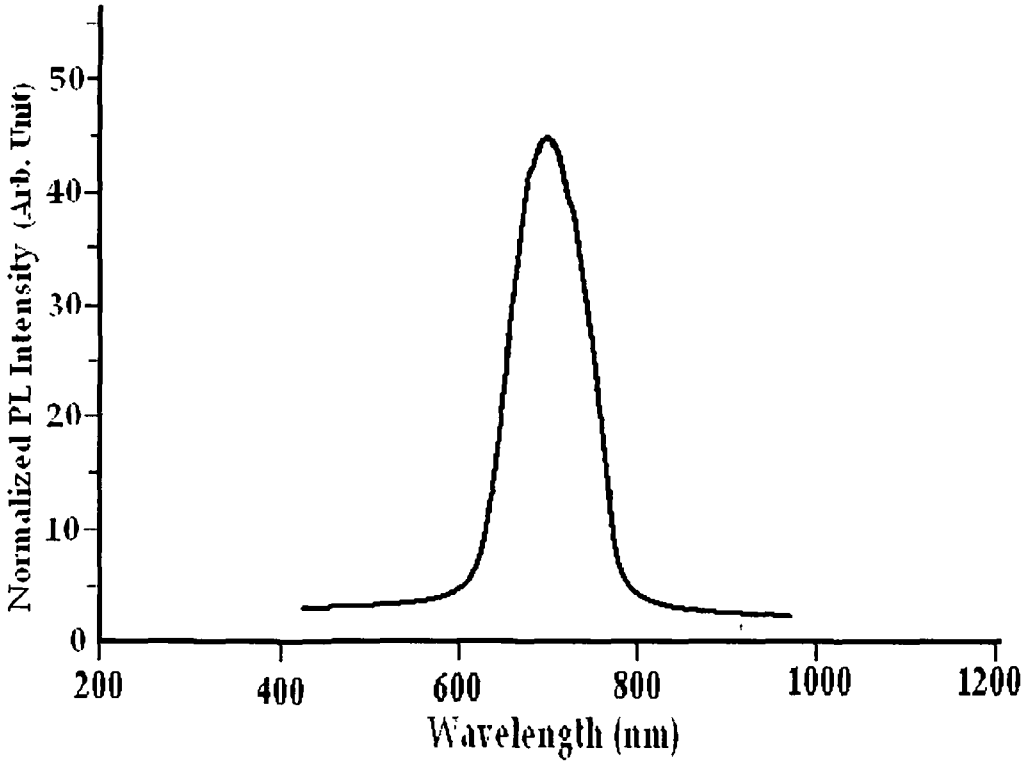

Figure 5.6: PL spectra of PbS quantum dots with excitation at 680nm

5.3.2.2 CdS quantum dots:

To estimate the optical operating range of CdS optoelectronic switch PL studies were carried out with excitation sources of wavelengths 200nm, 325 nm and 630 nm. In all the cases the PL peaks appeared at around 700 nm which is related to CdO phase as discussed in chapter III. The PL spectra recorded with 200 and 680 nm excitation sources are shown in fig. 5.7 and 5.8. To avoid repetition, the PL spectrum with excitation source 325 nm is not shown. For

CdS quantum dots, no emission was observed with excitation source of wavelength more than 630 nm.

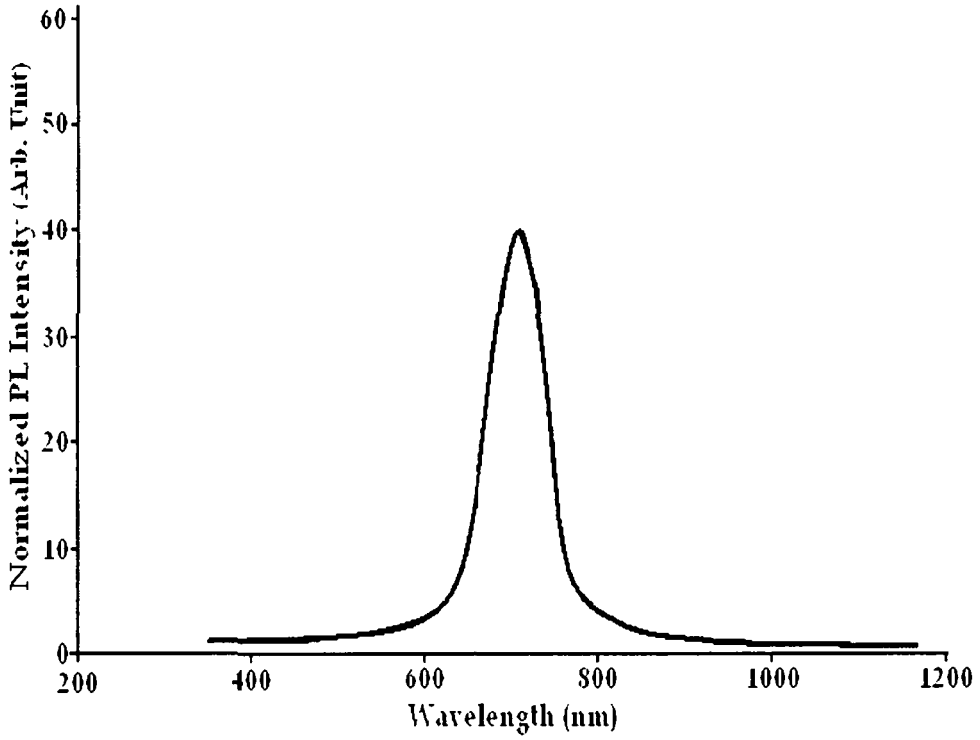

Figure 5.7: PL spectra of CdS quantum dots with excitation at 200 nm

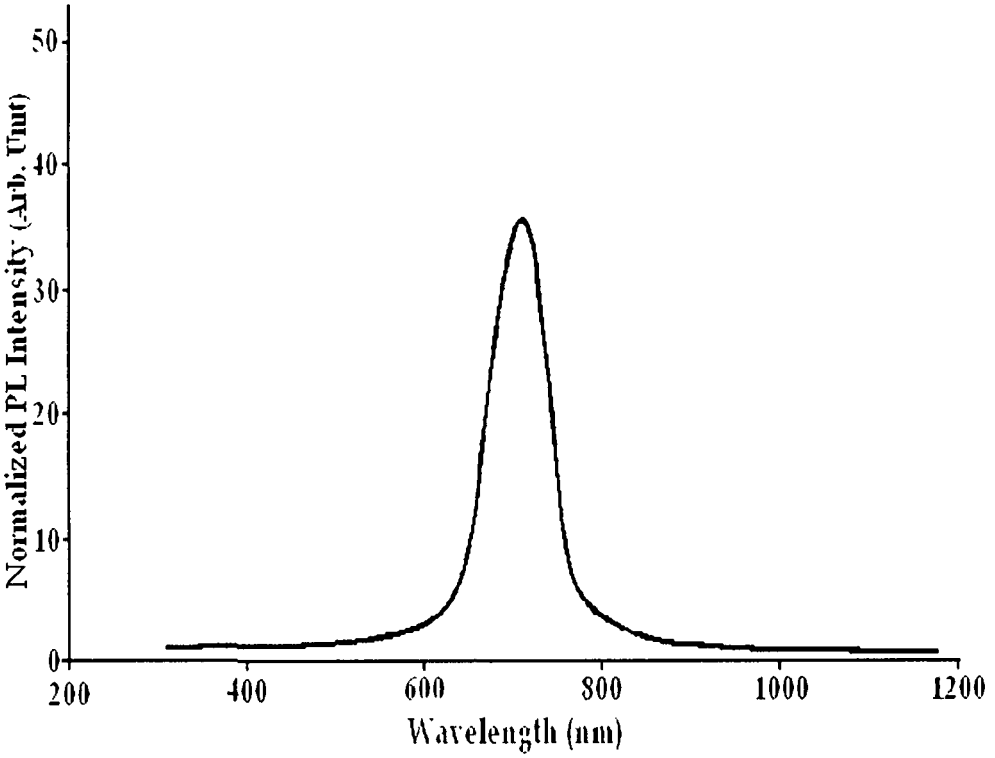

Figure 5.8: PL spectra of CdS quantum dots with excitation at 630 nm

5.3.2.3 *ZnS quantum dots:*

Similar to PbS and CdS quantum dots, the PL studies of ZnS quantum dots also reveal source independent emission regarding the PL peak position.

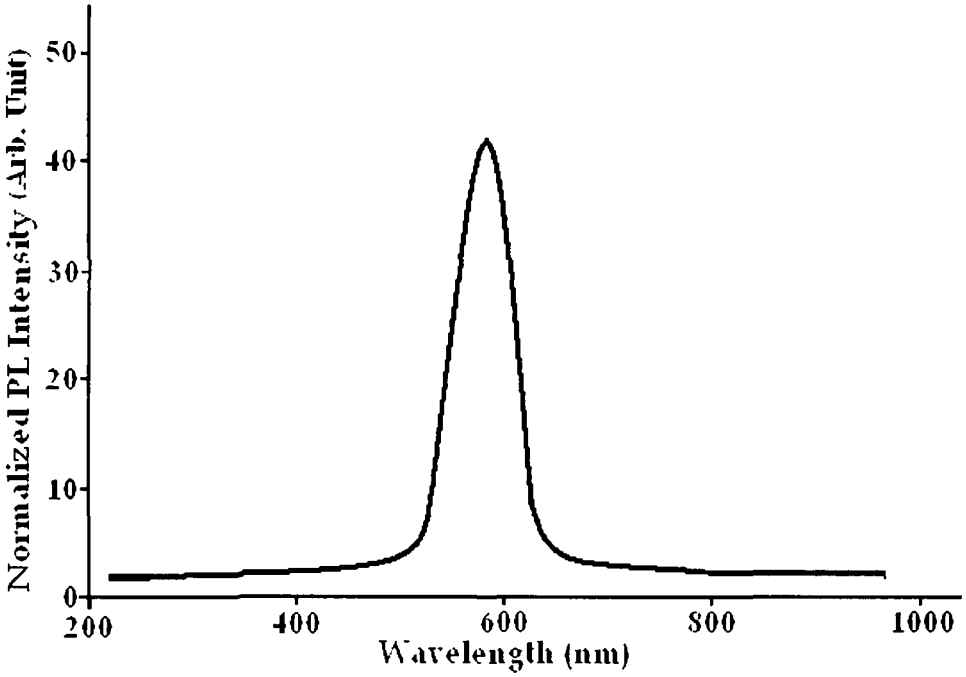

Figure 5.9: PL spectra of ZnS quantum dots with excitation at 200 nm

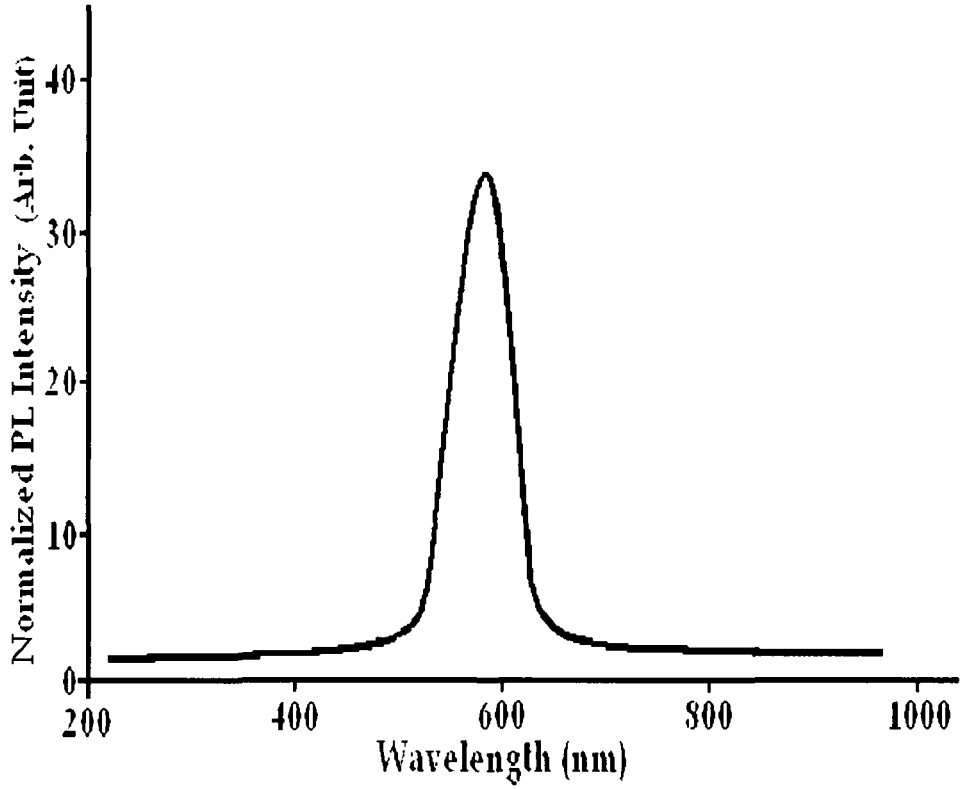

Figure 5.10: PL spectra of ZnS quantum dots with excitation at 460 nm

For the analysis, three excitation sources with wavelengths 200 nm, 325 nm and 460 nm were used and the corresponding PL peaks appeared at 591 nm. No emission was observed in ZnS samples with excitation source of wavelength more than 460 nm. The PL spectra of ZnS quantum dots excited with 200 nm and 460 nm are shown in figure 5.9 and 5.10, while that with 325 nm were already presented in chapter III.

5.3.3 *Switching speed:*

From the PL studies of quantum dots it has been revealed that quantum dots can convert a wavelength lying within a specific range, depending on the sample, into another optical output of different wavelength. This is the principle of optical switches. Thus our prepared quantum dots can be used as optical switches. We can estimate the switching speed of corresponding optical switch from the PL experiment because it is the trapping and detrapping of electrons by the traps (e.g. vacancies, surface states) that cause the switching phenomena [29-31]. From luminescence studies, the different transitions are identified and corresponding transition speed of electrons between any two traps can be estimated. This transition speed is the response speed of the device which depends on the types of traps.

From the PL data it can be shown that PbS quantum dots can convert optical signal lying between 200-680 nm range into a signal of wavelength 700 nm. Similarly CdS quantum dots accepts signal within the range 200-630 nm and yield output at 700 nm and ZnS quantum dots can convert any wavelength within 200-460 nm giving output at 591 nm. The switching speed of the quantum dots optical switches is estimated to be ~10^{-14} sec.

5.3.4: *Experimental setup for optoelectronic and electronic switching:*

Two ends of 99% pure fine gold wire of 0.01 mm diameter are fixed very close to each other within micron range. A small drop of quantum dot sample is gently dropped over the ends of the gold wire to make the micro contact and

dried under vacuum. The free ends of the gold wire are connected to a mV range bias source with one micro ammeter in series. All the connections are made with silver paste to avoid air gap resistance in the contacts. Nd:YAG laser has been used to illuminate the sample. The experimental setup is shown in figure 5.11.

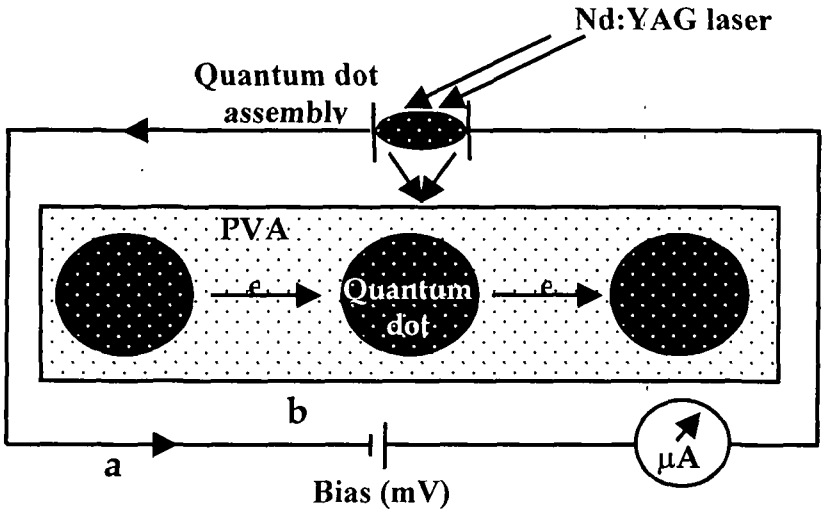

Figure 5.11: (a) Experimental setup for electronic and optoelectronic switching (b) schematic presentation of quantum dots in polymer matrix

5.3.5: General behaviour of quantum dot electronic and optoelectronic switch:

We have studied the electronic and optoelectronic switching behaviour of our prepared quantum dot samples and plotted the characteristic curves between current generated and bias voltage for three illumination intensities ϕ_1, ϕ_2 and ϕ_3. The general pattern of such curve is shown in figure 5.12.

First we consider the plot ABCDEFG for intensity ϕ_1, photocurrent starts to flow at point A and produces a steep rise at point B and than saturates at point C. It falls at point D and again rises at point E and then saturates again at point at point F. Next the reasons are explained.

Optical signal excite charge carriers and produces corresponding trap related transition in quantum dots. But to produce effective current, electrons must tunnel from one dot to another through the insulating matrix.

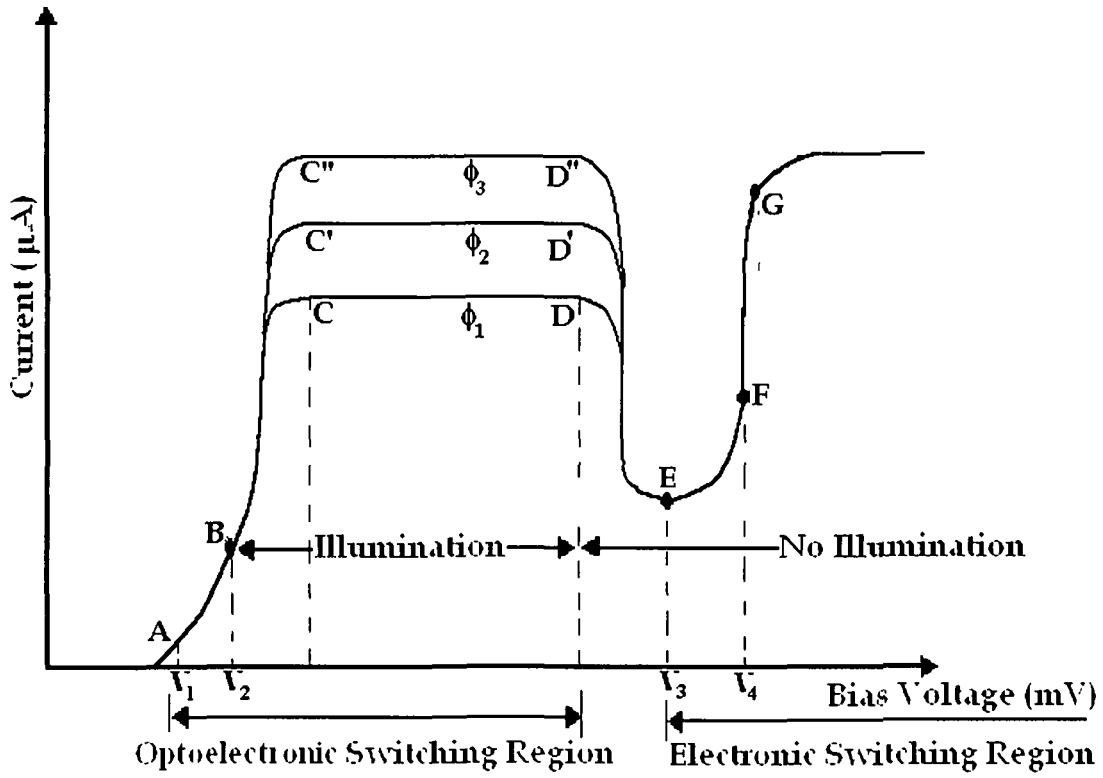

Figure 5.12: Pattern of optoelectronic and electronic switching characteristics of quantum dots (ϕ → illumination intensity, $\phi_1<\phi_2<\phi_3$)

That is why a minimum bias voltage is needed to cause electronic current through polymer. This voltage corresponds to the point A and is denoted by V_1. At point B the bias voltage V_2 produces breakdown phenomenon by causing all the charge carriers to tunnel through the polymer wall at a time and produces steep rise in photocurrent. This process can be compared with the breakdown phenomenon of avalanche photodiode. Furthermore, at point C, photocurrent is saturated due to the saturation of tunneling of charge carriers and no further change in it is observed from C to D. The similar behaviour of photocurrent observed with higher illumination intensity with only difference that photocurrent saturates with higher magnitude.

To observe the effect of bias in the absence of illumination, we switch off the optical source (laser) at point D. The photocurrent falls but does not reach zero, rather, it starts rising again at point E corresponding to the bias voltage V_3

with steep rise at point F corresponding to the bias V_4 and then saturates at point G.

In the absence of illumination, photocurrent tends to cease, but at the critical point E, bias V_3, itself can excite some of the charge carriers even in the absence of light while at point F, the bias V_4 causes the avalanche breakdown by detrapping all the charge carriers at a time, resulting in steep rise in output current. The phenomena may be compared to zener breakdown of semiconductor diode. Furthermore, at the point G, the current is saturated as trapping and detrapping of charge carriers is saturated at this point.

The portion AB and EF indicate optoelectronic switching and electronic switching respectively. Interestingly, in the actual plots, we find that, both the portions show similar kind of steep rise, which infer the same optoelectronic and electronic switching speed. This behaviour also suggests that both the switching phenomena are caused by same mechanism, that is, trap related charge carrier transition.

It is experimentally found that up to point E, corresponding to bias voltage V_3 quantum dots act as optoelectronic switch but beyond it, it acts as electronic switch.

5.3.6 Optoelectronic and electronic switching characteristics:

5.3.6.1 PbS quantum dots:

Investigation of optoelectronic and electronic switching phenomena of PbS quantum dot assembly embedded in PVA matrix were carried out with three illumination intensities ϕ_1, ϕ_2 and ϕ_3 ($\phi_1<\phi_2<\phi_3$). The presence of surface traps and related transitions are the origin of the switching behaviour. The optoelectronic and electronic switching characteristics are shown in fig 5.13 and corresponding data are presented in table 5.1 and 5.2.

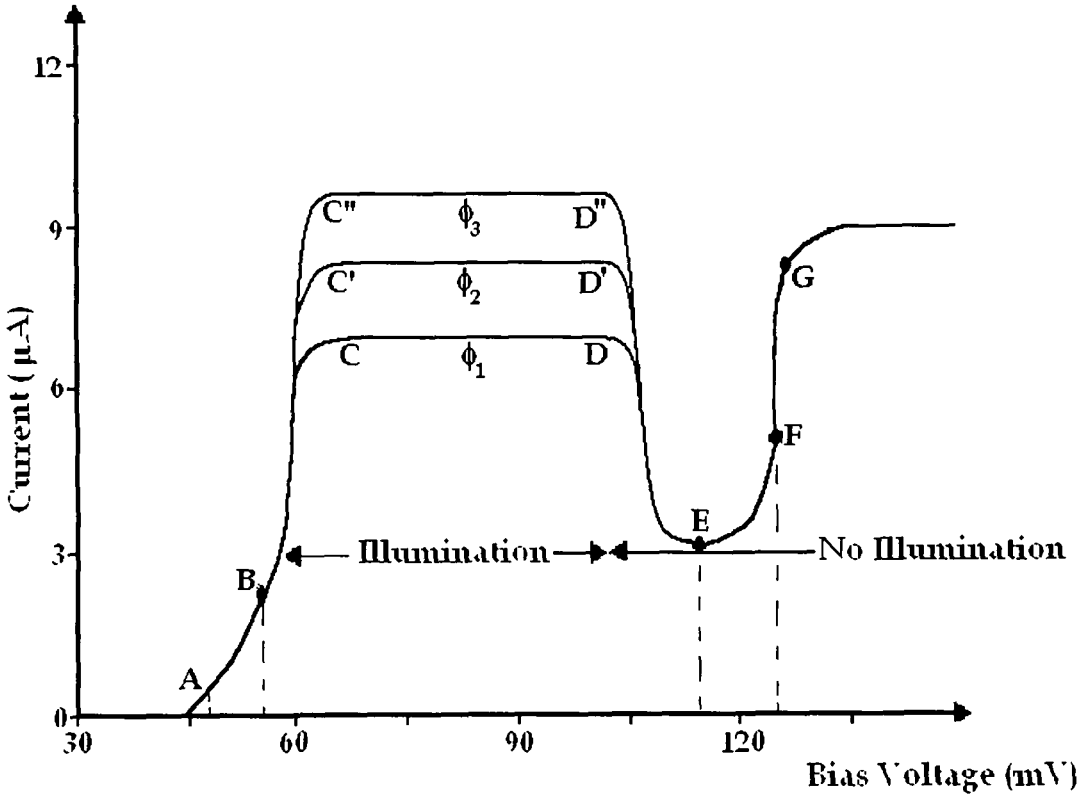

Figure 5.13: Switching characteristics of PbS quantum dots

Table 5.1: Optoelectronic switching data of PbS quantum dots

Illumination	Saturation Current (μA)	V_1 (mV)	V_2 (mV)	Optical Operating Range (nm)
ϕ_1	6.9			
ϕ_2	8.4	48.2	55.7	200 - 680
ϕ_3	9.7			

Table 5.2: Electronic switching data of PbS quantum dots

V_3 (mV)	V_4 (mV)	Saturation Current (μA)
114.6	125.4	9.1

5.3.6.2 *CdS quantum dots:*

Both optoelectronic and electronic switching phenomena of CdS quantum dot assembly embedded in PVA matrix are studied under the three

illumination intensities ϕ_1, ϕ_2 and ϕ_3. The switching characteristics are shown in fig 5.14 and related data are represented in table 5.3 and 5.4. The reason behind the switching phenomena is the transition between CdO center (donor level acting as trap) and valance band of CdS quantum dots [32].

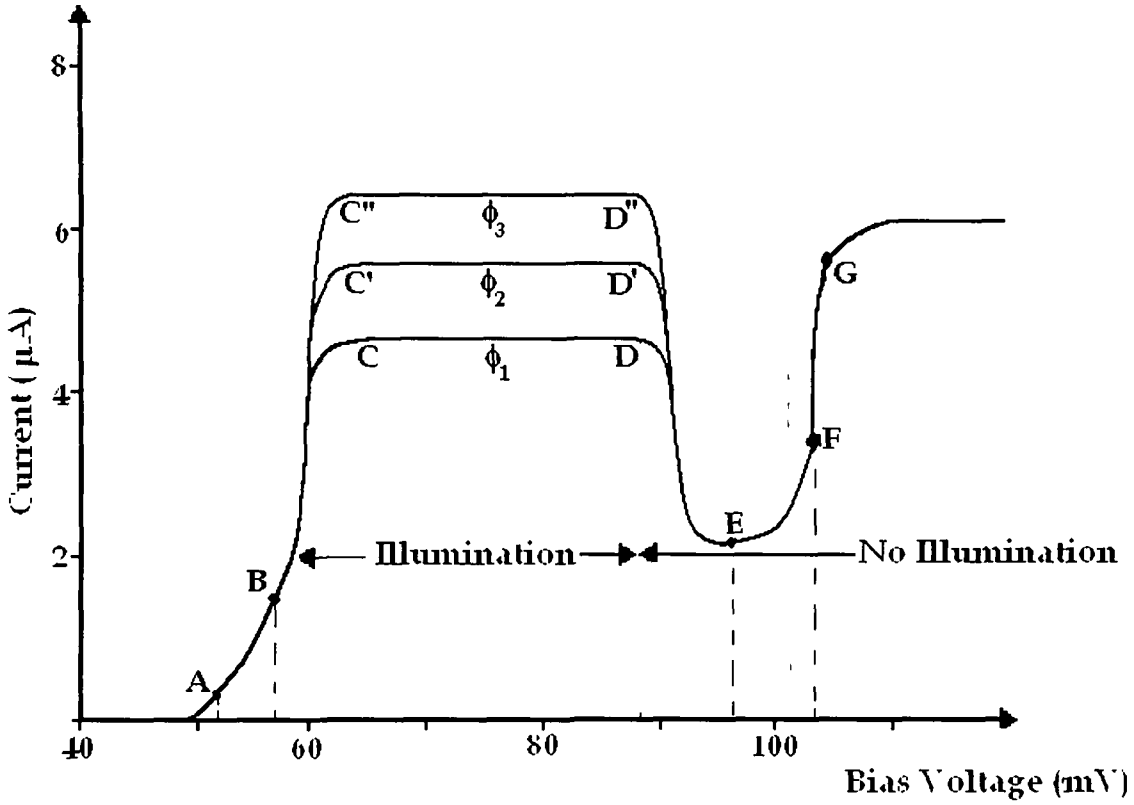

Figure 5.14: Switching characteristics of CdS quantum dots

Table 5.3: Optoelectronic switching data of CdS quantum dots

Illumination	Saturation Current (μA)	V_1 (mV)	V_2 (mV)	Optical Operating Range (nm)
ϕ_1	4.6			
ϕ_2	5.5	52.1	57.2	200 - 630
ϕ_3	6.4			

Table 5.4: Electronic switching data of CdS quantum dots

V_3 (mV)	V_4 (mV)	Saturation Current (μA)
96.5	123.5	6.0

5.3.6.3 *ZnS quantum dots:*

To investigate optoelectronic and electronic switching phenomena in ZnS quantum dots, the quantum dots sample are illuminated with three intensities.

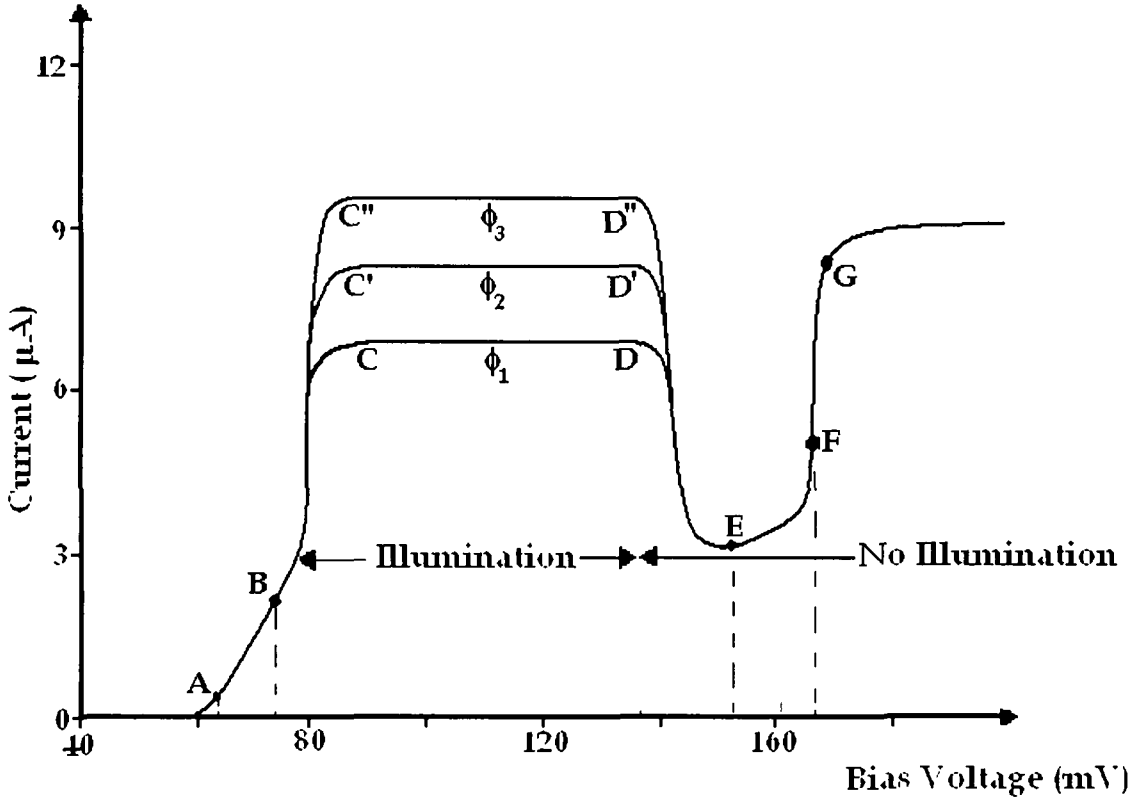

Figure 5.15: Switching characteristics of ZnS quantum dots

Like PbS and CdS quantum dots the transition from surface states caused by trapping and detrapping of charge carriers are attributed as the origin of the switching phenomena [33]. The optoelectronic and electronic switching characteristics are shown in fig. 5.15 and the corresponding data are represented in table 5.5 and 5.6 respectively. The results are in close agreement with previous work [34]

Table 5.5: Optoelectronic switching data of ZnS quantum dots

Illumination	Saturation Current (μA)	V_1 (mV)	V_2 (mV)	Optical Operating Range (nm)
ϕ_1	6.9			
ϕ_2	8.2	64.1	74.5	200 - 460
ϕ_3	9.5			

Table 5.6: Electronic switching data of ZnS quantum dots

V_3 (mV)	V_4 (mV)	Saturation Current (μA)
132.7	166.9	8.7

In this chapter we have studied the application of PbS quantum dots (bare) in the field of nonlinear optics. As we are using a low power laser source so DFWM experiment is limited for PbS quantum dots only, since it has a large strong confinement regime due to the large Bohr excitonic radius (~20 nm). And nonlinear optical properties of semiconductor quantum dots are expected to be greatly enhanced in this strong confinement regime.

The prepared PbS, CdS and ZnS (bare) quantum dots have been tested for possible application in optoelectronic as well as electronic switches. The results show that the quantum dot assembly can be used as efficient optoelectronic switch and also optical switch of high speed.

References:

1. Maiman T.H., *Nature,* **187** (1960) 493.
2. Franken P. A., Hill A. E., Peters C. W., and Weinreich G., *Phys. Rev. Lett.,* **7** (1961) 118 N.
3. Bloembergen N., *Nonlinear Optics,* World Scientific Publishing, Singapore, 1996.
4. Sakai J-I., Advanced Science and Technology Series-*Phase Conjugate Optics,* McGraw-Hill, New York, 1992.
5. Sauter E.G., *Nonlinear Optics,* John Wiley & Sons, New York, 1996.
6. Laud B.B., *Laser and Nonlinear Optics,* New Age International (P) Ltd., New Delhi, 2000.
7. Wang Y., *Ace. Chem. Res.,* **24** (1991)133.
8. Denzler D., Olschewski M., and Sattler K., *J. Appl. Phys.,* **84** (1998) 2841
9. Bakkers E.P.A.M., Reitsma E., Kelly J. J., and Vanmaekelbergh D., *J. Phys. Chem. B,* **103** (1999) 2781.
10. de Nalda R., del Coso R., Requejo-Isidro J., Olivares J., Suarez-Garcia A., Solis J, and Afonso C.N., *J. Opt. Soc. Am. B,* **19** (2002) 289.
11. Fern´ee M.J., Warner J., Watt A., Cooper S., Heckenberg N.R. and Dunlop R.H., *Nanotechnology,* **15** (2004) 16.
12. Wang Y. and Mahler W., *Opt. Commun.,* **61** (1987) 233.
13. Gerdova I. and Hache´ A. *Opt. Commun.,* **246** (2005) 205.
14. Takada T., Mackenzie J. D., Yamane M., Kang K., Peyghambarian N., Reeves R. J., Knobbe E. T., and Powell R. C., *J. Mater. Sci.,* **31** (1996) 423.
15. Woggon U., *Optical Properties of Semiconductor Quantum Dot* Managing editor Höhler G, Springer-Verlag, Berlin, (1997) pp-177.
16. Yamaki T., Asai K., Ishigure K., Sano K. and Ema K., *Synth. Metals,* **103** (1999) 2690.
17. Wolff P.A., Yuen S.Y., Harris K.A., Cook J.W. and Schetzina J.F. Jr., *Appl. Phys. Lett.,* 50 (1987) 1858.

18. Lu S.W., Sohling U., Mennig M. and Schmidt H., *Nanotechnology,* **13** (2002) 669.

19. Fick J., Schell J., L´evy R., Martucci A. and Guglielmi M., *Pure Appl. Opt.,* **6** (1997)527.

20. Yang Y., Fei H., Wei Z., Yang Q., Sun G. and Han L., *J. Luminescence,* **66 & 67**(1996) 133.

21. Kiessling A., Baade T., and Wenke L., *J. Mod. Opt.,* **43** (1996)1525.

22. Kurian P.A., and Vijayan C., 2004 *ISRS-2004* December 20-22 Chennai, India.

23. Littlewood P.B., *J. Phys. C: Solid State Phys.,* **12** (1979) 4459.

24. Schoolar R.B., and Dixon J.R., *Phys. Rev.,* **137** (1965) A667.

25. Chestnoy N., Harris T.D., Hull R., and Brus L.E., *J. Phys. Chem.,* **90** (1986) 3393.

26. Chen W., Wang Z., Lin Z., and Lin L., *J. Appl. Phys.,* **82** (1997) 3111.

27. Macdonald R.I., *IEEE Journal on Selected Areas in Communication,* **6**(1988) 1141.

28. Chowdhury S., Mohanta D., Ahmed G.A, Dolui S.K., Avasthi D.K. and Choudhury A., *J. Luminescence,* **114** (2005) 95.

29. Sengupta A., Jiang B., Mandal K. C.,and Zhang J. Z., *J. Phys. Chem. B***103** (1999), 3128.

30. Sengupta A., Mandal K.C.,and Zhang J.Z., *J. Phys. Chem. B***104** (2000), 9396.

31. Boroditsky M., Gontijo I., Jackson M., Vrijen R., and Yablonovitchb E., Krauss T., Cheng Chuan-Cheng, Scherer A., Bhat R. and Krames M., *J. Appl. Phys.,* **87**(2000), 3497.

32. Behera S.N., Sahu S.N. and Nanda K.K, *Ind. J. Phys.,* **74A**, 81, 2000.

33. Chen W., Wang Z., Lin Z., and Lin L., *J. Appl. Phys.,* **82** (1997) 3111.

34. Nath S.S., *"Synthesis of semiconductor quantum dots on polymer matrix and their applications in Electronics, photonics, and nonlinear optics",* PhD thesis, 2004.

CHAPTER VI

The ongoing miniaturization of solid state devices make it possible to fabricate electronic devices such as single electron transistor (SET) which are small enough to have device characteristics sensitive to the motion of single electron within them even at room temperature. Quantum dots may be used to fabricate single electron transistor [1] that can be viewed as an electron box, which has separate junctions for the entrance and exit of single electrons. It may also be viewed as field effects transistor, in which the channel is replaced by two tunnel junctions forming the metallic island. The voltage applied to the gate electrode affects the amount of energy needed to change the number of electrons. This device works on coulomb blockade effects. The advantage of this device is higher sensitivity, theoretically, by several orders of magnitude and low power consumption.

A quantum dot, also termed as artificial atom, can contain roughly a million of atoms together with an appropriate number of tightly bound electrons. However, a dot can also contain a small number of free electrons, which can be varied as desired. Just like in a real atom, these electrons are attracted to a central location being trapped in a bowl-like parabolic potential well. Because of the small dimension of the well, at sufficiently low operating temperatures electrons occupy quantized energy levels, and thus have a discrete excitation spectrum. Measurements of the orbital energies in these 'atoms' allows us to probe directly many important laws of quantum mechanics. Also quantum dots provide an experimental system to probe our understanding of single-particle and many-particle physics. One of the main efforts currently under task is the study of the applicability of a single-particle model to a many-particle system. If the size of the quantum dot is sufficiently small and the charging energy E_c is much greater than the thermal energy K_BT, no electron tunnels to and from the quantum dot. Thus the number of electron

inside the dot becomes fixed. The charging effect, which blocks the injection /ejection of a single charge into/from a quantum dot, is called Coulomb blockade effect [2]. Therefore, the condition for observing Coulomb blockade effect at room temperature is [3, 4]

$$E_c=e^2/2C >> K_BT,$$

where C is the capacitance of the quantum dot and T, the temperature of the system. The charging energy manifests itself in a different way in the nonlinear current voltage characteristics, in the form of stepwise increase known as the Coulomb staircase [5, 6]. Another condition for observing Coulomb effect is that the tunnel resistance must be much larger than h/e^2 = 26 kΩ [4].

The Coulomb blockade (CB) regime in transport through quantum dots provides a near perfect system to probe the applicability of the single particle model to a system involving many electrons. Particularly, the CB regime is characterized by a large charging energy, E_c which suppresses transport through the device except at points of degeneracy in dot occupation number. This charging energy represents the interaction energy of the electrons on the dot; hence, E_c represents a characteristic energy of the many-particle system. Coulomb blockade in isolated quantum dots at low temperatures is characterized by transport through a single level of the dot spectrum [5]. As such, the measured transport properties provide statistics of a single level on the background of a many-particle interacting system.

Some of the many-body effects have already been investigated in lithographically defined quantum dots, including the physics of Coulomb charging and the Kondo effect. Measurements of transport properties in a magnetic field have been used to study the filling of energy levels and the validity of Hund's rule in these electrostatically defined quantum dots [7]. Unexpected effects have been reported in these systems, including the pair wise loading of electrons into quantum dots [8].

Since quantum dots are of the order of a few atomic dimensions, direct electrical probing is a cumbersome job for practical applications. Direct use of

conventional lithographic techniques such as electron beam lithography [9] or scanning probe microscope related nanolithography [10, 11] become slow when used to define nanoscale features. Recently self-assembly techniques have attracted interest for nanoscale device applications because these techniques offer the potential to fabricate nanoscale elements such as quantum dots and electronic device configurations of these nanoscale elements without direct use of conventional lithographic techniques [12]. A number of self-assembly techniques have been reported for fabricating nanoscale structures of clusters, quantum dots, and wires [13, 14].

6.1 Frequency dependent capacitance voltage (C-V) characteristics of PbS quantum dots:

It has been reported that organic/nanocrystal composites have been used in number of important optoelectronic devices operating in the visible region [15]. We have studied the capacitance-voltage (C-V) and current-voltage (I-V) response of quantum dots (bare and coated PbS) at different frequency range to investigate electrical behavior of the samples. A similar study was carried out with CdS quantum dots recently by Mohanta *et al.* [16].

The capacitance-voltage (C-V) and current-voltage (I-V) measurements were carried out with variable frequency LCR meter (Hioki 3532-50 LCR Hi-Tester) in the frequency range 300-900 Hz, 10-50 kHz and 1.2-5.0 MHz. For comparison, first, we have recorded the C-V and I-V characteristics of the polymer matrix (PVA) alone using a thin polymer film of thickness ~20 μm by connecting to the LCR meter through silver (Ag) contact established on the two surfaces of the films. The results are presented in fig. 6.1. Similarly, to carry out the analysis with quantum dots, thin films (20 μm) of both bare and coated PbS quantum dots embedded in PVA are taken and connected to the LCR meter through silver (Ag) contacts. Thus the arrangement can be viewed as nano PbS/Ag capacitor.

Figure 6.2 and 6.3 show the capacitance-voltage characteristics of bare and coated nano PbS / Ag junction at specified frequencies respectively in Hz. It is clear that in the low frequencies, capacitance increases almost linearly with applied voltage. But the rate of increment is more in coated samples than the bare ones.

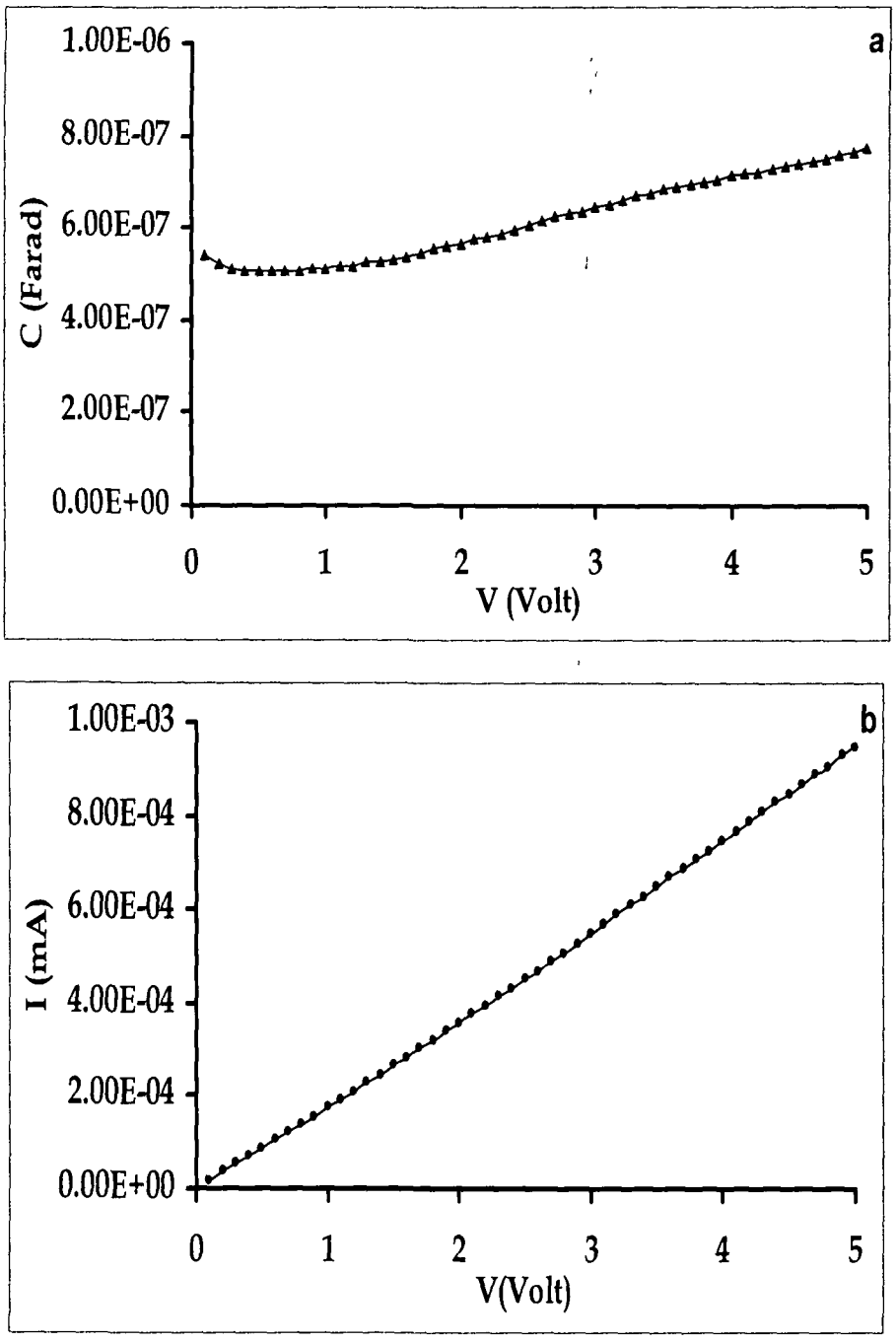

Figure 6.1: C-V (a) and I-V (b) characteristic of the polymer matrix (PVA) at 300Hz

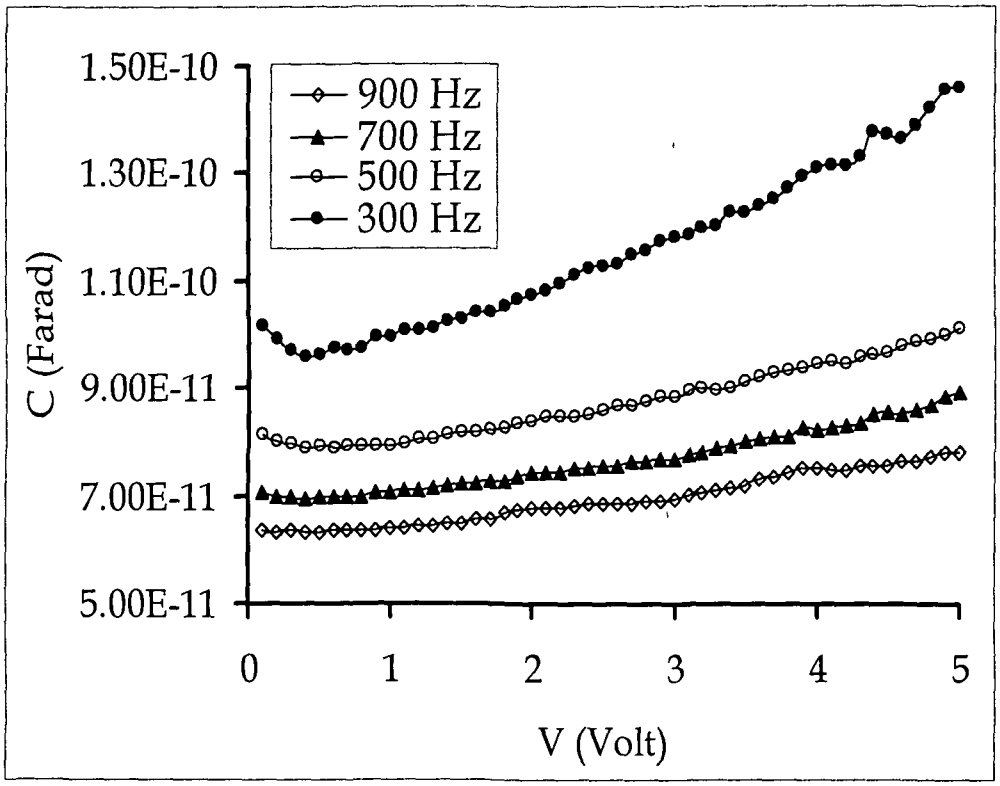

Figure 6.2: C-V characteristic of bare nano PbS / Ag junction (300-900 Hz)

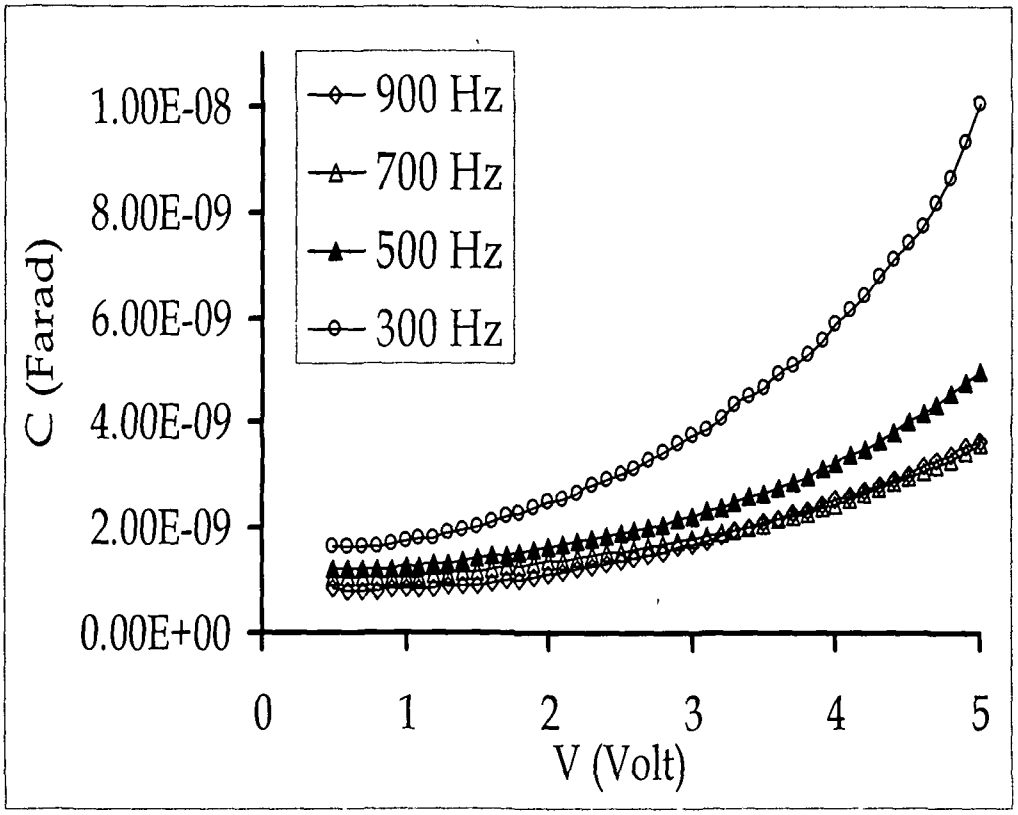

Figure 6.3: C-V characteristic of coated nano PbS / Ag junction (300-900 Hz).

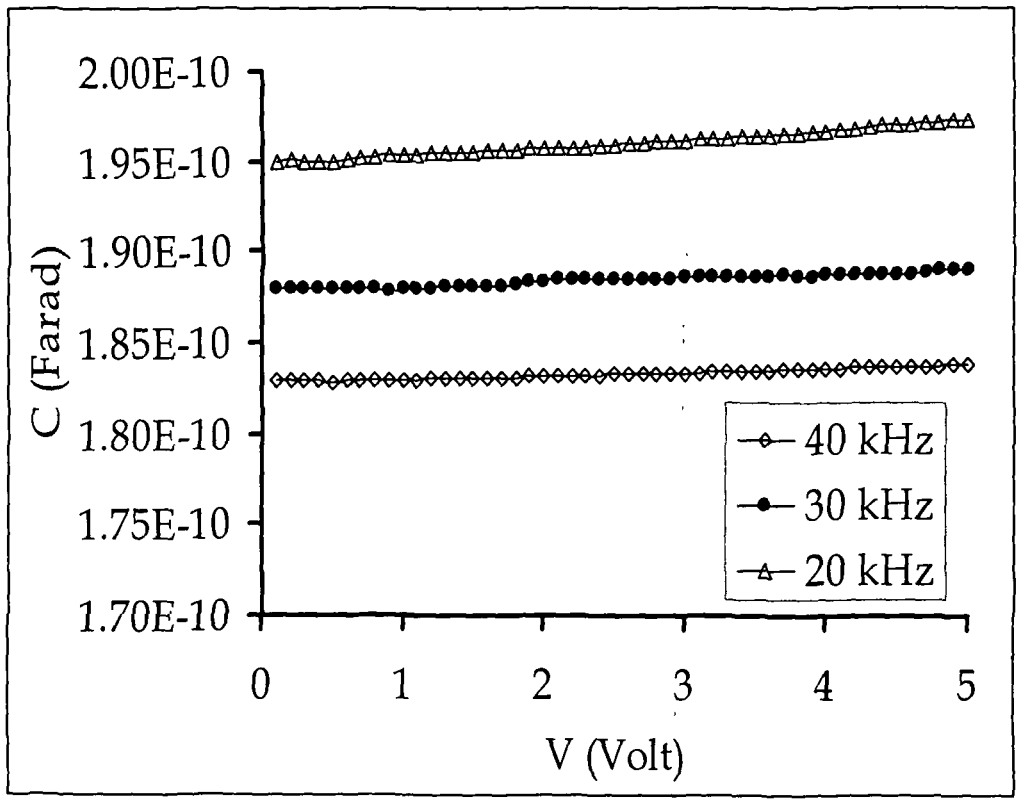

Figure 6.4: C-V characteristic of bare nano PbS / Ag junction (20-40 kHz)

In our system, we have a thin film of PbS (bare and coated) quantum dots embedded in a matrix, such two near by quantum dots separated by a thin film of PVA itself act as a capacitor and there will be series of such capacitors within the area under consideration. Again using Ag contact over the surface forms a metal semiconductor junction. Therefore the total capacitance will be the sum of capacitance due to the nano PbS/Ag junction and capacitance of the quantum dots. For coated quantum dots formation of PbS /SiO_2 junction is also possible.

Due to large surface to volume ratio, the quantum dots contain large number of surface traps due to dangling bond, and other defects. So when an electric field is applied it might be possible that the injected charge fall into these traps. Thus by holding the charge, the quantum dots contribute to the total capacitance of the system together with the normal depletion layer contribution. As these trap states are being filled, the probability for newly

injected charge to flow through the system increases. As a result there will be considerable increase in current (to be discussed later in this chapter).

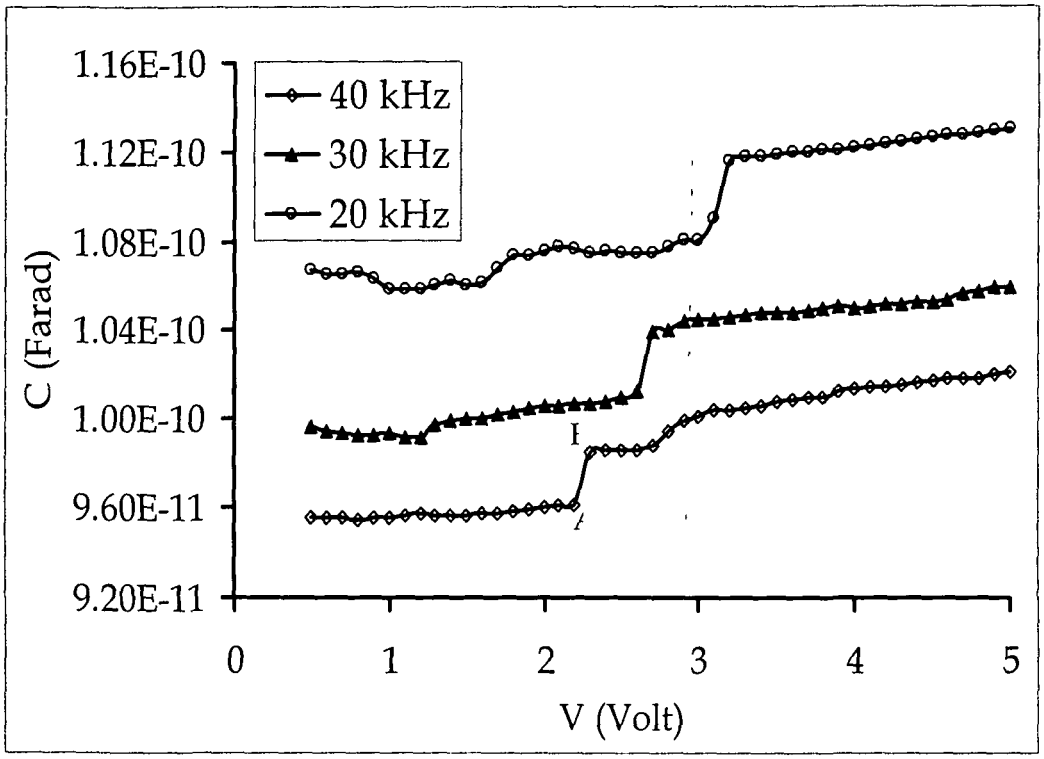

Figure 6.5: C-V characteristic of coated nano PbS / Ag junction (20-40 kHz)

However the injection of charge carriers may not affect the C-V response significantly. This is what we observe for uncoated PbS/Ag junction at higher frequency range 20-40 kHz (figure 6.4). For a particular frequency the capacitance of the system remains almost constant with increase in applied voltage.

The C-V characteristics of coated PbS/Ag nanojunction are shown in figure 6.5. It has been observed that with increase in frequency range (Hz to kHz) the capacitance of the system decreases (from ~10^{-8} to 10^{-10} F). Interestingly, some abrupt change in capacitance at particular applied voltages has been observed in the C-V plot.

It has been mentioned earlier that the total capacitance of the system is comprised of the nano PbS/Ag junction and capacitance due to PbS quantum

dot. Theoretically, the capacitance of a single quantum dot surrounded by a medium of dielectric constant ε depends on its size as [17]

$$C(r) = 4\pi\varepsilon_0\varepsilon r$$

Thus for PbS (coated) quantum dot having radius 6 nm (considering the largest dot) the capacitance can be calculated as ~13.3×10^{-19} F (taking ε= 2 for PVA). Again the charging energy, E_c= 59 meV which is much greater than K_BT (~ 26 meV), satisfies the condition for observing Coulomb blockade. The resistance of the system is ~MΩ, thus the second condition [4] for observing Coulomb blockade is also fulfilled. For applied voltage 2.2 V (denoted by A in 20 kHz C-V response in figure 6.5), the no of electrons in such a quantum dot will be approximately 18. For applied voltage 2.3 V (denoted by A in 20 kHz C-V response in figure 6.5), the no of electrons will be approximately 19. So there is a transfer of single electron. There are two reasons for requirement of extra energy to add additional electrons to the quantum dots. First, the electrons inside the dot will repel each other and make it difficult for other electrons to enter the dot. As number of electrons in the dot increases, repulsion also increases and it takes more energy to add another electron. Second, The Pauli exclusion principle requires electrons to be in different quantum levels in the dot. Additional electrons must be promoted into higher energy level [18]. The calculation will be exactly same for 30 kHz and 40 kHz.

Thus theoretically we can explain the rise in capacitance at the particular observed voltages as due to Coulomb blockade. But with the present arrangement experimental confirmation is not possible as we cannot separately measure quantum dot capacitance. However there must be some relationship between the theoretical and experimental observation. Coulomb blockade only in case of coated sample infers that the PbS/SiO_2 nanojunction may be responsible for such behavior.

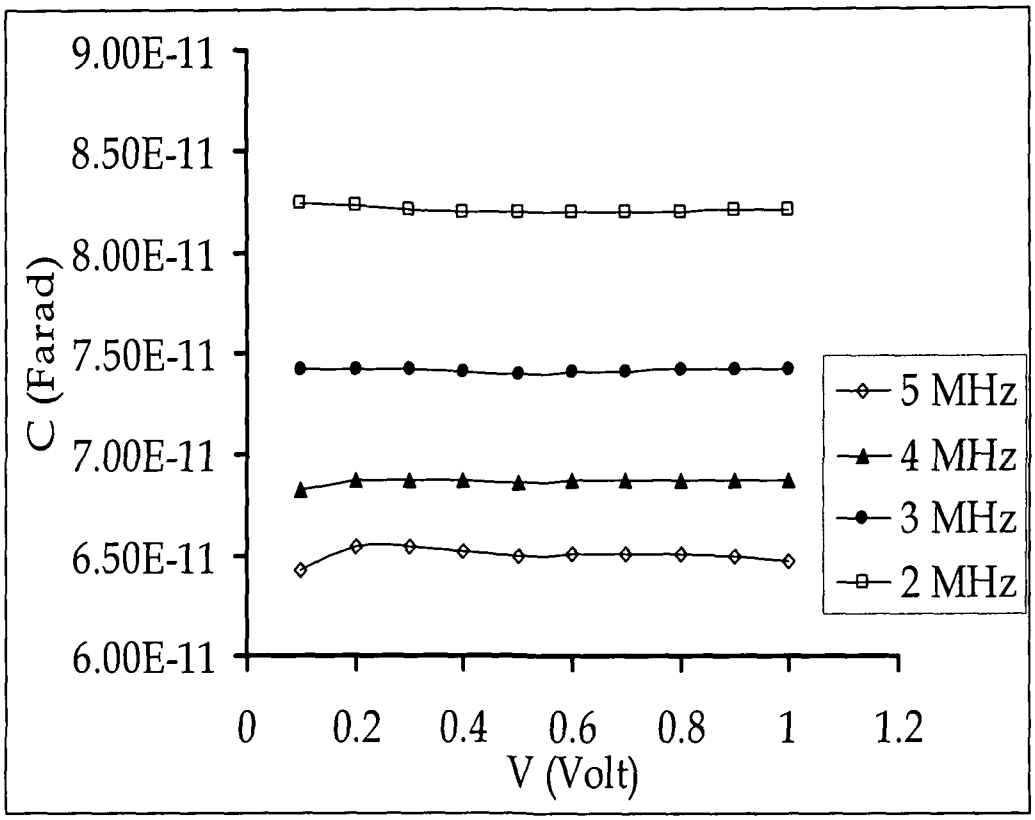

Figure 6.6: C-V characteristic of bare nano PbS / Ag junction (2-5 MHz)

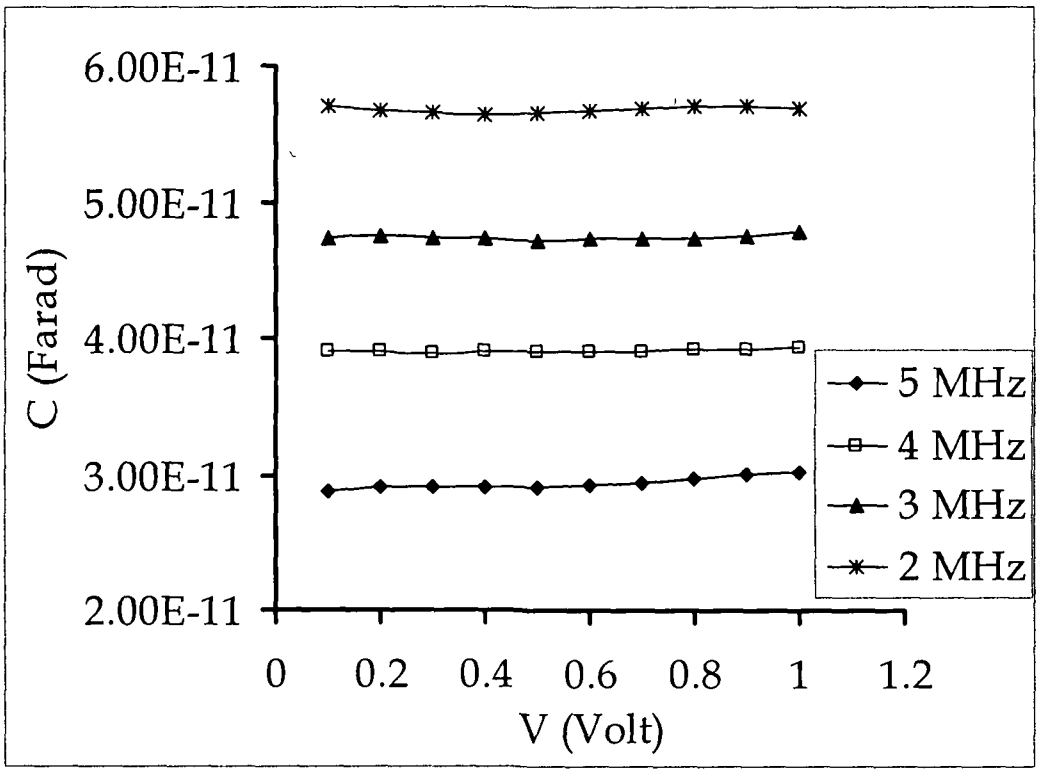

Figure 6.7: C-V characteristic of coated nano PbS / Ag junction at (2-5 MHz)

However, at high frequency range [2-5 MHz] both bare and coated PbS quantum dots/Ag junction show almost constant response. Also the capacitance of the system as a whole drops considerably with increase in frequency (figure 6.6 and 6.7).

6.2 Frequency dependent current voltage (I-V) characteristics of PbS quantum dots:

The I-V measurement of bare and coated nano PbS /Ag junctions were carried out at low frequency (300-900 Hz), mid-frequency (20-40 kHz) and high frequency (1-5 MHz) range.

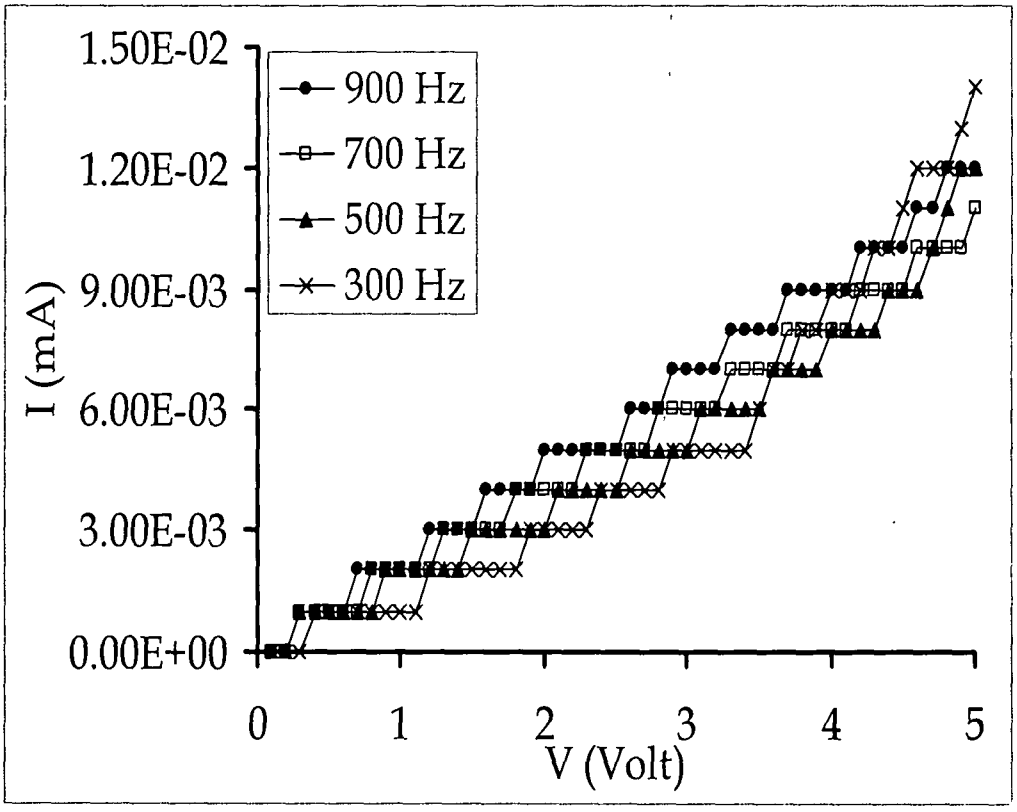

Figure 6.8: I-V characteristic of bare nano PbS /Ag junction (300-900 Hz)

At low frequency range, as shown in figure 6.8, it has been observed that in case of bare nano PbS/Ag, the current increases stepwise with increase in applied voltage. Nonlinear current-voltage relations are the result of Coulomb-blockade and Coulomb-staircase phenomena in the electrical charging of nanoscale electrical conductors. Strong step structures due to the Coulomb-

staircase are normally observed in systems with highly asymmetric junctions, especially when the resistance of one junction is much greater than that of the other [19]. This is very likely in our case. Also, such C-V characteristic is possible for the polymer which is known as molecular eigenvalue staircase. However molecular eigenvalue staircase feature is

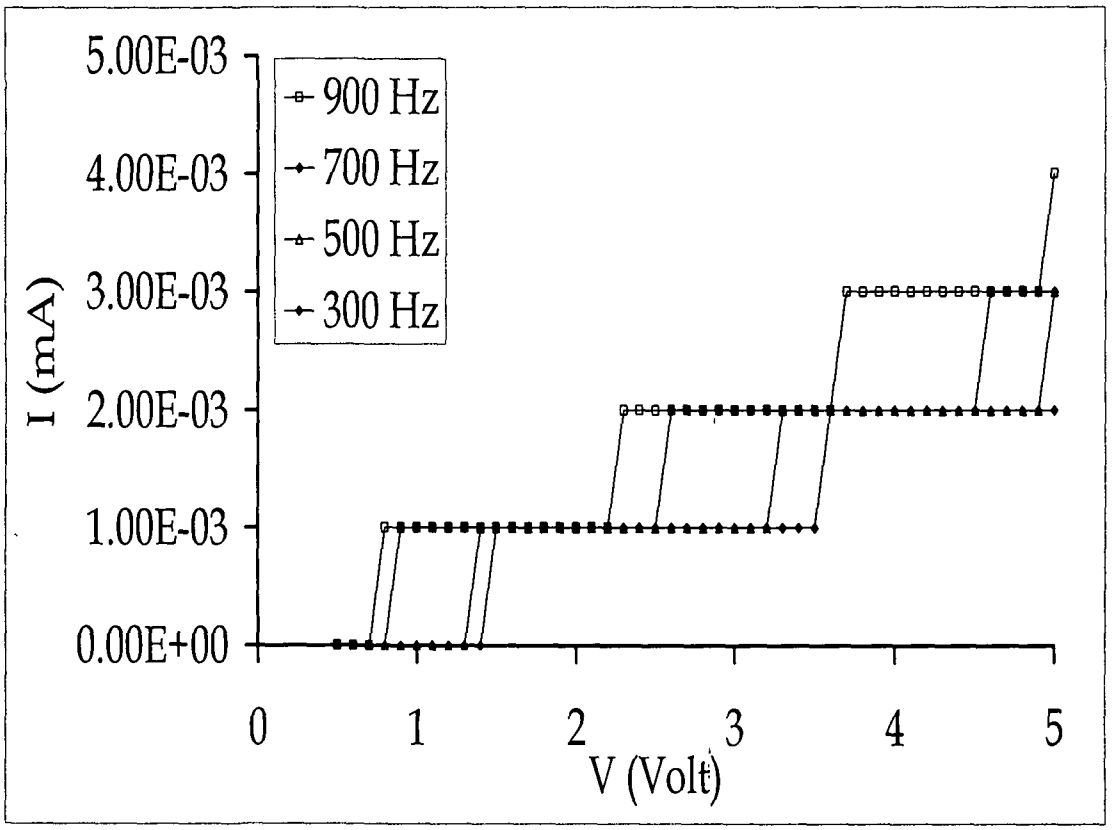

Figure 6.9: I-V characteristic of coated nano PbS / Ag junction (300-900 Hz)

observable only for smaller molecule like object [20]. From the analysis it has been observed that for a particular frequency, the step width decreases with increase in applied voltage. Theoretically, the current steps ΔI should occur at voltage intervals $\Delta V \approx e/C$. In our case for a single quantum dot e/C=0.12 V, whereas experimentally observed value was~ 0.1 V.

In case of coated nano PbS / Ag junction (figure 6.9) also, the same step like structure has been observed, but the width of the plateau region is more than that of junction containing bare quantum dots. This may be due to the SiO_2

coating which acts as barrier for charge transportation from or to the quantum dots. At higher frequency range (kHz and MHz), both bare and coated nano

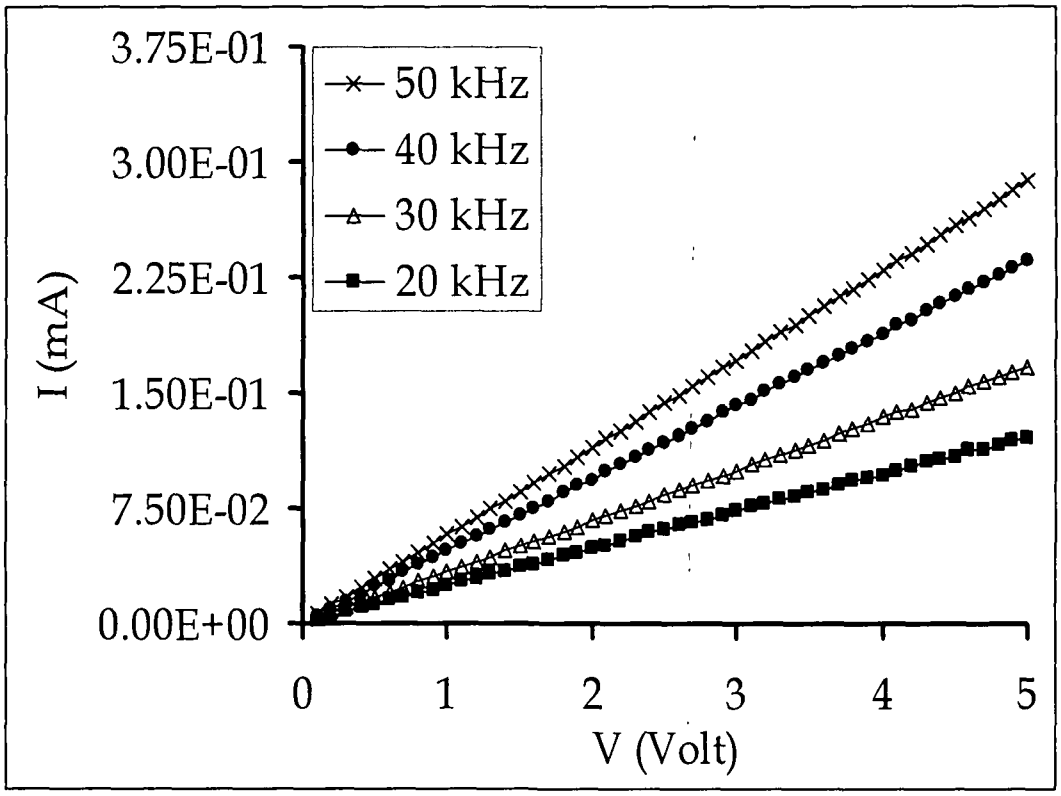

Figure 6.10: I-V characteristic of bare nano PbS /Ag junction (20-50 kHz)

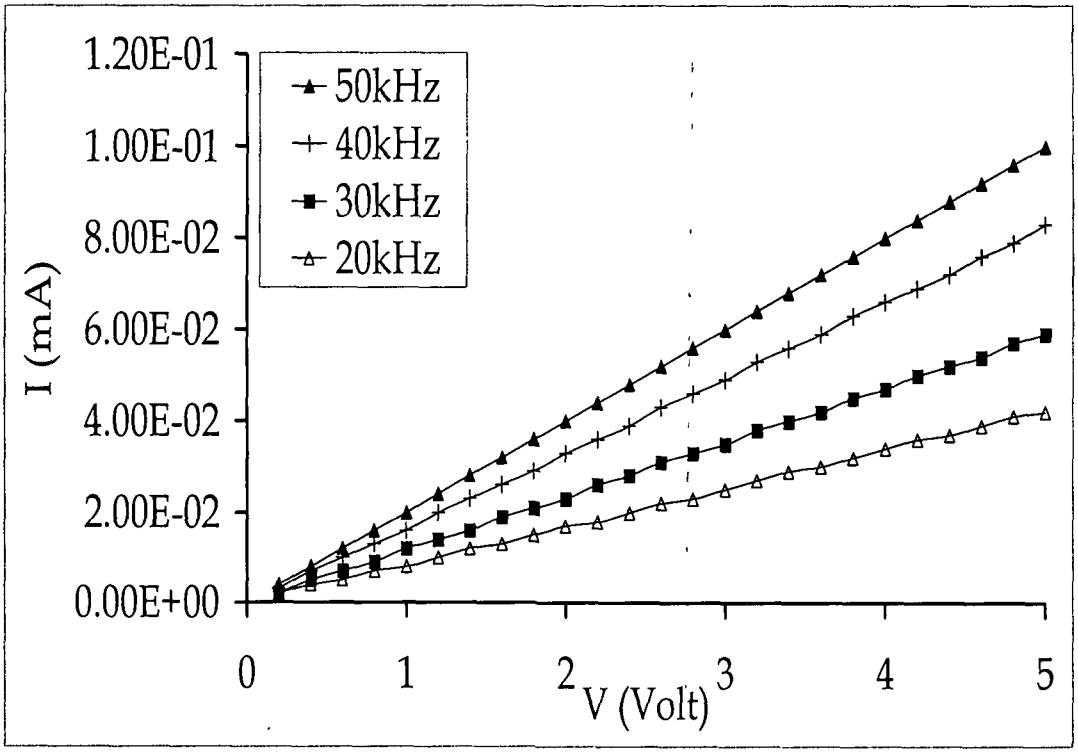

Figure 6.11: I-V characteristic of coated nano PbS / Ag junction (20-50 kHz)

PbS/ Ag junction exhibit linear dependence of current with applied voltage. The corresponding I-V characteristics have been plotted in figures 6.10-6.13.

It is expected that quantum dots which contain trapped carriers while trying to follow a.c. signal provide conducting channels through the sample giving rise to current establishment. Large becomes the signal frequency, more would be the number of carriers participate for current establishment by dislodging themselves from the trapped centers (surface states).

However the magnitude of current in case of bare nano PbS/Ag (figure 6.12) junction is much higher as compared to coated once (figure 6.13). The highest current recorded for bare nano PbS/Ag junction at 5 MHz was 4.45 mA while for coated nano PbS/Ag junction was 1.37 mA. On the basis of present understanding the low current in the later case may be thought of due to lower content of surface states or traps.

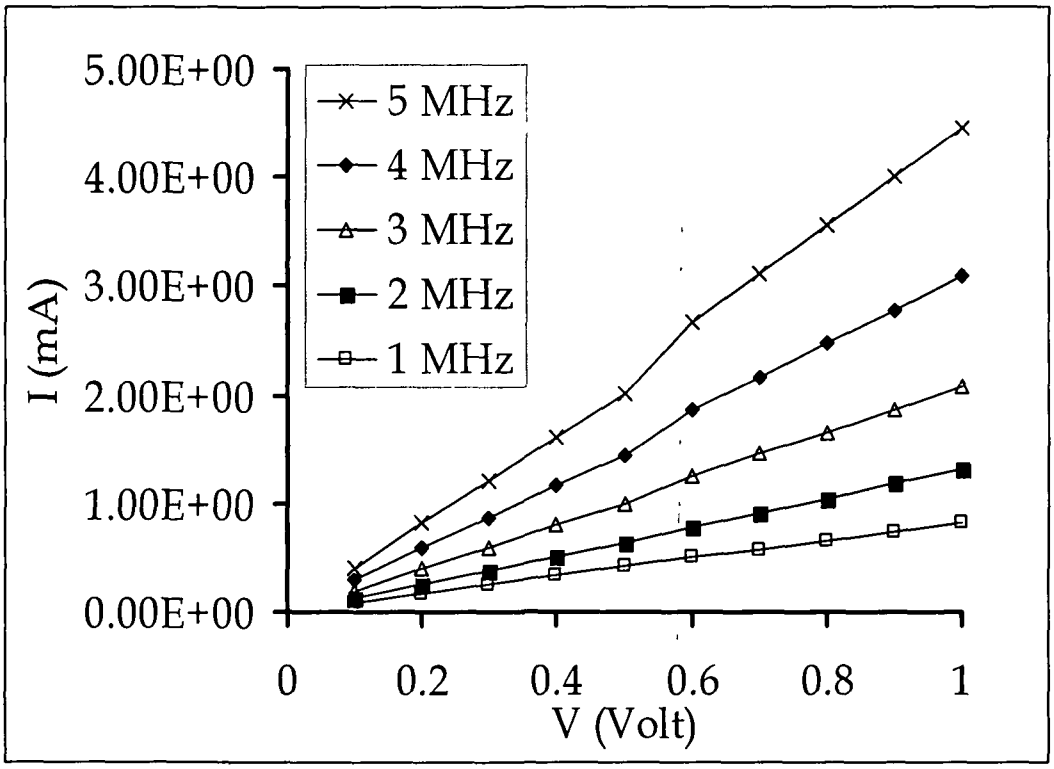

Figure 6.12: I-V characteristic of bare nano PbS / Ag junction (1-5 MHz)

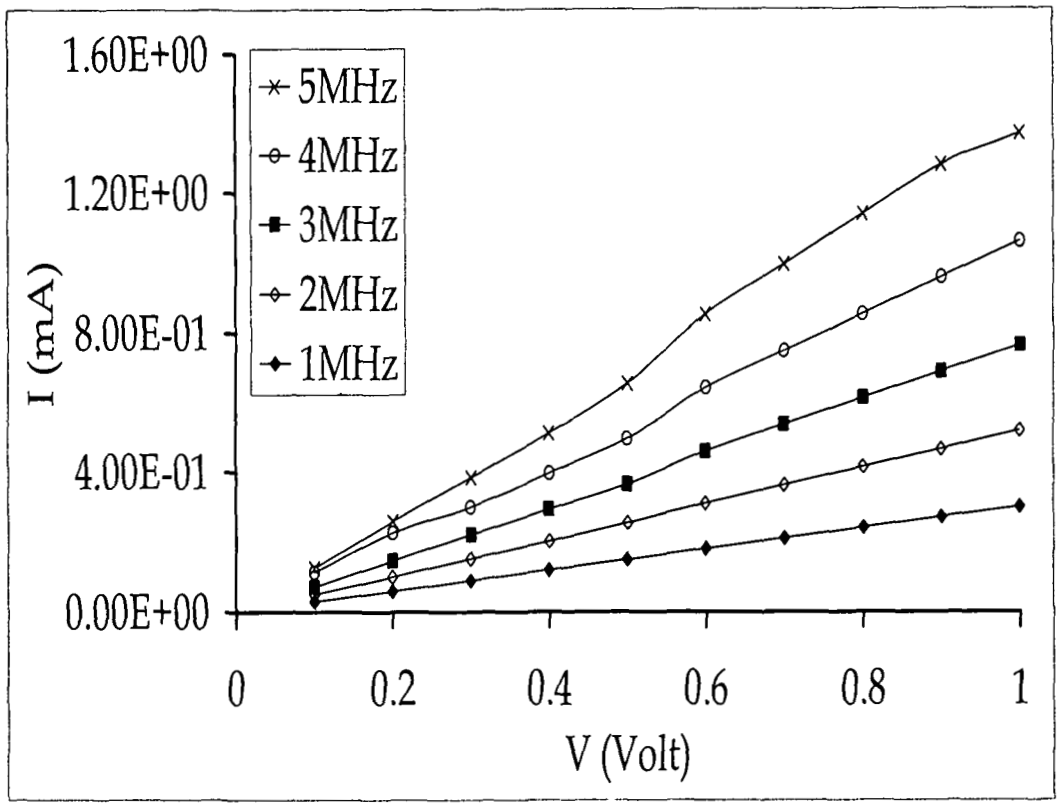

Figure 6.13: I-V characteristic of coated nano PbS / Ag junction (1-5 MHz)

In this chapter we have investigated frequency dependent electrical behavior of both bare and coated PbS quantum dots. The investigation of the electrical behavior shows the possibility of application of PbS quantum dots as electrical components like capacitor in low frequency range. Also, the study reveals that the electrical behavior, both C-V and I-V, depends on the applied frequency.

References:

1. Devoret M.H. and Christian G., *Physics World*, September 1998.
2. Francesco F.,*Topics in Nanotechnology*, 2004/5 - ver. 1 - part 5 - pp-7.
3. Jiang P., Liu Z.-F. and Cai S.-M. *J. Appl. Phys.*, **90** (2001)2039.
4. Beenakker C. W., *J.Phys. Rev. B*, **44** (1991) 1646.
5. Schrönenberger C., Houten V.H. and Beenakker C.W.J., *Physica B*, **189** (1993) 218.
6. Jortner J. and Rao C. N. R., *Pure Appl. Chem.*, **74** (2002)1491.
7. Tarucha S., Austing D. G., Honda T., van der Hage R.J., Kouwenhoven L. P., *Phys. Rev. Lett.*, **77** (1996) 3613.
8. Zhitenev N.B., Ashoori R.C., Pfeiffer L.N., West K.W., *Phys. Rev. Lett.*, **79** (1997)2308.
9. Johnson K.S., Thywissen J.H., Dekker N.H., Berggren K.K., Chu A.P., Younkin R., Prentiss M., *Science*, **280** (1998) 1583.
10. Dai H., Franklin N. and Han J., *Appl.Phys.Lett.*, **73** (1998)1508.
11. Hong S., Zhu J. and Mirkin C.A., *Science*, **286** (1999) 523.
12. Lee T., Liu J. Chen N-Po., Andres R.P., Janes D.B. and Reifenberger R., *J. Nanoparticle Res.*, **2** (2000) 345.
13. Murray C.B., Kagan C.R. and Bawendi M.G., *Science*, **270** (1995) 1335.
14. Andres R.P., J.D. Bielefeld, Henderson J.I., Janes D.B., Kolagunta V.R., Kubiak C.P., Mahoney W.J. and Osifchin R.G., *Science*, **273** (1996)1690.
15. Mcdonald S.A., Konstantatos G., Zhang S., Cyr W.P., Klem E. J.D., Levina L. and Sargent E.H., *Nature Materials*, **4** (2005) 138.
16. Mohanta D. and Choudhury A., *Eur. Phys. J. B*, **45** (2005) 63.
17. Murray C.B., Kagan C.R. and Bawendi M.G., *Annu. Rev. Mater. Sci.*, **30** (2000) 545.
18. Ashoori R.C., *Nature*, **379**, (1996), 413.
19. Kim J. J., Lee J.O., Kim J., Yoo K.H., Park J.W .and Choi J.B., *J. Kor. Phys. Soc.*, **33** (1998) 750.
20. Mujica V., Kemp M., Roitberg A., Ratnera M *J. Chem. Phys.*, **104** (1996) 7296.

CHAPTER VII

Thesis conclusion and future prospects:

7.1 Thesis conclusion:

We have successfully fabricated IV-VI (PbS) and II-VI (CdS and ZnS) semiconductor quantum dots on polymer matrix PVA with average particle size <15 nm. The average size of quantum dots was measured from X-ray diffraction (XRD) patterns using Scherrer formula and transmission electron microscopy (TEM) confirmed the sizes.

Next, we have applied a composite of PVA and SiO_2 for overcoating the quantum dots. Small reduction in size (1-3 nm) was observed for the coated quantum dots.

The optical absorption spectra provide information of blue shift and gives evidence for formation of particles in nanoscale range. Using the observed nanocrystalline band gap in the UV-Vis absorption spectra the particle size were calculated theoretically. Then PL study was carried out for both bare and coated quantum dots. The PL intensity of the coated quantum dots were significantly more than the bare once. The PL emission in case of bare quantum dots were mostly attributed to surface state emission whereas PL emission due to e-h recombination were recorded in case of coated CdS and ZnS quantum dots. Also the PL behavior of coated quantum dots were affected little after they were aged for 60 days whereas considerable increase in PL intensity was recorded with time for the bare quantum dots.

Effects of SHI were investigated in case of various polymers for modification of their properties like electronic and ionic conduction, atmospheric stability, crystallinity etc. [1,2]. But when a semiconducting particle is embedded in a polymer what physical phenomena would come to the forefront? To explore the effect of SHI irradiation on both bare and coated

quantum dots we have selected Ni^{12+} beam of energy 160 MeV for irradiation experiments. We found redshift in the absorption spectra of bare PbS, CdS and ZnS quantum dots after SHI irradiation which is stronger with respect to increase in ion fluence and expect that there might be grain growth due to Ostwald ripening under ion irradiation. However, for coated quantum dots we found no such size enhancement. We believe that the high melting point of SiO_2 may protect the quantum dots so that they can not agglomerate to form bigger particles.

Size independent PL behavior has been observed in case of both bare and coated quantum dots after SHI irradiation. However PL intensity significantly increases after irradiation which is due to thermal detrapping of charge carriers initiating high energy emission as well as increase in defect concentration after irradiation. New peaks were detected due to the formation of CdO and PbO in case of coated CdS and PbS quantum dots after SHI irradiation.

As an effort to study the nonlinear behavior of PbS quantum dots for their application in DFWM, we have successfully used low power He-Ne laser as the laser source. Also we have successfully shown that the prepared quantum dots can behave as optoelectronic as well as electronic switch depending on the input condition.

Electrical studies were carried out to investigate possible device application of polymer embedded quantum dots. For this we have studied capacitance-voltage (C-V) and current-voltage (I-V) responses of bare and coated PbS quantum dots at different frequencies. This is comparatively a new study which reveals frequency dependent C-V and I-V response of both bare and coated PbS quantum dots.

7.2 Future prospect:

We expect effective results if further research is carried out on quantum dots in the following directions:

7.2.1 New materials to synthesize quantum dot:

In the present work we have limited our study for II-VI and IV-VI semiconductor quantum dots. This may be extended for III-V semiconductor such as InP and GaP. The structural quality of the self-assembled quantum dots and their compatibility with conventional III-V technology has permitted the demonstration of high performance prototype devices such as semiconductor QD lasers [3].

7.2.2 Possible modifications in synthesis and characterization procedure:

For arresting the growth of semiconductor nanoparticles polymer matrix PVA was used. It was observed that the particles were not stable enough against SHI and also optical properties were modified with time. For better size and photo stability conjugate polymer and zeolites [4-9] could be used as a matrix in future. Also, using such matrix, the quantum dots may be fabricated with more uniform size distribution. Again for similar reasons apart from colloidal chemistry we can follow sol-gel [10] or micelle method [11] and could compare the results. In our method of fabrication we did not study the effect of pH over the particle size and other properties that could be included in future study. Synthesis of quantum dots may be tried using electro-deposition technique which permits easy control of input electrical signal.

For characterization of the samples along with XRD, UV-Vis spectroscopy, TEM and PL, Atomic force Microscopy (AFM) and Scanning Electron Microscopy (SEM) can be used for better understanding of the surface morphology of the synthesized samples.

7.2.3 Lower energy (KeV) ion beam irradiation:

In this work, SHI irradiation at high energy (160 MeV) was carried out to explore the modification on structural and optical properties of the quantum dots. At such high energy the ion beam simply irradiates the sample, the ions do not remain inside the samples. Using low energy ion beam (KeV) we can

implant different ions in the sample and can study there affect specially on luminescence and electrical properties.

7.2.4 *New areas for quantum dot application:*

The application of quantum dots has been investigated in the realm of nonlinear optics and electrical properties in the present work. The future study may effectively include the application of quantum dots as fluorescent tags or biological markers since luminescence properties of the quantum dots have been studied extensively in the present research. By using these markers, the locations of different components of cells can be observed and imaged simultaneously [12, 13].

References:

1. Kumar A., Saikia D., Singh F., Avasthi D.K., *Solid State Ionics,* **176** (2005) 1585.
2. Hussain A.M.P., Kumar A., Saikia D., Singh F., Avasthi D.K., *Nucl. Instr. Meth. B,* (in press).
3. Fafard S., Hinzer K. and Allen C.N. *Brazilian Journal of Physics,* **34,** (2004) 550.
4. Brigham E.S., Weisbecker C.S., Rudzinski W.E., and Mallouk T.E., *Chem. Mater.,* **8,** (1996) 2121.
5. Ozin G.A., Ozkar S. and Stuckyt G.D., *J. Phys. Chem.,* **94** (1990) 7562.
6. Wang Y. and Herron N., *J. Phys. Chem.,* **91** (1987) 257.
7. Wang Y. and Herron N., *J. Phys. Chem.,* **92** (1988) 4988.
8. Stein A., Ozin G.A., and Stucky G.D., *J. Am. Chem. Soc.,* **112** (1990) 904.
9. Hemon N., Wang Y., Eddy M.M., Stucky G.D., Cox D.E., Moller K., and Beid T., *J. Am. Chem. Soc.,* **111** (1989) 530.
10. Dawnay E.J.C., Fardad M.A., Green M. and Yeatman E.M., *J. Mater. Res.,* **12** (1997) 3115.
11. Larson D.R., Zipfel W. R., Williams R.M., Clark S.W., Bruchez M.P., Wise F.W., Webb W.W., *Science,* **300** (2003)1434
12. Bruchez M. Jr., Moronne M., Gin P., Weiss S., Alivisatos A.P., *Science,* **281** (1998) 2013
13. Michalet X., Pinaud F., Lacoste T.D., Dahan M., Bruchez M.P., Alivisatos A.P. and Weiss S., *Single Mol.,* **2** (2001), 261

List of Publications

A. In referred journal:

(i) **S. Chowdhury**, G. A. Ahmed, D. Mohanta, S. K. Dolui, D. K. Avasthi and A. Choudhury, *'Luminescence study of bare and coated CdS quantum dots: effect of SHI irradiation and ageing'* ***Nucl. Instrum. and Meth.B*** **240** (2005) 690.

(ii) **S. Chowdhury**, D. Mohanta, G. A. Ahmed, S. K. Dolui, D. K. Avasthi and A. Choudhury, *'Effect of 160MeV Ni12+ ion irradiation on PbS quantum dots'* ***J. Luminescence*** **114** (2005) 95.

(iii) **S. Chowdhury**, S. K. Dolui, D. K. Avasthi and A. Choudhury, *'Irradiation Induced grain growth and PL study of PbS quantum dots'*, ***Ind. J. Phys.*** (In Press).

(iv) D. Mohanta, G. A. Ahmed, **S. Chowdhury**, K. Baruah, K. Hazarika, F. Singh, D.K. Avasthi and A. Choudhury, *'Luminescence from irradiated cadmium sulfide quantum dots'*, ***Nucl. Instr. and Meth.*** **B.** (accepted)

(v) D. Mohanta, S. S. Nath, A. Bordoloi, **S. Chowdhury**, S. K. Dolui and A Choudhury, Ion irradiation response of semiconductor nanoparticles embedded in polymer matrix, *Annu. Report 2001-2002, Nuclear Science Centre, p-116*

(vi) D. Mohanta, S.S. Nath, A. Bordoloi, **S. Chowdhury**, S.K. Dolui and A. Choudhury, *Asian J. Phys.* **12** (2003) 57.

B. Presented in conference:

(i) D. Mohanta, G. A. Ahmed, S. Chowdhury, K. Baruah, K. Hazarika, F. Singh, D.K. Avasthi and A. Choudhury, *'Luminescence from irradiated cadmium sulfide quantum dots'* Paper presented in Indo German Workshop on Synthesis and Modification of Nano-Structured Materials by Energetic Ion Beams Feb. 20-24, 2005 at NSC New Delhi.

(ii) S. Chowdhury, S.K. Dolui, D. K. Avasthi, A. Choudhury, *'Irradiation Induced grain growth and PL study of PbS quantum dots'* Paper presented in Condensed Matter Days 04 at NEHU, Shillong 25-27 August, 04.

(iii) S. S. Nath, D. Mohanta, A. Bordoloi, S. Chowdhury, S.K. Dolui and A. Choudhury, *Proc. Of Nat. Conf. on Laser & Its Application,* Nov5-7, 2001, Dept. of Physics, Dibrugarh University, Dibrugarh.

(iv) S. S. Nath, D. Mohanta, A. K. Bordoloi, S. Chowdhury, A.M.P. Hussain, S.K. Dolui and A. Choudhury, *Preparation of ZnO quantum dots and its characterization,* Proceedings of the 47th Annual Technical Session, Assam Science Society, Dibrugarh, 2nd Feb, 2002.

(v) S. Chowdhury, S.S. Nath, D. Mohanta, S.K. Dolui and A. Choudhury, *'Preparation, characterization and size estimation of PbS quantum dots'* Paper presented in National Conference of Materials and Application, Kurukshetra 11-13 February, 2004.